# A SIMULATION-BASED FATIGUE LIFE ESTIMATION METHOD FOR NONLINEAR SYSTEMS UNDER NON-GAUSSIAN LOADS

by

ONKAR K. MANDE

A dissertation submitted in partial fulfillment of the
requirements for the degree of

DOCTOR OF PHILOSOPHY IN
MECHANICAL ENGINEERING

2023

Oakland University
Rochester, Michigan

Doctoral Advisory Committee:

Zissimos P. Mourelatos, Ph.D , Chair
Ryan Monroe, Ph.D
Dorin Drignei, Ph.D.
Randy J. Gu, Ph.D.

*To my wife and son*
*To my mother father and Sisters*

## ACKNOWLEDGMENTS

I am filled with immense gratitude as I thank those who made this dissertation possible. I owe profound thanks to my advisor, Prof. Zissimos P. Mourelatos, for his invaluable guidance, inspiration, and support throughout my research journey. His introduction to random vibrations, fatigue, and reliability in his courses shaped my focus, and I'm deeply thankful for the opportunity. His constant encouragement made working with him incredibly rewarding.

I sincerely thank my Doctoral Advisory Committee Prof. Ryan Monroe, Prof. Randy Gu, and Prof. Dorin Drignei for their insightful advice that significantly influenced my work. I wish to express gratitude to Prof. Mourelatos for his dedicated review of my research.

I acknowledge the essential support of my work organizations, ESTECO North America and BETA CAE Systems, for generously contributing time and access to software tools. My friends and colleagues Dr. Santosh Patil, Dr. Dimitris Papadimitriou, Dr. Vasiliki Tsianika, Dr. Vasileios Geroulas, and Ravi Nimbalkar were a source of encouragement and guidance. I'm sincerely thankful.

Lastly, I'm forever grateful to my family - my parents, wife, sisters, and son - for their unwavering spiritual support throughout this dissertation and life. I could not have done this without them.

I'm humbled and filled with immense joy to have worked with such inspiring individuals. This dissertation would not have been possible without them.

Onkar K. Mande

ABSTRACT

A SIMULATION-BASED FATIGUE LIFE ESTIMATION METHOD FOR NONLINEAR SYSTEMS UNDER NON-GAUSSIAN LOADS
by

ONKAR K. MANDE

Adviser: Zissimos P. Mourelatos

In the fields of durability and stochastic structural dynamics, it is customary to focus on linear structures subjected to Gaussian excitations. However, real-world engineering systems often exhibit nonlinear behavior and are exposed to non-Gaussian loads. Calculating fatigue life for such nonlinear systems under non-Gaussian loading presents many challenges such as complex nonlinear dynamics, multifaceted statistical characteristics, and time-dependent effects resulting in a very high computational effort. To overcome these hurdles, this research uses non-Gaussian Karhunen-Loeve expansion (NG-KLE) to not only predict the expected fatigue life but also obtain the Probability Density Function (PDF) of fatigue life. It integrates a sub-domain-based technique to significantly reduce the computational demands while preserving accuracy, by efficiently obtaining long time trajectories of random processes. This development is very useful for excitation signals that far exceed the process correlation length.

The NG-KLE method serves as the main tool for characterizing the excitation process by estimating its non-Gaussian marginal distribution and autocorrelation function. A Karhunen-Loeve (KL) expansion is executed only for the first subdomain, and then extended to subsequent subdomains by establishing correlations between the KL expansion coefficients of adjacent subdomains. This innovative approach is adapted to

non-Gaussian (NG) excitation, allowing for efficient characterization of both the input and output random processes using NG-KLE, enabling the generation of very long synthetic output random stress process samples. The fatigue life corresponding to each output stress trajectory contributes to the estimation of the PDF of fatigue life. The proposed generalized fatigue life estimation approach accommodates both Gaussian and non-Gaussian processes for both narrow and wide band signals. To demonstrate its effectiveness, we use a duffing oscillator system and a practical example involving a truck assembly modeled by the Finite Element Method (FEM).

TABLE OF CONTENTS

LIST OF TABLES

LIST OF FIGURES

NOMENCLATURE

| | |
|---|---|
| PCE | Polynomial Chaos Expansion |
| KL | Karhunen-Loeve Expansion |
| CAE | Computer Aided Engineering |
| PSD | Power Spectral Density |
| PDF | Probability Density Function |
| CDF | Cumulative Distribution Function |
| QMC | Quasi Monte Carlo |
| MCS | Monte Carlo Simulation |
| $P_f$ | Instantaneous Probability of failure |
| g($\mathbf{X}$) | Limit state function |
| $f_{\mathbf{X}}(x)$ | Joint probability density function of random variables X |
| $P_{\boldsymbol{f}}(0,T)$ | Cumulative probability of failure between 0 and time T |
| $\mathbf{X}$ | Vector of input random variables |
| $\mathbf{F}(t)$ | Vector of input random processes |
| EOM | Equations of motion |
| $\mathbf{D}_f$ | Failure Domain |
| $P_f^0$ | Instantaneous probability of failure at the initial time |
| D | Cumulative Damage |

| | |
|---|---|
| $d$ | Incremental fatigue damage |
| $S_i$ | Stress level |
| $N_{f,i}$ | Number of cycles the specimen will fail under stress Si |
| $E(D)$ | Expectation of damage |
| $f_s(s)$ | PDF of peak stress level |
| DOF | Degree of freedom |
| $[m]$ | Vibratory system mass matrix |
| $[c]$ | Vibratory system damping matrix |
| $[k]$ | Vibratory system stiffness matrix |
| EOLE | Expansion Optimal Linear Estimation |
| OLH | Optimal Latin Hypercube |
| OSE | Orthogonal Series Expansion |
| FRF | Frequency response function |
| $S_{FF}(\omega)$ | Power spectral density of input random process |
| $S_{YY}(\omega)$ | Power spectral density of output random process |
| $H(\omega)$ | Frequency response function |
| $R_{YY}(t_1, t_2)$ | Autocorrelation function of the output process |
| $\rho$ | Correlation coefficient |
| $\sigma_Y$ | Standard deviation of output process |

| | |
|---|---|
| $\mu_Y$ | Mean value of output process |
| $C_{YY}(t_1, t_2)$ | Autocovariance function of output process |
| $\rho_{YY}(t_1, t_2)$ | Autocorrelation coefficient function of input process |
| $\lambda$ | Dominant eigenvalues from an eigenvalue decomposition of the covariance matrix |
| $\Phi$ | Eigenvectors from an eigenvalue decomposition of the covariance matrix |
| Z | Vector of independent standard normal random variables |
| $h(t)$ | Impulse response function |
| $\xi$ | Standard normal random variable |
| $\xi(t)$ | Standard normal random process |
| $\Psi_i$ | One dimensional Hermite polynomials |
| $b_i$ | Expansion coefficients of the Polynomial Chaos Expansion |
| $S_e$ | Equivalent stress level |
| $S_m$ | Mean Stress |
| $S_a$ | Stress amplitude |
| $S_u$ | Ultimate strength of the material |
| $G$ | Shear modulus |
| $d$ | wire diameter |
| $C$ | Spring index |
| $\tau$ | Shear stress |

| | |
|---|---|
| $K_W$ | Wahl factor |
| $D$ | coil diameter |
| $\omega$ | Circular frequency in rad/sec |
| $M$ | Number of trajectories of the output process |
| $S_k$ | Skewness coefficient |
| $K_u$ | Kurtosis coefficient |
| $\beta$ | Weibull scale parameter |
| $\eta$ | Weibull shape parameter |
| $S(t)$ | Output stress process |
| $f(t)$ | Input force process |
| $S_f$ | Fatigue strength coefficient |
| $[m]$ | Vibratory system mass matrix |
| $[C]$ | Vibratory system damping matrix |
| $[k]$ | Vibratory system stiffness matrix |
| $Z$ | Vector of independent standard normal random |

LIST OF SYMBOLS

| | |
|---|---|
| $\zeta$ | Damping co-efficient |
| $\omega_n$ | Natural frequency |
| $\Sigma$ | Spectral decomposition of the covariance matrix |
| $\tau$ | Relative time |
| $R_F(\tau)$ | Autocorrelation function |
| $\rho_F(\tau)$ | Autocorrelation coefficient |
| $S_{FF}(\omega)$ | Power spectral density |
| K | Coupling matrix |
| $t_1^-$ | negative time step at subdomain junction |
| $t_1^+$ | positive time step at subdomain junction |
| $T$ | Total time duration |
| $C(\lvert s-t\rvert)$ | Covariance function |
| $L$ | Lower triangular matrix of Cholesky decomposition |
| $I$ | Identity matrix |
| $\bar{\boldsymbol{H}}$ | a vector in terms of K and L |
| $\theta_1$ | Standard normal variable for domain 1 |
| $\theta_2$ | Standard normal variable for domain 2 |
| $\in$ | Relative error |
| A | Pierson-Moskowitz scaling parameter (alpha) |
| B | Pierson-Moskowitz scaling parameter (beta) |

| | |
|---|---|
| $dt$ | Discretize timestep |
| $e$ | Euler's number |
| $\bar{\xi}_i$ | random coefficient |
| $j$ | imaginary unit |
| $K^T$ | Transpose of Coupling matrix |
| $T_{max}$ | Maximum time duration of each stress trajectory |
| $m$ | A multiple of the maximum time duration of each stress trajectory |
| $D_{mean}$ | Mean Damage |
| $E_{life}$ | Expected fatigue life |
| $N_{traj}$ | Number of trajectories of the output stress process |
| $N_{cycle}$ | Number of cycles per hour |
| $f_s(s)$ | Probability density function of peak stresses |
| $\tau_F^{cor}$ | Correlation length of input process |
| $N_{cycle}$ | Number of cycles per hour |

# CHAPTER ONE

# INTRODUCTION

## 1.1 Background

The occurrence of fatigue failure in vehicle components has long been recognized as a prominent contributor to accidents. This form of failure is a cumulative process, wherein materials progressively develop brittle cracks and ultimately fracture under the influence of fluctuating stresses [1, 2]. Notably, the manifestation of fatigue failure in mechanical parts lacks overt deformations, underscoring the pivotal role of fatigue life prediction in the domain of automotive part maintenance and operation. Recent years have witnessed a surge in research works aimed at predicting vehicle fatigue life, encompassing a spectrum of topics such as simulating random excitation, analyzing the response of vehicle components, and devising methods for fatigue life calculation.

In practical scenarios, a moving vehicle experiences non-Gaussian excitations in a real-world environment, a departure from the Gaussian assumption. Consequently, conventional Gaussian random signals fall short in capturing these non-Gaussian processes. Literature presents two distinct approaches to simulate non-Gaussian excitation [3, 4, 5, 6], one using the first four moments and power spectral density, while the other uses a probability density function and the Power Spectral Density (PSD) to characterize a non-Gaussian random process. The response analysis, comparatively straightforward, has garnered attention [7, 8]. In the context of nonlinear problems, the computation of output time trajectories necessitates using the corresponding input time trajectories. This operation, referred to as uncertainty propagation, entails the use of multiple trajectories to obtain accurate statistics for the output random process. This, in turn, mandates a comprehensive characterization (i.e., generation of time trajectories) of both input and output random processes in the time domain. However, the pursuit of uncertainty propagation commonly demands a prolonged time horizon to yield meaningful results. In the context of stationary processes, the practical application of the Karhunen-Loeve expansion (KLE) over a long-time domain compared to the correlation length of the process remains challenging.

## 1.2 Motivation

Failure is a cumulative event where materials gradually produce brittle cracks and eventually break due to fluctuating stresses [8], and presents a critical challenge, especially in vehicle components [9]. Notably, fatigue failure in mechanical parts can remain imperceptible, making accurate fatigue life prediction a vital task in automotive maintenance and operation. Recent years have seen a surge in research efforts aimed at predicting vehicle fatigue life, encompassing diverse aspects such as simulating random excitation, analyzing vehicle component responses, and devising fatigue life calculation methodologies.

The behavior of nonlinear vibratory systems under stochastic excitation is very significant across various disciplines, including time-dependent reliability, random vibrations, durability, and fatigue analysis. Achieving precise predictions requires the quantification and propagation of input uncertainty through the system to evaluate the resultant output uncertainty. Given the dynamic nature of these systems, a time-dependent analysis is essential. However, the inherent complexity of characterizing nonstationary and non-Gaussian input random processes [10-13] poses significant challenges. Literature also highlights the impact of non-Gaussian excitation on damage accumulation [14,15], underscoring the need for accurate characterization.

In the pursuit of accurate fatigue life predictions, the consideration of a long-time horizon becomes crucial. The temporal evolution of stress and strain patterns, influenced by various factors, necessitates an extended observation period to capture the process statistics and ensure meaningful results. However, applying conventional methodologies like the Karhunen-Loeve expansion (KLE) to long time domains relative to the process correlation length presents computational challenges. The computational effort required for uncertainty propagation in large time horizons can be prohibitive. Thus, innovative approaches are sought to address this issue, enabling the accurate estimation of fatigue life for long periods.

## 1.3 Literature Review

Spectral decomposition techniques are commonly used to characterize Gaussian random processes. A suite of methods has evolved, including Borgman's approach [16, 64], Shinozuka's method [17, 18], Karhunen-Loeve expansion (KLE) [19, 20], and Expansion Optimal Linear Estimation (EOLE) [21], among others. While KLE primarily caters to Gaussian processes, its applicability can be extended to non-Gaussian processes [22]. KLE represents random processes using a weighted sum of uncorrelated eigenfunctions derived from the process covariance matrix, leveraging spectral decomposition. For stationary processes, knowledge of the process Power Spectral Density (PSD) is required to construct the covariance matrix.

Methods like Borgman and Shinozuka [16-18,64], using Fourier transform principles, treat phase angles of harmonics as independent random variables. The assumption of ergodicity enables these methods to equate temporal and ensemble statistics for sample trajectories. KLE decomposes the covariance function into uncorrelated eigenfunctions, while EOLE [22] is a KLE variant. Autoregressive time series models [23, 24] offer an alternative by presuming linear dependencies between states based on previous states, with computation of linear dependency coefficients typically involving a likelihood function maximization. The application of KLE to a significantly long-time domain compared to the correlation length remains challenging [25], as the number of KLE terms required for a given mean-square error experiences substantial growth with domain size. This poses challenges in scenarios requiring extensive trajectory durations. Two prominent hurdles surface: the covariance matrix size increases, particularly with fine discretization, and eigenvalue analysis becomes computationally demanding. Moreover, the context of uncertainty propagation in nonlinear dynamic problems or linear scenarios driven by non-Gaussian processes demands an accurate solution to enhance output process statistical moment accuracy without intensive time integration of lengthy input trajectories. A generalized methodology, using the marginal PDF of the input process and its autocorrelation function (or PSD) [26], with a subdomain NG-KLE approach, addresses these challenges. Notably, addressing scenarios involving many lengthy input random trajectories for nonlinear systems necessitates an innovative strategy. An initial phase leverages short time horizons for system evaluations, thereby generating output random trajectories to estimate the output marginal PDF and autocorrelation function. Subsequently, a subdomain NG-KLE methodology generates long output random process trajectories, facilitating fatigue life estimation via the proposed generalized methodology. This strategy streamlines computations and accommodates nonlinearities, enhancing the efficacy of fatigue life prediction.

## 1.4 Methodology

The fatigue failure of vehicle components is a critical contributor to accidents. Fatigue failure, a cumulative event wherein materials progressively develop brittle cracks culminating in failure due to fluctuating stresses, is of paramount significance [27]. The behavior of nonlinear vibratory systems under stochastic excitation, with its ramifications spanning time-dependent reliability, random vibrations, durability, and fatigue, requires an accurate assessment. To achieve accurate predictions, quantifying and propagating input uncertainty through the system, thereby assessing output uncertainty, is a pivotal pursuit. The dynamics of such systems necessitate a time-dependent analysis. Unlike the relatively straightforward characterization of stationary and Gaussian random processes [28-30], the characterization of nonstationary and non-Gaussian input random processes poses a formidable challenge [31-33]. Existing literature underscores the heightened sensitivity of damage accumulation under non-Gaussian excitation [34,35]. An accurate characterization of nonstationary and non-Gaussian random processes requires the process probability density function (PDF) and PSD which require a significant amount of data. Conventional techniques, as the spectral representation method [36], use the Gaussian assumption. To simulate non-Gaussian processes, existing methodologies entail nonlinear transformations of underlying Gaussian processes, based on the Grigoriu translation process theory [37].

This study presents a novel approach to simulate non-Gaussian excitation to simulate real-world conditions. The proposed method provides therefore an accurate fatigue life estimation for vehicle components. This dissertation introduces a simulation-based approach to characterize the output random process of nonlinear vibratory systems with random parameters excited by nonstationary Gaussian processes. The proposed methodology uses a limited number of simulations and has broad applications in diverse domains encompassing time-dependent reliability, random vibrations, and fatigue prediction. We apply this innovative methodology to time-dependent reliability for nonlinear dynamic systems subject to non-Gaussian excitation. The research aims to predict fatigue life of nonlinear vibratory systems exposed to non-Gaussian loads. The initial step involves characterizing the non-Gaussian input process using a non-Gaussian Karhunen Loeve expansion (NG-KLE) based on a provided marginal PDF and a target correlation function. For nonstationary processes, the process marginal PDF is represented by a series of Hermite polynomials of the standard normal random variable. The resulting coefficients of the series are estimated using a Polynomial Chaos Expansion (PCE). The series is subsequently extended in time, thereby expressing the process using Hermite polynomials of a standard normal process $\xi(t)$. The final step involves employing KLE to express $\xi(t)$ using uncorrelated standard normal variables, effectively representing the non-Gaussian process using independent standard normal random variables. To enhance accuracy, the first six Hermite polynomials are employed in the process expression. Given the non-linear nature of the system, solving for numerous input random trajectories, particularly for long duration vibratory systems, proves prohibitively expensive and impractical. Thus, the study's methodology first employs a non-Gaussian Karhunen-Loeve expansion (NG-KLE) method to characterize the process using a few output trajectories of short duration generated from the system. The NG-KLE approach primarily characterizes the excitation process by estimating its non-Gaussian marginal distribution and autocorrelation function. This step allows us to generate multiple output stress trajectories. Then, each generated output trajectory of the non-Gaussian stress process undergoes rain-flow counting based on a 4-point algorithm [38] to identify each damage cycle. A mean-stress correction is also used to obtain fully reversed amplitude cycles crucial for fatigue life estimation. Furthermore, the expected life is calculated using an alternate approach based on the total probability theorem [39], showing a good agreement between the prediction of the two methods. A contribution of this study and its proposed methodology is the utilization of a generalized least squares approximation to characterize non-Gaussian random processes using NG-KLE. Furthermore, the methodology considers fully reversed amplitudes, a mean-stress correction, and the calculation of the PDF of peak stresses for fully reversed cycles [40]. The latter allows us to use a narrow-band assumption without loss of accuracy. Consequently, this methodology is applicable to both narrow-band and wide-band processes. The study also addresses the pressing challenge of accurately generating long horizon random processes using a unique approach based on a subdomain KLE. This holds significant relevance, particularly in cycle counting methodologies, a critical component for accurate fatigue life estimation. In summary, the study introduces a new simulation-based methodology for assessing fatigue life of nonlinear vibratory systems subjected to non-Gaussian loads.

# CHAPTER TWO

# SIMULATION-BASED FATIGUE ANALYSIS AND LITERATURE REVIEW

## 2.1 Fatigue and Reliability Background

Predicting fatigue damage of structural components to variable loading conditions is a complex issue. Random loading conditions perplex even more the calculation of fatigue life as random excitations induce uncertainty in the stress output of a mechanical system. There are several approaches to estimate fatigue damage that can be divided into two major categories, i.e., stress-based and strain-based methodologies [41].

In the stress-based approaches cycles, as well as magnitudes of oscillatory stresses need to be calculated at the stress concentration areas and compared to the strength of the material defined by the *S-N* curve. If the damage computed exceeds a certain level, then failure is assumed for the component. Furthermore, for the estimation of the damage, a fatigue damage rule is needed. It is a common practice to use the linear damage rule, or Miner's rule [42], due to its simplicity, applicability, and accuracy.

In the strain-based approaches, local stresses and strains are estimated at the point where fatigue cracking is most likely to occur. It is assumed that yielding will initiate at this point. In this methodology, a smooth laboratory specimen is used, which undergoes the same cyclic deformation as the actual notched component. Therefore, the effects of local yielding are included, and the material's strain-life curves are employed by inducing strain-controlled axial fatigue testing on the laboratory specimen. This method is sometimes referred to as local strain analysis.

All the fatigue damage theories include deterministic approaches in the calculation of the life of a structural component. The structural component might be the suspension of a vehicle system, a bridge truss or even a skyscraper undergoing cyclic loading. This loading is random in nature, which means that it cannot be predicted as it does not follow a deterministic pattern. Examples can be an earthquake motion, wind loading or the roughness of a road path that excites the suspension of a vehicle.

Different approaches need to be applied in order to account for the uncertainty of an oscillatory motion that causes fatigue failure to a system. Therefore, the reliability of a system is defined. Reliability of a component or a system is the probability that the system or component will perform its intended functionality according to design specifications for a prescribed time period. All these components or systems are designed such that they sustain variable types of loadings. The time $T_f$ at which a member fails, is a random variable depending on the applied random loading. Moreover, the load time-history data defines a random process. Since $T_f$ is a random variable, it is a common practice that its expected value is used to define the fatigue life of the system.

Fatigue failure is a cumulative event due to cyclic loading. The fatigue damage $d = \frac{a}{a_f}$ is the ratio of the current crack length $a$ to the final crack length $a_f$ at failure. The linear damage Palmgren-Miner model [43, 44] $d = \frac{n}{N_f}$ is commonly used, where $n$ is the number of cycles at a constant amplitude cyclic load (e.g., stress) and $N_f$ is the number of cycles for the specimen to fail at the same stress level.

However, in fatigue, uncertainty is not induced only from the random nature of the excitation of a system. Stress and strain-based approaches involve laboratory testing.

The construction of the *S-N* curve includes the testing of “identical” coupons under “identical” laboratory conditions. Inherent variability in the microstructure of a material as well as variability in the testing conditions induce high uncertainty in the estimation of fatigue life and needs to be included in the computational methods of fatigue damage.

The Palmgren-Miner linear damage model has been proved accurate for random loading if stresses are not high enough to induce plastic deformation [42]. We first count (estimate) the number of cycles $n_i$ at each stress level $S_i$ and use the material S-N curve to calculate the number of cycles $N_{f,i}$ the specimen will fail under the cyclic load $S_i$. The damage model is then used to calculate the incremental damage $d_i$. The cumulative damage $D$ is calculated by summing up the incremental damage $d_i$ over all the load (stress) levels $i$ as

$$D = \sum_i d_i = \sum_i \frac{n_i}{N_{f,i}} \tag{2.1}$$

For a zero-mean, stationary random stress signal and under the strong assumption of a narrow-band random process, the linear damage model provides the following expected damage [46]

$$E(D) = \frac{v_0 T}{A} \int_0^\infty s^m f_s(s) ds \tag{2.2}$$

where $v_0$ is the mean up-crossing rate, $T$ is the signal duration, $A$ and $m$ are coefficients of the S-N curve ($N_f \cdot S^m = A$) and $f_s(s)$ is the PDF of the peak stress ($S$) level. The distribution $f_s(s)$ is used for cyclic counting under the narrow-band assumption (existence of a negative stress trough equal in magnitude with a positive stress peak to form a load cycle). The difference between a wide-band and a narrow-band process is shown in Fig. 2.1. Note that in Eq. (2.1) $D$ is a random variable and its range of values (e.g., 95th percentile minus 5th percentile) can be wide. Thus, the expected value $E(D)$ may be of limited practical significance.

It can be shown that for a zero-mean, Gaussian, narrow-band process (e.g., harmonic process with constant frequency and random amplitude), $f_s(s)$ is Rayleigh distributed as

$$f_s(s) = \frac{s}{\sigma_x^2} exp\left(-\frac{s^2}{2\sigma_x^2}\right) \tag{2.3}$$

where $\sigma_x^2$ is the variance of the underlying process $X(t)$. In this case, the linear damage model yields the following expected value $E(D)$ of damage [47].

$$E(D) = \frac{v_0 T}{A}\left(\sqrt{2}\sigma\right)^m \Gamma\left(\frac{m}{2}+1\right) \tag{2.4}$$

For a zero-mean, Gaussian, wide-band process with irregularity factor $\alpha = \frac{v_0}{v_p}$ (ratio of zero up-crossing frequency to peak frequency), the distribution $f_s(s)$ is provided by the following Rice formula [22,75].

$$\begin{aligned} f_s(s) = (1-\alpha^2)\frac{1}{\sqrt{2\pi(1-\alpha^2)}\sigma_x} \cdot exp\left(-\frac{s^2}{2(1-\alpha^2)\sigma_x^2}\right) \\ + \alpha\Phi\left(\frac{\alpha}{\sqrt{1-\alpha^2}} \cdot \frac{s}{\sigma_x}\right)\frac{s}{\sigma_x^2} \cdot exp\left(-\frac{s^2}{2\sigma_x^2}\right) \end{aligned} \tag{2.5}$$

The Powell distribution of peak stresses $f_s(s) = -\frac{1}{v_p}\frac{d(v_{s^+})}{ds}$ where $v_{s^+}$ is the up-crossing rate for stress level $S$ and $v_p$ is the peak frequency, does not use the gaussian assumption and is therefore more general than the Rice formula of Eq. (2.5). However, it cannot be used for cycle counting unless we assume a narrow-band process. Both $v_{s^+}$ and $v_p$ can be calculated numerically for a non-Gaussian distribution [48,75].

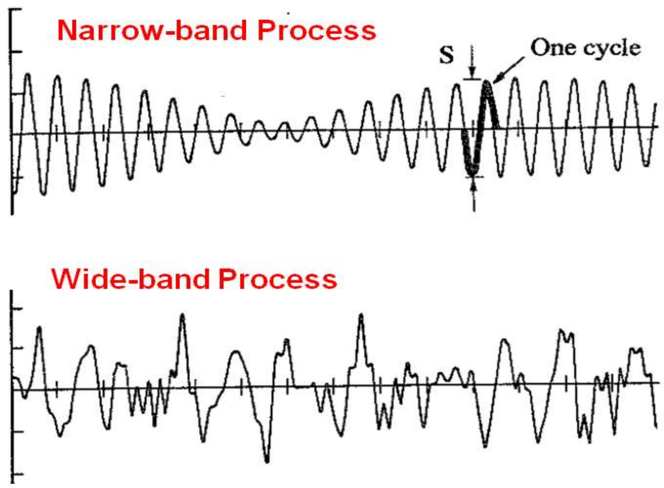


Figure 2.1  Narrow-band / Wide-band process (From: P.H. Wirsching, T.L. Paez, H. Ortiz, Random Vibrations: Theory and Practice, John Wiley & Sons, 1995)[105]

Dirlik [49,75] has developed an empirical peak stress distribution using Monte Carlo simulations and rain-flow cycle counting as a weighted average of an exponential and two Rayleigh distributions. Dirlik's peak stress distribution is considered more accurate compared to Rayleigh or Rice distributions for wide-band processes [49,50]. However, it can only be used to estimate the expected (not the actual) cumulative damage using Eq. (9). Fatigue failure occurs if $D$ is greater than one ($D > 1$). The fatigue life $T_L$ is random because of 1) randomness of the input (represented by a provided spectrum), 2) inherent variability of the test component (material properties, dimensions, etc.), and 3) uncertainty in the definition of the S-N curve (randomness of $m$ and $A$ coefficients). The fatigue reliability $R(T)$ at time $T$ is defined as the probability that $T_L$ is greater than $T$; i.e.,

$$R(T) = Pr(T_L > T) \text{ or } R(T) = Pr(D < 1) \quad (2.6)$$

The main shortcomings of the above state-of-the-art fatigue reliability methods (Equations 2.4 to 2.6) are: 1) Equation (2.1) provides only the mean value of damage. In this research, we will estimate the entire PDF of damage; 2) The restrictive narrow-band assumption is used to allow cycle counting based on the peak stress distribution; 3) The stress process is assumed Gaussian. Equations (2.6) to (2.7) are based on the Gaussian assumption which simplifies the estimation of fatigue life significantly. If the excitation is Gaussian and the system is linear, the output stress is also Gaussian and one of the aforementioned approaches can be applied. However, many loads are non-Gaussian resulting in non-Gaussian stresses.

## 2.2 Need of Long-time Trajectories

In fatigue analysis, the need for long- time trajectories arises from the inherent nature of fatigue failure mechanisms and the desire to accurately predict the lifespan of a component or structure under cyclic loading [51]. Fatigue failure occurs due to the accumulation of damage over time, where repeated cyclic loading induces microscopic cracks and material degradation. These cracks gradually propagate until they reach a critical size, leading to catastrophic failure. To predict the fatigue life of a component, engineers and researchers simulate the cyclic loading conditions over an extended period to observe how the material degrades and cracks propagate. This simulation involves tracking the stress and strain variations in the material as the cyclic loading is applied repeatedly. The goal is to determine how many cycles the material can endure before failure occurs.

Several reasons emphasize the need for long-time trajectories in fatigue analysis:

- Accurate Damage Accumulation: Fatigue failure is a gradual process, and accurately capturing the accumulation of damage requires observing the material's behavior over a sufficient number of cycles. Short-duration simulations might miss critical fatigue-related phenomena that only manifest after a certain duration.
- Cumulative Effect: Fatigue damage is cumulative, meaning that each cycle contributes to the overall degradation of the material. Long-time trajectories allow us to capture the compounding effect of cyclic loading over time, leading to a more accurate estimation of fatigue life.
- Statistical Significance: Fatigue behavior exhibits statistical variability. Long-duration simulations help establish statistically significant trends and patterns in the material's response, leading to more reliable predictions of fatigue life.
- Low-Cycle and High-Cycle Fatigue: Different fatigue regimes, such as low-cycle and high-cycle fatigue, operate over different frequency ranges. Longer time trajectories are essential to capture the behavior in both regimes and accurately assess the material's fatigue resistance across the entire spectrum.
- Environmental and Load Variability: Real-world conditions involve variations in loads, temperatures, and other environmental factors. Longer simulations allow for a better representation of these variable conditions, leading to more comprehensive fatigue life predictions.
- Complex Loading Patterns: Some applications involve complex loading patterns that take time to fully manifest their effects on fatigue. Longer time trajectories are necessary to observe the interactions between different loading conditions.

In summary, long time trajectories in fatigue analysis enable us to observe and quantify the gradual deterioration of materials under cyclic loading, resulting in more accurate predictions of fatigue life and better-informed engineering decisions regarding component design, maintenance intervals, and operational safety.

## 2.3 Cycle Counting Techniques

In fatigue analysis, cycle counting techniques play a crucial role in simplifying complex variable amplitude loading histories into manageable sequences of constant amplitude loading events, each indicative of fatigue damage. There are two kinds of these techniques: the one-parameter technique and the two-parameter technique. The former includes methods such as level crossing cycle counting, peak valley counting, and range counting. However, these methods struggle to capture the relationship between loading cycles and the detailed local stress-strain behavior that greatly influences fatigue failure [52]. On the other hand, the two-parameter cycle counting methods, such as the well-regarded rain-flow counting method, are notably more effective. As highlighted by Dowling [53], the rain-flow counting algorithm stands out for its impressive accuracy in predicting fatigue life. Conceived with a touch of inspiration from raindrops gracefully descending upon a pagoda roof and tracing their path down the edges, the rain-flow method, pioneered by Matsuishi and Endo in 1968 [48], meticulously identifies stress cycles. This involves capturing both the stress range and mean value inherent in each cycle within a complex loading sequence inherent in a wide-band random process.

Embracing these advanced cycle counting techniques not only helps untangle the intricate relationship between loading patterns and fatigue behavior but also opens the door to more precise and well-informed predictions of fatigue life across various engineering scenarios.

### 2.3.1 Four Point Rain-flow Counting Algorithm

The rain-flow counting algorithm, originally developed by Matsuishi and Endo (1968) [48], was conceived by observing the analogy of raindrops falling on a pagoda roof and running down the edges of the roof. The rain-flow method is used to identify stress cycles, that is, the stress range and mean value for each cycle, in a complex loading sequence such as a realization (time trajectory) of a wide-band random process. There are several variations to the rain-flow cycle counting method including three- and four-point versions[53]. In the four-point cycle counting rule, four consecutive points in a stress history data are used in order to extract a cycle [38]. The steps below describe how a cycle is extracted:

- The stress time data are rearranged so that the signal starts with the highest peak or the lowest valley, whichever is greater in absolute magnitude. Then, four consecutive points $(S_1, S_2, S_3, S_4)$ are identified.
- Define two ranges. One inner range $\Delta S_i = |S_2 - S_3|$ and one outer range $\Delta S_o = |S_1 - S_4|$.
- If $\Delta S_i \leq \Delta S_o$ then one cycle is extracted from point $S_2$ to $S_3$ and points $S_1$ and $S_4$ are connected to each other.

The same process is carried out until all cycles are identified and extracted. One simple example is illustrated in Figure 2.2.

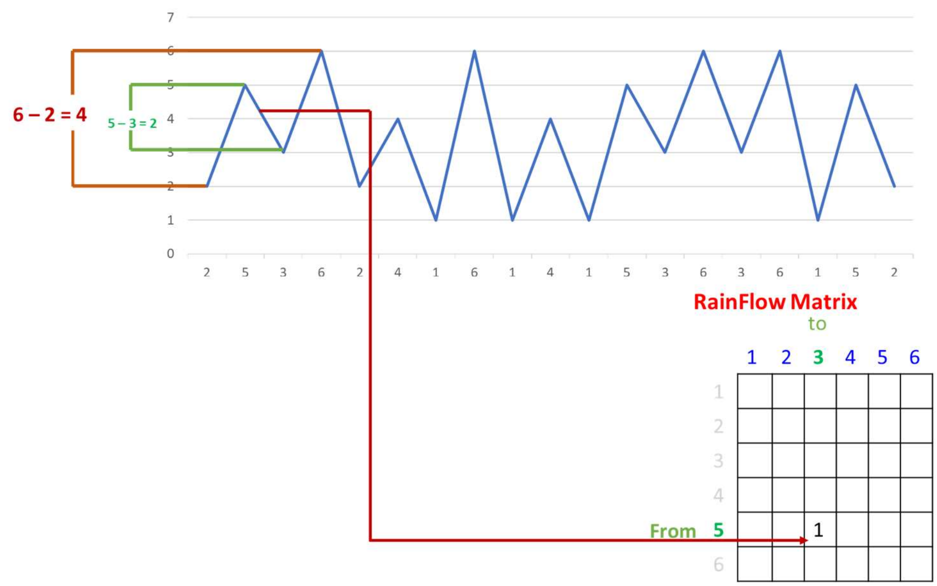


Figure 2.2 Rain-flow counting technique and extraction of a cycle

After all cycles are identified and extracted, the data are organized in a "From-To" table. In this table, the “From” values denote all points $S_2$ while the “To” values denote all points $S_3$. When the four-point counting method is used, some of the data points will remain and will not form a closed loop. These points form the so-called residue. In order to calculate the cycles in the residue, first the residue is duplicated to form a sequence [residue + residue]. Using this sequence, the same rain-flow counting technique is applied. Then, the newly extracted cycles are added to the already extracted ones.

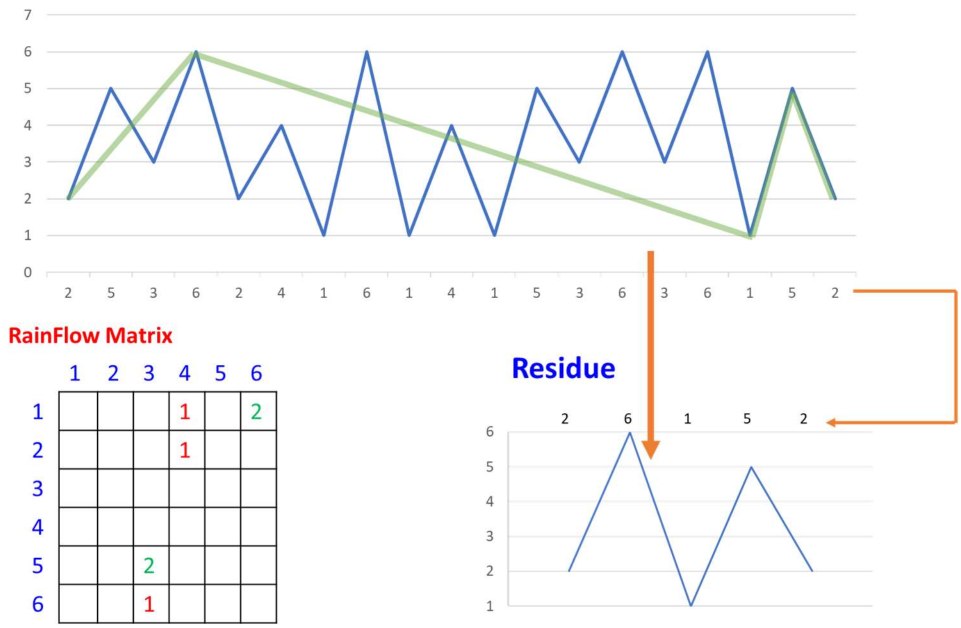


Figure 2.3 Rain-flow matrix and residue

The residue contains the largest unclosed cycles present in time history. If the time history was for one lap of a durability proving ground, to calculate the damage for 1000 laps, every element of the matrix would be multiplied by 1000. The residue would be appended 1000 times over and the unclosed cycles then counted and added to the rain-flow matrix. The 'Rain-flow Matrix' and 'Residue' are the end results of the rain-flow counting process. They contain the following information:

- Cycle amplitude – Across the top of the display is the "To" stress level for the cycle. Across the side is the "From" stress level for the cycles. The range or amplitude of the cycle is |To-From|.
- Cycle mean – The mean of the cycle is (To+From)/2. The mean stress determines if the cycle is compressive or tensile, which affects the accumulated damage.
- Number of cycles – The number of the cycles is indicated, sometimes with colors dictating specific number of cycle thresholds.

This cycle information is in a much more compact and manageable form than the original time history data. Only the sequence, or order, in which the cycles are applied over time are not kept. Figure 2.4 provides a schematic of the rain-flow counting process.

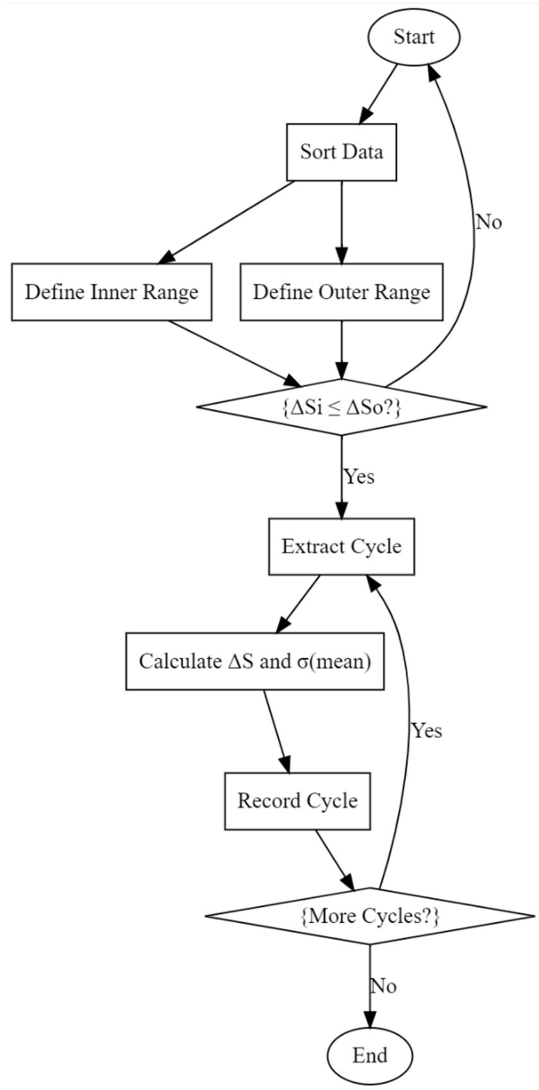


Figure 2.4 Rain-flow counting algorithm

## 2.4 Mean Stress Effect in Stress-based Fatigue Life

Fatigue damage of a component correlates strongly with the applied stress amplitude $S_a = \frac{S_{\max} - S_{\min}}{2}$ or applied stress range $S_r = S_{\max} - S_{\min}$ and is also influenced by the mean stress $S_m = \frac{S_{\max} - S_{\min}}{2}$ [56]. In the high cycle fatigue region, normal mean stresses have a significant effect on fatigue behavior of components because they are responsible for the opening and closing state of microcracks. Because the opening of microcracks accelerates the rate of crack propagation and the closing of the microcracks retards the growth of cracks, a tensile normal mean stress reduces the fatigue strength, while a compressive normal mean stress is beneficial in the terms of fatigue strength. The shear mean stress does not influence the opening and closing state of microcracks and therefore has little effect on crack propagation. There is very little or no effect of mean stress on fatigue strength in the low-cycle fatigue region in which the large plastic deformation erases any beneficial or detrimental effect of a mean stress.

The S-N curve states that

$$S_{ar} = S_f'\left(2\,N_f\right)^b \tag{2.7}$$

where $S_{ar}$ is the fully reversed stress amplitude (corresponding to zero mean load), $S_f'$ is the fatigue strength coefficient, $b$ is the fatigue strength exponent, $N_f$ is the number of cycles of failure and $2N_f$ is the number of reversals. If for a cyclic load there is a mean stress, an equivalent fully reversed stress amplitude $S_{ar}$ must be calculated using one of the available mean stress correction approaches. The most well-known mean stress correction for stress-based fatigue using the S-N curve are briefly described below.

Goodman Mean Stress Correction

$$S_{ar} = \frac{S_a}{1-\left(\frac{S_m}{S_u}\right)} \tag{2.8}$$

where $S_u$ is the material ultimate strength.

Gerber Mean Stress Correction

$$S_{ar} = \frac{S_a}{1-\left(\frac{S_m}{S_u}\right)^2} \tag{2.9}$$

Soderberg Mean Stress Correction

$$S_{ar} = \frac{S_a}{1-\left(\frac{S_m}{S_y}\right)} \tag{2.10}$$

where $S_y$ is the material ultimate strength.

Morrow Mean Stress Correction

$$S_{ar} = \frac{S_a}{1-\left(\frac{S_m}{S'_f}\right)} \tag{2.11}$$

where $S_f'$ is fatigue strength coefficient. Note that the above equation is equivalent to

$$S_a = \left(S_f' - S_m\right)\left(2N_f\right)^b \tag{2.12}$$

Smith, Watson and Topper (SWT) Mean Stress Correction

$$S_{ar} = \sqrt{(S_{\max S_a)}} = S'f(2Nf)^b \qquad (2.13)$$

if $S_{max} > 0$. If $S_{max} \leq 0$, there is no crack initiation.

It should be noted that for relatively small mean stress loading, the Morrow and the SWT approaches are considered better than the Goodman method. The Goodman mean stress correction formula is preferred if none of the fatigue properties are available. For metals, it appears to work particularly well for aluminum alloys. Below are some practical comments on the mean stress correction methods.

- The Goodman method employing the ultimate tensile strength $S_u$ is highly inaccurate and should not be employed where life estimates are desired in fatigue analysis.
- The Morrow equation with the true fracture strength $S_f'$ is reasonably accurate in most cases. However, true fracture strengths are often unavailable and must be estimated.
- The Morrow method with the intercept constant $S_f'$ is also reasonably accurate for steels, but often gives grossly non-conservative life estimates for aluminium alloys.
- The SWT method provides good results in most cases, and for aluminum alloys it is somewhat more accurate than the Morrow $S_f'$ equation. The SWT method has the advantage of simplicity and is a good choice for general use.
- When sufficient data is available for fitting the adjustable parameter $\gamma$, the Walker method gives superior results.

It should be noted that for relatively small mean stress loading, the Morrow and the SWT approaches are considered better than the Goodman method [57]. The Goodman mean stress correction formula is preferred if none of the fatigue properties are available. In metals and appears to work particularly well for aluminum alloys. The Morrow approach was used in the presented simulation-based general fatigue method.

## 2.5 Summary

This chapter provides a comprehensive detail of fundamental concepts in fatigue analysis and the important aspect of fatigue reliability, considering both short and long-time horizons. It introduces the linear damage rule and the S-N curve, emphasizing their role in quantifying fatigue damage accumulation. The chapter also discusses uncertainties in S-N curve calculations, highlighting the importance of accounting for material properties and testing conditions to enhance reliability. Various mean stress correction methods are presented, along with their applications and accuracy across different scenarios. The significance of peak stress distribution and the four-point rain-flow counting technique is explained in relation to quantifying fatigue damage in complex loading histories. Moreover, the chapter addresses the challenge of calculating fatigue life under uncertainty, emphasizing the need for robust methodologies to ensure accurate predictions over extended time horizons.

# CHAPTER THREE

# NON-GAUSSIAN PROCESS CHARACTERIZATION

## 3.1 Process Characterization Introduction

Several techniques are well-suited for handling non-Gaussian data. The Independent Component Analysis (ICA) [50] extracts statistically independent components from mixed sources in non-Gaussian and non-linear scenarios. The copula approach captures complex dependencies between random variables irrespective of their marginal distributions [51]. The Polynomial Chaos Expansion (PCE) efficiently propagates uncertainty through models with non-Gaussian input distributions using orthogonal polynomials [52]. The Gaussian Mixture Models (GMM) approximate complex non-Gaussian data distributions by combining Gaussian components [53]. The Kernel Density Estimation (KDE) [54] accurately estimates non-Gaussian data distributions by smoothing data points. Finally, Quantile Regression robustly estimates conditional quantiles of a response variable, making it suitable for modeling data with non-Gaussian tails. These techniques find applications across fields such as finance, engineering, and data science, providing valuable tools for analyzing and modeling non-Gaussian data.

To fully characterize a non-stationary and non-Gaussian random process, the joint probability density functions of all orders must be specified. This is impractical because it requires a large amount of data. The Spectral Representation Method (SRM) [55] is commonly used for Gaussian processes. The available methods to simulate a non-

Gaussian process use a non-linear transformation of underlying Gaussian processes based on the rigorous mathematical framework of Grigoriu's translation process theory [37,58]. A translation process is a monotonic transformation of a Gaussian process. Details are provided in [58]. Almost all methods use an iterative process to identify the non-linear transformation to obtain the required non-Gaussian characteristics. The iterative procedure is based on the spectral density function of the process [58] or its correlation function. In the former case, the approach is applicable to stationary processes and the latter uses translation processes. In this research, we characterize a stationary and non-Gaussian process using a PCE-KL (Polynomial Chaos Expansion – Karhunen Loeve expansion) approach, based on a target first-order marginal PDF and a target second-order correlation function [11, 58]. For a non-stationary process, the marginal PDF varies in time. PCE [59] represents the marginal PDF of the process as a series of Hermite polynomials of the standard normal random variable $\xi$. The series is then extended in time to express the process in terms of Hermite polynomials of a standard normal process $\xi(t)$. KL expansion [60] is finally used to express $\xi(t)$ in terms of uncorrelated standard normal variables. The method, therefore, represents a non-Gaussian process in terms of independent standard normal random variables.

## 3.2 Polynomial Chaos Expansion

The roots of polynomial chaos expansion (PCE) trace back to Norbert Wiener's pioneering work in 1938, where the theory of homogeneous chaos took shape [59]. Building on this foundation, Cameron and Martin's demonstration of PCE's convergence in the $L^2$ sense added a robust mathematical underpinning [60]. However, it was Ghanem and Spanos who brought PCE into broader prominence by combining it with stochastic Galerkin techniques, opening doors to a plethora of applications [61]. This sparked a wave of investigations into PCE's construction, limitations, and its varied applications across disciplines [11, 58, 61]. The strength of PCE goes beyond computational efficiency. It enables practitioners with analytical expressions for stochastic moments such as mean, variance, and global sensitivity indices [62] without the need for further original model evaluations.

PCE's practical significance is not without challenges, particularly when confronted with rising input dimensions. The so-called "curse of dimensionality" looms, leading to a proliferation of terms and training runs, eroding computational efficiency. Efforts to surmount this obstacle have given rise to sparse PCE approximations. These innovative strategies artfully select expansion terms with non-zero coefficients, optimizing the trade-off between precision and computational cost. Among these strategies, sparse quadrature, stochastic collocation, and stratified sampling methods have emerged as notable contenders.

In conclusion, Polynomial Chaos Expansion has evolved into a practical tool with wide-ranging applications. The combined contributions of Wiener, Cameron, Martin, Ghanem, and Spanos [57-60] have paved the way for exploring its capabilities in addressing complex systems. Further research into sparse PCE techniques promises to extend its applicability to higher-dimensional challenges.

### 3.3 Computation of PCE Coefficients

Polynomial Chaos methods present two fundamental pathways for deriving expansion coefficients, i.e. Intrusive and Non-Intrusive Polynomial Chaos. The Intrusive Polynomial Chaos paradigm establishes strong links with Stochastic Finite Element methods [63]. In this approach, model equations undergo discretization in both design and probability spaces, and coefficients emerge through Galerkin projection [64]. While offering precision, this method often necessitates the creation of custom solvers. Consequently, its utility diminishes in complex scenarios where existing deterministic codes are at hand. This challenge becomes particularly pronounced in multi-physics scenarios, where simulation routines can be resource intensive. On the contrary, Non-Intrusive Polynomial Chaos (NIPC) emerges as a versatile alternative. It circumvents the need for new discretized equations by leveraging established responses at discrete points within the probability space. Deterministic evaluations unfold at these designated points, allowing seamless integration of existing external solvers in a black-box fashion. This approach not only enhances computational efficiency but also allows to use deterministic solvers.

Numerous strategies have been explored to ensure accurate computation of Polynomial Chaos Expansion (PCE) coefficients [65]. Spectral projection involves projection onto basis elements to enforce orthogonality. Conversely, the quadrature-based (collocation) technique relies on a one-dimensional quadrature rule, often following a Gaussian distribution. In tackling the challenge posed by high dimensions, sparse quadrature emerges as a promising alternative. This methodology replaces full-tensor quadrature with lower-order rules, enhancing scalability. Moreover, various methodologies have been devised, including sampling-based, oversampling, gradient-enhanced polynomial chaos, and sub-sampled points approaches [66]. However, these strategies primarily focus on approximating expectations or integrals, which limit their applicability. In response to the limitations of projection-based methods, the regression-based approach, specifically employing the Least Squares method, has gained prominence. This method utilizes normal variates $\xi$ as coordinates. The ensuing deterministic coefficients govern the behavior of the regression-based Least Squares surrogate. This surrogate approach closely mirrors the statistical regression of the exact solution within the Polynomial Chaos basis.

For this research, the selection of the Least Squares approximation is considered, aligning it with the specific characteristics of the problem. Further insights into this methodology are explored in the following section.

## 3.4 PCE-KL Expansion

In time-dependent reliability assessment through simulation, a pivotal challenge lies in devising efficient methodologies capable of generating sample functions[67]. This task is considerably more sophisticated than simulating mere random variables, as the sample functions must obey a provided covariance function, all while ensuring accuracy compared to the target marginal distribution. The term “characterization” within the context of a stochastic process indicates the development of a stochastic metamodel that generates trajectories, or time series, of the process under consideration. Each trajectory undergoes cycle counting, and the Miner's rule model is employed to estimate the damage of the pertinent realization of the random process. For stationary and Gaussian processes, several techniques, including the Karhunen Loeve (K-L) expansion [20], the Shinozuka method [17-18], the Expansion Optimal Linear Estimation method (EOLE) [4], or the Orthogonal Series Expansion (OSE) [22], have been proposed for characterizing the process in the time domain. However, for a non-Gaussian process, the process characterization becomes notably intricate. In 2005, Phoon et al. [68] proposed the utilization of the Karhunen–Loeve (K–L) expansion with non-Gaussian random variables. The main feature of this technique resides in its ability to uphold the target covariance function while iteratively updating the probability distributions of the K–L random variables. This approach provides significant appeal due to its seamless extension to non-stationary and multi-dimensional domains in a comprehensive manner. Computational insights highlight that, in practice, simulation time is predominantly governed by the number of K-L terms [69]. In the context of a stationary and non-Gaussian process, a Polynomial Chaos Expansion – Karhunen-Loeve expansion (PCE-KL) approach is very attractive. This approach uses a target first-order marginal Probability Density Function (PDF) and a target second-order correlation function[70]. The process marginal PDF is expressed as a series of Hermite polynomials of the standard normal random variable $\xi$. This series is then temporally extended to represent the process in terms of Hermite polynomials associated with a standard normal process $\xi(t)$. Subsequently, the Karhunen-Loeve (KL) expansion is employed to represent $\xi(t)$ as a composition of uncorrelated standard normal variables. Thus, this method encapsulates a non-Gaussian process using independent standard normal random variables. In the estimation of a normal or non-normal random variable $Z$, one-dimensional Hermite polynomials $\Psi_i$ of standard normal random variables ξ are used. The expression for Z takes the form of a summation involving these polynomials, with coefficients $b_i$ as shown below

$$Z = \sum_{i=0} b_i \Psi_i(\xi) = b_0 + b_1\xi + b_2(\xi^2 - 1) + b_3(\xi^3 - 3\xi)$$
$$+b_4(\xi^4 - 6\xi^2 + 3) + (b_5\xi^5 - 10\xi^3 + 15\xi) + b_6(\xi^6 - 15\xi^4 + 45(\xi)^2 - 15) \dots\dots \quad (3.1)$$

The Hermite polynomials $\Psi_i$ are defined as $\Psi_i(\xi) = (-1)^i \frac{\varphi^{(i)}(\xi)}{\varphi(\xi)}$ where $\varphi^{(i)}(\xi)$ is the ith derivative of the standard normal PDF $\varphi(\xi)$. This combination of ideas and advanced math comes together to create a complete system that helps us understand and simulate processes that change over time. This system handles tricky aspects like how things relate to each other (covariance), how values are spread out (distribution), and unusual patterns (non-Gaussian behavior). This makes it easier for us to study and analyze these processes in a strong and meaningful way.

## 3.5 Non-Gaussian Process Characterization Using PCE-KL

In [31], a sampling-based approach was employed to directly estimate the expectation outlined in equation for each term within the expansion. This involved computing the mean of products over a designated number of sampled points. A common selection in this context is Monte Carlo Simulation (MCS), which usually validates the accuracy of non-sampling methodologies. MCS presents advantages concerning the dimensionality of the problem, as its convergence properties remain unaffected by the number of dimensions engaged. This particular attribute positions MCS as a viable option for generating reference values against which other methods can be assessed. Building upon prior research [69], more efficient sampling techniques are also introduced, such as Quasi-Monte Carlo sampling (QMC) and Optimal Latin Hypercube sampling (OLHS) [31,68]. However, these techniques tend to be computationally demanding for non-linear systems. Consequently, their application is preferably reserved for validation purposes [70]. In contrast to the sampling-based methodologies, which focus on approximating expectations or integrals, we use in this work a regression-based technique to construct a surrogate model of a non-Gaussian process using Polynomial Chaos Expansion (PCE) [52,68]. The non-Gaussian process is defined by a non-Gaussian marginal PDF (or equivalently CDF) and an autocorrelation function which can be obtained by a provided PSD. The latter provides the correlation structure. The steps to generate a non-Gaussian process using PCE are provided below [71].

First, a random sample $x_i$ from a known distribution with a CDF $F_X(x)$ is obtained. A random number $b_i$ between 0 and 1 is generated so that $x_i$ is obtained as

$$x_i = F_X^{-1}(b_i) \tag{3.2}$$

Thus, if

$$Z(z) = \varphi(\xi) = b_i \text{ from } [0,1] \tag{3.3}$$

then

$$\xi = \varphi^{-1}(b_i) \tag{3.4}$$

and

$$z = Z^{-1}(b_i) \tag{3.5}$$

If $N_s$ pairs of $\xi$ and $z$ are generated using Equations (3.4) and (3.5) where $N_s$ is much larger than the number $P$ of $\Psi$ terms in Equation (3.1), we have:

$$\begin{pmatrix} \Psi_0\left(\xi^{(0)}\right) & \Psi_1\left(\xi^{(0)}\right) & \dots & \Psi_P\left(\xi^{(0)}\right) \\ \Psi_0\left(\xi^{(1)}\right) & \Psi_1\left(\xi^{(1)}\right) & \dots & \Psi_P\left(\xi^{(1)}\right) \\ \vdots & \vdots & \ddots & \vdots \\ \Psi_0\left(\xi^{(N_s)}\right) & \Psi_1\left(\xi^{(N_s)}\right) & \dots & \Psi_P\left(\xi^{(N_s)}\right) \end{pmatrix} \begin{Bmatrix} b_0 \\ b_1 \\ \vdots \\ b_P \end{Bmatrix} = \begin{Bmatrix} Z\left(\xi^{(0)}\right) \\ Z\left(\xi^{(1)}\right) \\ \vdots \\ Z\left(\xi^{(N_s)}\right) \end{Bmatrix} \tag{3.6}$$

The system can be expressed in compact form as

$$\Psi * b = Z \tag{3.7}$$

where $\Psi$ is the so-called design matrix of size $N_s$ x $P$ and $b$ is the vector of size $P$ containing the unknown coefficients. To ensure accuracy in calculating $b$, $N_s \gg P$ resulting in an over-determined system of equations in (3.6). Then $b$ can be obtained as a least-squares approximation using the Moore-Penrose (or pseudoinverse) as

$$b \approx \left(\Psi^T \Psi\right)^{-1} \Psi^T Z \tag{3.8}$$

In this research, we found that using only 6 terms in b provides good accuracy, i.e. Equation (3.6) follows the provided marginal distribution $F_X(x)$ and the provided autocorrelation function.

Using the orthogonality properties of the Hermite polynomials, the covariance $C_{ZZ}(t_1, t_2)$ of $Z(t)$ between times $t_1$and $t_2$is equal to

$$C_{ZZ}(t_1, t_2) = \sum_{i=1} b_i(t_1) b_i(t_2) \cdot (i!) \cdot \left(E[\xi(t_1)\xi(t_2)]\right)^i \tag{3.9}$$

For a given $C_{ZZ}(t_1, t_2)$, Equation (3.9) is used to calculate the covariance matrix $C_{\xi\xi}(t_1, t_2) = E[\xi(t_1)\xi(t_2)]$ of $\xi(t)$. Based on $C_{\xi\xi}(t_1, t_2)$, a Karhunen-Loeve (K-L) expansion [67] is used to express $\xi(t)$ in terms of independent standard normal variables $\xi_i, i = 0,1,2, \dots, N$ as:

$$\xi(t) = \sum_{i=1}^{N} \sqrt{\lambda_i} \cdot f_i(t) \cdot \xi_i \tag{3.10}$$

where $\lambda_i$ and $f_i(t)$ are the eigenvalues and eigenvectors of $C_{\xi\xi}(t_1, t_2)$. If Equation (3.10) is substituted in Equation (3.1), a series expansion of $Z(t)$ in terms of the independent standard normal variables $\xi_i$ can be obtained. This series expansion is used to create trajectories (sample functions) of the non-stationary and/or non-gaussian process $Z(t)$ by sampling the $N$ random variables $\xi_i, i = 1,2, \dots, N$.

# CHAPTER FOUR

# SIMULATION-BASED FATIGUE LIFE ESTIMATION METHOD FOR NONLINEAR SYSTEMS UNDER NON-GAUSSIAN LOADS

## 4.1 Introduction

This Chapter introduces an innovative framework for analyzing the fatigue behavior of linear or non-linear systems subject to non-Gaussian input processes [73-77]. Details on the developed framework are provided in Sections 4.2 and 4.3. Section 4.4 uses a nonlinear Duffing oscillator example to demonstrate all developments.

## 4.2 Proposed Methodology: A Simulation-based Fatigue Life Estimation

Figure 4.1 provides a schematic of a nonlinear vibratory system with random parameters $\boldsymbol{Y}$ excited by a non-Gaussian process $F(t)$. The response of the system is a non-Gaussian process $X(t)$ even if the input process $F(t)$ is Gaussian.


Figure 4.1 Schematic of input–output notation

The characterization of the input random process $F(t)$ is obtained using one or more provided time trajectories. If the process is assumed ergodic, a single trajectory is sufficient. However, if ergodicity is not assumed, a small number of trajectories, say 10-

50, is required. The non-Gaussian Karhunen-Loeve expansion (NG-KLE) method is employed to characterize $F(t)$ using its non-Gaussian marginal distribution and autocorrelation function. This allows us to generate multiple excitation time trajectories which are then used to obtain the corresponding response trajectories using time integration of the system equations of motion.

Below we describe the steps to estimate the fatigue life.

**Step 1:** Characterization of Input Random Process *F(t)*

This is carried out either by providing a marginal PDF and an autocorrelation function or by using a number of provided time trajectories to estimate the marginal PDF and the autocorrelation function. In the latter case, an empirical marginal PDF is first calculated and then a PCE approach is employed to estimate the process marginal PDF. The autocorrelation function is calculated by estimating a second-order statistical moment using the provided trajectories. Subsequently the newly developed non-Gaussian KLE (NG-KLE) method is used to generate multiple trajectories of the input process.

**Step 2:** Computation of System Output Trajectories

For each generated excitation (input) time trajectory, the system equations of motion are time integrated to obtain the corresponding output trajectory. For this task, a finite element model may be used for complex geometries. This step constitutes the most computationally expensive task. For this reason, we obtain the output trajectories for a relatively short time horizon (i.e. 10-20 correlation lengths) and use these trajectories to characterize the output process. Then the NG-KLE approach is used to generate trajectories of longer duration (i.e. 100-150 correlation lengths) similarly to the input process characterization.

**Step 3:** Estimation of Fatigue Life

After we have obtained output stress trajectories of long duration from Step 2, we employ either the total probability theorem approach (Section 4.3.2) or the PDF of peak stresses approach (Section 4.3.3) to estimate the fatigue life.

## 4.3 Estimation of Fatigue Life

To predict the fatigue life of a system, we use the system's stress output process as input to a fatigue model as illustrated in Figure 4.2. The estimation of the system's lifespan is achieved using three distinct approaches – the damage accumulation approach, the total probability theorem approach, and the PDF of peak stresses approach as shown in Figure 4.3.

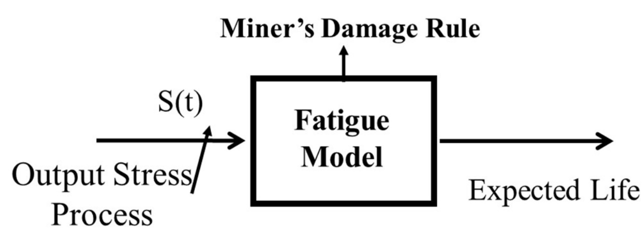


Figure 4.2 Schematic of fatigue model

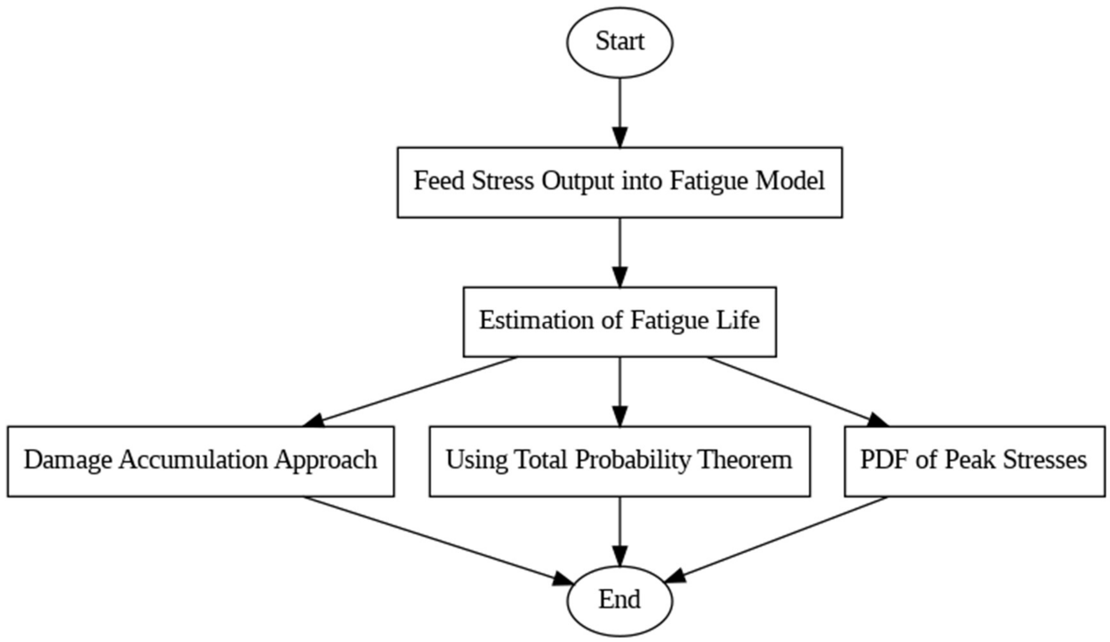


Figure 4.3 Approaches to estimate fatigue life

### 4.3.1 Damage Accumulation Approach

The damage accumulation approach is commonly used in the industry due to its simplicity. It uses only a single stress signal of duration $T_{max}$. The signal is rain-flow counted to obtain the damage *D* which is commonly much less than 1. The latter is a value which signifies fatigue failure. The life $E_{life}$ for a total damage *D* = 1 is then estimated as

$$E_{life} = \frac{1}{D} * T_{max} \tag{4.1}$$

This approach assumes that the stress signal of duration $T_{max}$ is repeated until the total damage reaches the value of 1. This is a very unrealistic assumption, but its simplicity has made it popular. The method may oversimplify the real-world behavior of materials, especially in cases where the stress history is complex and non-linear.

4.3.2 Total Probability Theorem Approach

The second approach for estimating the expected fatigue life is based on the total probability theorem. The Total Probability Theorem states that the duration of the process (or operation) should be a multiple of the maximum time duration of each stress trajectory [68,77], denoted as $T_{max}$ . Specifically, it is represented as $m * T_{max}$. This theorem is significant in fatigue analysis as it links the cumulative damage experienced by the system with the operation's duration.

Let $D_i, i = 1,2, \dots, N$ represent the damage of the $i$-th stress trajectory of duration $T$ (see Figure 4.6). Since *D* is a random variable, $D_i, i = 1,2, \dots, N$ is a realization of this random variable. The total probability theorem states that the mean value $D_{mean}$ of *D* is given as

$$D_{mean} = \frac{1}{N} \sum_{i=1}^{N} D_i \tag{4.2}$$

Therefore, the expected life $E_{life}$ for a total damage *D* = 1 is

$$E_{life} = \frac{1}{D_{mean}} * T_{max} \tag{4.3}$$

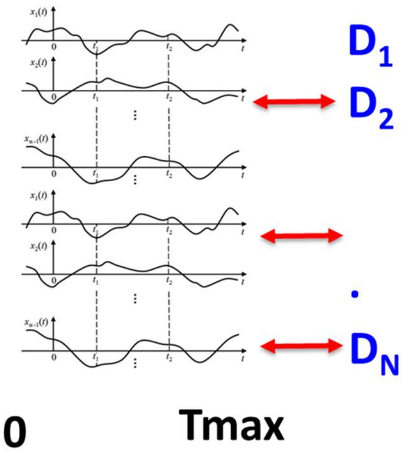


Figure 4.4 Damage for each of $N$ stress trajectories [106].

4.3.3 Estimation of Fatigue Life using PDF of Peak Stresses of Fully Reversed Cycles

This developed approach to estimate fatigue life is complementary to the total probability theorem approach of Section 4.3.2. It uses the PDF of peak stresses for fully reversed cycles. Each of the generated trajectories of the output stress process is rain-flow counted to identify each damage cycle which is then mean-stress corrected to obtain the corresponding fully reversed amplitude $S_{ar}$ as shown in Figure 4.7. The histogram of all samples of the fully reversed amplitudes is then obtained. Figure 4.8 shows a representative example. Note that the PDF of $S_{ar}$ can be easily obtained from the histogram. It is critical to mention that the PDF of fully reversed amplitudes allows us to calculate the expected fatigue damage $D$ using Equation (4.4) which holds for narrow-band processes. This PDF is also known as the PDF of peak stresses for a narrow-band process.

$$D = \frac{n}{A}\int_{0}^{\infty} S_m\, f_s(s) ds \tag{4.4}$$

In this equation, $n$ is the number of damage cycles, $A$ is provided from the S-N curve, $s$ represents the stress level, and $f_s(s)$ denotes the probability density function of peak stresses.

The mean-stress correction we use in this study follows the Morrow model (Eq. 4.5) which adjusts the stress amplitude to account for the mean-stress effect

$$S_{ar} = \frac{S_a}{1 - \left(\frac{S_m}{S'_f}\right)} \tag{4.5}$$

where $s'_f$ is fatigue strength coefficient, $S_m$ is the mean stress and $S_a$ is the stress amplitude. Other mean-stress correction models can also be used.

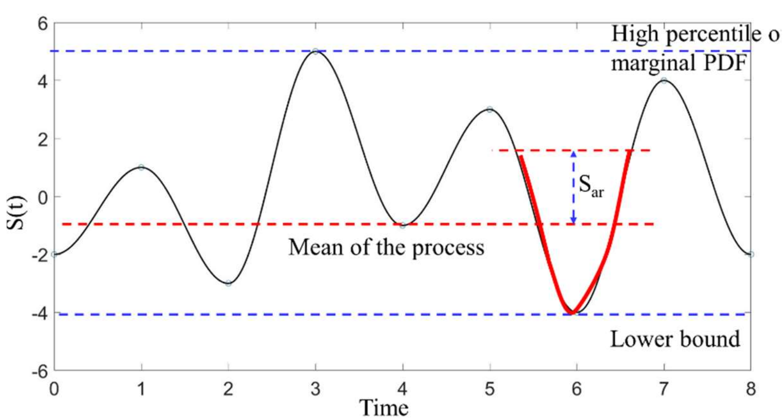


Figure 4.5 Explanation of fully reversed amplitude $S_{ar}$

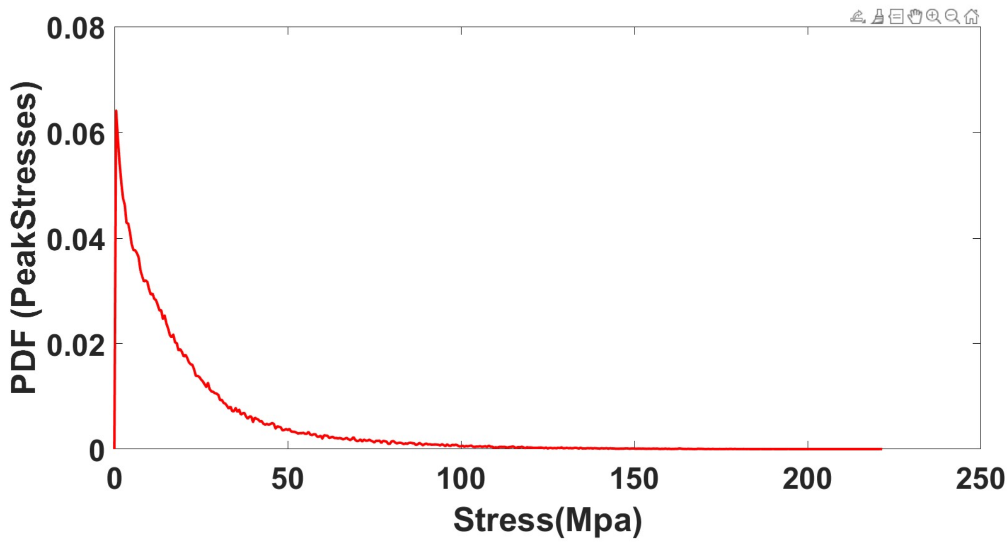


Figure 4.6 Histogram of fully reversed amplitudes $S_{ar}$

The total number $n$ of damage cycles in Equation (4.4) is calculated for a large number of trajectories $N_{traj}$ (e.g. 2000) of the output stress process during rain-flow counting to identify the damage cycles. The number of cycles per hour is then equal to

$$N_{cycle} = n * \frac{3600}{N_{traj} * T_{max}} \tag{4.6}$$

where $T_{max}$ is the duration of each stress trajectory in seconds. Finally, the damage $D$ per hour is computed as

$$D = \left(\frac{N_{cycle}}{A}\right) \int_0^\infty s^m f_s(s) ds \tag{4.7}$$

and the expected life in hours is

$$E_{Life} = \frac{1}{D} \tag{4.8}$$

This approach accommodates both wide-band and narrow-band processes, as the PDF of peak stresses $fs(s)$ pertains to fully reversed cycles (i.e. cycles after a mean-stress correction). It is also accurate for both Gaussian and non-Gaussian processes.

Creating long stress trajectories is essential when working with the PDF (Probability Density Function) of peak stresses for a few key reasons. To accurately represent this PDF, we need many stress peak samples, which means simulating lots of loading cycles and long stress histories. These peaks are the highest points in the stress data, and you need long stress data to find enough of them for accurate statistics. Peaks can be irregular, and they don't happen all the time, so longer stress data helps ensure we catch these infrequent high points. Some of these high peaks can be rare but very important for fatigue analysis, and longer data helps include them. Short data might miss important peaks and lead to an incomplete or biased PDF. In summary, using long stress data ensures we have enough peaks for an accurate distribution and better statistics.

## 4.4. Duffing Oscillator Example

The application of the proposed methodology is demonstrated using a Duffing oscillator, a single Degree-of-Freedom (DOF) vibratory system (Figure 4.7) known for its complex nonlinear behavior [31,77,91].

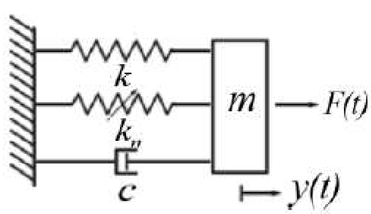


Figure 4.7 Schematic of Duffing oscillator [99].

The equation of motion

$$m\ddot{y}(t) + c\dot{y}(t) + ky(t) + k_n y^3(t) = F(t) \tag{4.9}$$

includes a nonlinear stiffness term $k_n y^3(t)$. The system parameters include a mass $m$ of 25 kg, and a linear damping and spring coefficient of $c = 15 kg/s$ and $k = 100\ N/m$, respectively. The nonlinear stiffness is $k_n = 1000 * k$. The undamped natural frequency is $\omega_n = \sqrt{\frac{k}{m}} = 2\ rad/s$ and the damping factor $\zeta = \frac{c}{2m\omega_n} = 0.15$. The linear spring $k$ is a coil spring whose stiffness is provided by

$$k = \frac{Gd}{8NC^3} \tag{4.10}$$

The dynamic response of the system is first calculated in order to determine the deflection $y(t)$ of the spring. The dynamic component of the shear stress is then estimated as

$$\tau = K_w \frac{8Dky(t)}{\pi d^3} \text{ where } K_w = \frac{4C-1}{4C-4} + \frac{0.615}{C}. \tag{4.11}$$

The static shear stress $\tau_m$ not considered in obtaining the total stress $\tau$. Equation (4.11) uses the Wahl factor $K_w$ to account for the stress increase on the spring wire due to spring curvature. $K_w$ is a function of the spring index $C$ [77,80]. Table 4.1 provides all pertinent data for the coil spring.

Table 4.1 Coil spring parameters

| Quantity | Value (Units) |
|---|---|
| Wire diameter, $d$ | 1.91cm |
| Number of active turns | 10 |
| Coil diameter, $D$ | 15cm |
| Ultimate Stress, $S_{ut}$ | 1240 Mpa |
| Endurance limit, $S_f$ | 558 Mpa |
| Shear Modulus, $G$ | 81 Gpa |
| Spring Index, $C = D/d$ | 7.85 |

4.4.1 Generation of Non-Gaussian Excitation Processes

To demonstrate the simulation-based approach a stationary, we use two types of stationary excitation (input). A Gaussian and a non-Gaussian random process $F(t)$ is used having the same mean of 500 N, a standard deviation of 300 N and an exponential autocorrelation function with λ = 2 according to ISO 8608 standard [76] (Eq. 4.12). A Weibull marginal PDF is used

$$f_F(f) = \frac{b}{a}\left(\frac{f}{a}\right)^{b-1} e^{-\left(\frac{f}{a}\right)^a}, \qquad f \geq 0 \tag{4.12}$$

where $a = 5$ and $b = 1.2$ are the scale and shape parameters, for which the mean, standard deviation, skewness coefficient and kurtosis coefficient are $\mu_F = 500$, $\sigma_F =$

300, $Sk_F = E[(f-\mu_F)^3]/\sigma_F^3 = 0.85$ and $Ku_F = E[(f-\mu_F)^4]/\sigma_F^4$ =3.7, respectively. Figure 4.8 shows the Weibull PDF and a normal PDF with the same mean and standard deviation for comparison purposes.

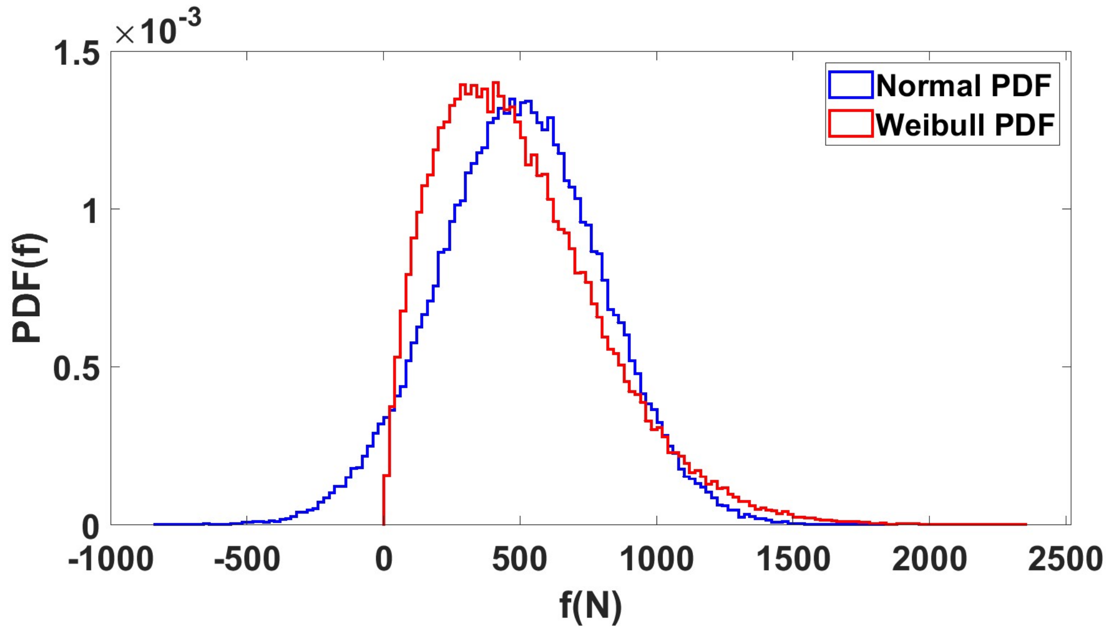


Figure 4.8 Marginal PDF for normal and Weibull distribution

The autocorrelation coefficient of $F(t)$ representing an exponential decay is

$$\rho_{FF}(\tau) = e^{-(\tau*\lambda)} \tag{4.13}$$

where $\tau$ is the relative time and λ = 2. Figure 4.9 shows the $\rho_{FF}(\tau)$ indicating that the correlation length of the input process is approximately equal to $\tau_F^{cor}$= 6sec. The autocorrelation function $R(\tau)$ is the inverse Fourier transform of the spectrum. Normalizing $R(\tau)$ by the corresponding variance $\sigma^2 = R(\tau = 0) = 0.001m^2$, provides the autocorrelation coefficient function $\rho_{FF}(\tau) = \rho_{FF}(t, t+\tau)$.

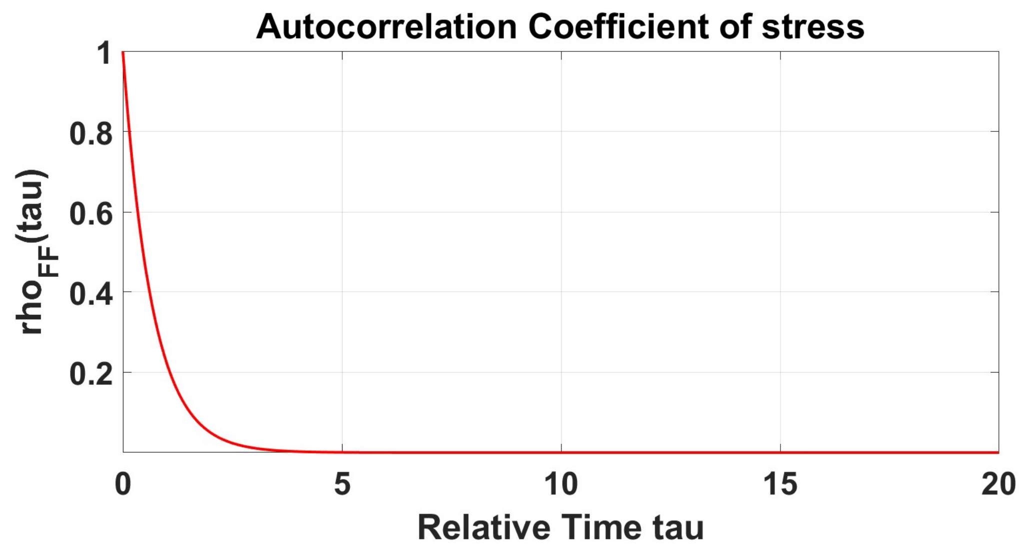


Figure 4.9 Autocorrelation coefficient of input random process

Using a time discretization $dt = 0.01$ sec for the $0 \leq t \leq 140$ sec time of interest, the covariance matrix of the covariance matrix $C_{FF}(t_i, t_j), i, j = 1, \dots, 2001$ of the input process was formed. Based on $C_{FF}(t_i, t_j)$, the covariance matrix $C_{\xi\xi}(t_i, t_j) = E[\xi(t_i)\xi(t_j)]$ of the Gaussian process $\xi(t)$ of PCE was calculated. Figure 4.11 shows the eigenvalues of $C_{\xi\xi}(t_i, t_j)$ if a normal or Weibull marginal PDF is used. For an accurate KLE, the first dominant eigenvalues were kept so that the ratio of the lowest ($100^{\text{th}}$) to the highest (1st) eigenvalue is less than 1%. Thus, the series expansion of the input process $F(t)$ uses 1167 and 650 independent standard normal variables $\xi_i$ for Nomal and Weibull.

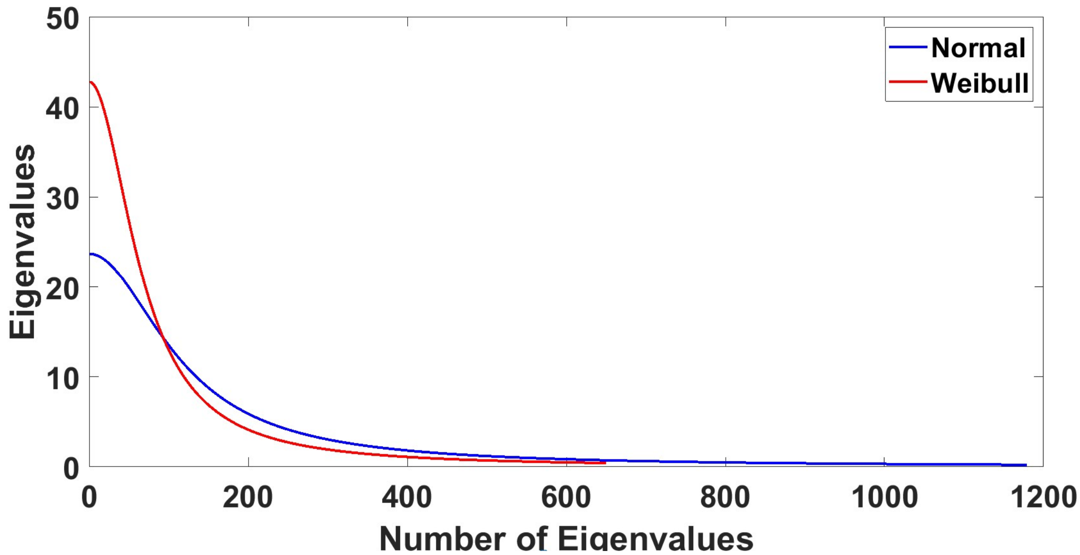


Figure 4.10 Number of eigenvalues of covariance matrix for a normal or Weibull marginal PDF

The $b$ coefficients of the PCE were calculated using Section 3.5. Table 4.2 shows their values for both the Gaussian and the non-Gaussian case. A KL expansion was then performed to generate trajectories of the stationary, non-Gaussian process $F(t)$ by sampling the standard normal variables $\xi_i, i = 1,2, \dots ,100$. Figure 4.11 show a few trajectories of Gaussian and the non-Gaussian trajectories of $F(t)$. Note that the instantaneous force $F(t)$ is greater or equal to zero for the non-Gaussian trajectories because the Weibull marginal PDF is defined only for $f \geq 0$. In contrast, the Gaussian trajectories can have negative values.

Table 4.2 Statistics for the target Input trajectories

| Quantity | Gaussian | Non - Gaussian |
|---|---|---|
| Mean | 500 | 500 |
| Standard Deviation | 300 | 300 |
| Skewness | 0 | 0.8 |
| Kurtosis | 3 | 3.70 |

Table 4.3 '*b*' coefficients for PCE

| Quantity | Gaussian | Non - Gaussian |
|---|---|---|
| $b_0$ | 501.345 | 499.91 |
| $b_1$ | 299.87 | 297.546 |
| $b_2$ | 0.0456 | 0.843 |
| $b_3$ | -0.022534 | -0.024325 |
| $b_4$ | -0.00212 | -0.002432 |
| $b_5$ | 0.0003532 | 0.00034234 |

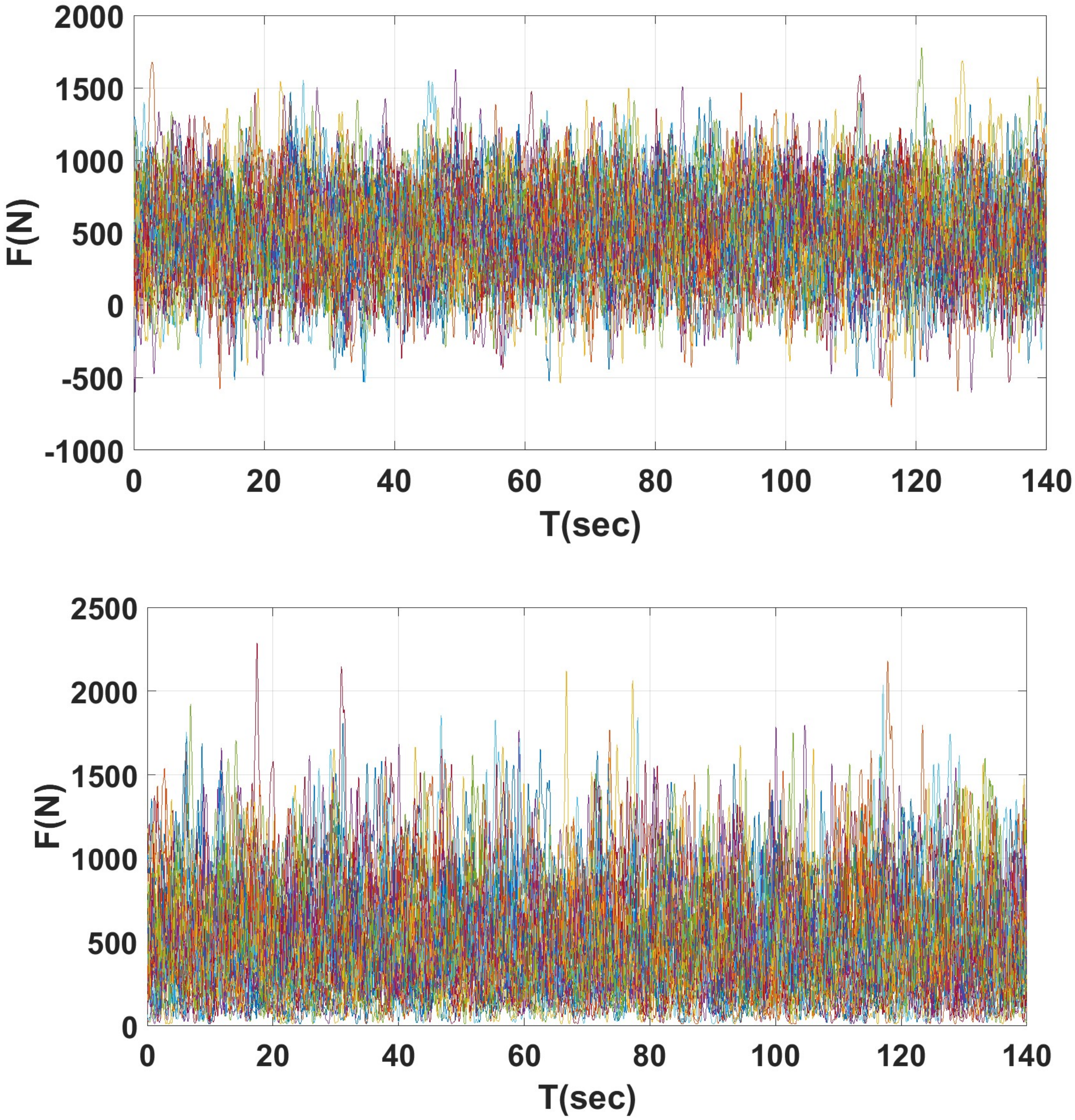


Figure 4.11 Random trajectories for (a) Gaussian (Normal) and (b) Non -Gaussian (Weibull) marginal distribution for $0 \leq T \leq 140$ sec

To demonstrate the accuracy of the proposed methodology in estimating the marginal PDF's Figure 4.12 shows that both estimated PDFs regenerated from the 2000 trajectories are very close to the exact normal and Weibull marginal PDFs even at the right rail which is important for fatigue life estimation. Figure 4.13 also shows that the autocorrelation coefficient of the input process is estimated very accurately. Finally, Table 4.4 shows that the estimated mean, standard deviation, and skewness and kurtosis coefficients are very close to the target values.

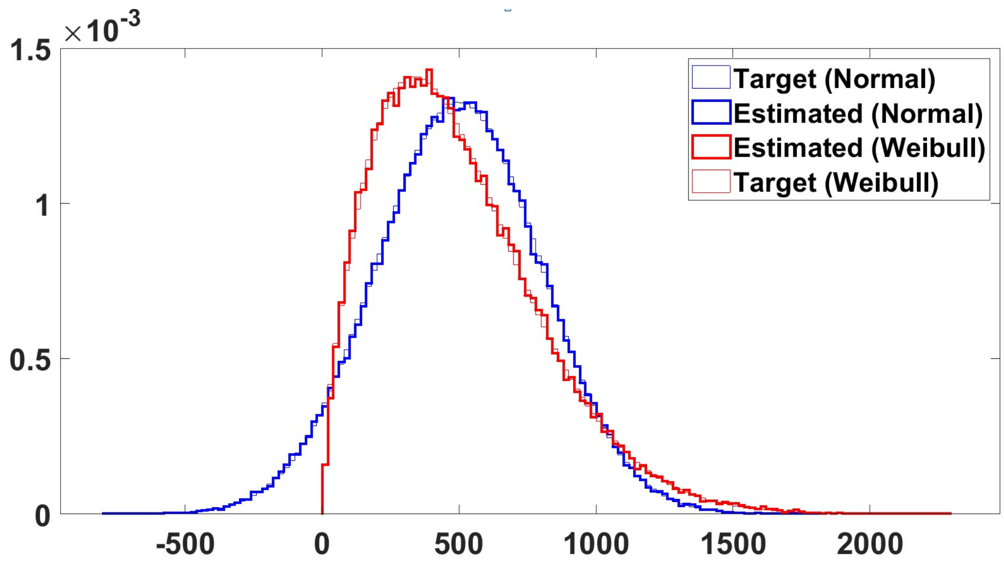


Figure 4.12 Accuracy of PCE estimated marginal PDF vs target marginal PDF

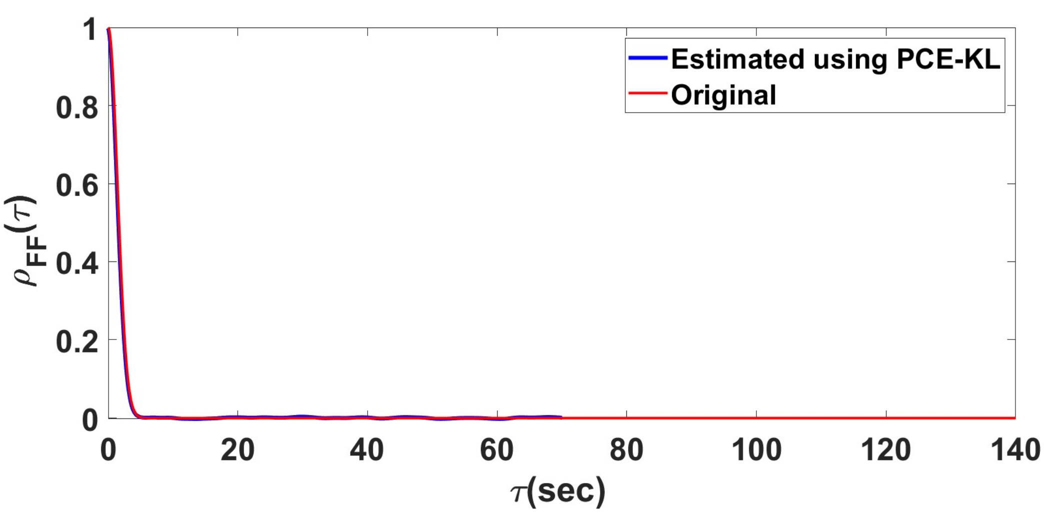


Figure 4.13 Estimated autocorrelation coefficient using PCE-KL

Table 4.4 Statistical moments of input random process

| Quantity | Gaussian | Non - Gaussian |
|---|---|---|
| Mean | 502 | 498.5 |
| Standard Deviation | 299.7 | 297.5 |
| Skewness | 0.0025 | 0.89 |
| Kurtosis | 3.004 | 3.78 |

### 4.4.2 Output Stresses and Estimation of their Marginal PDF

After obtaining input force trajectories using the estimated marginal PDF and NG-KLE techniques, we evaluate the Duffing Oscillator system response for each random input signal to determine the corresponding output stress signal. Figure 4.14 shows these output stress signals, which are obtained by solving the vibratory equation of motion of the duffing oscillator.

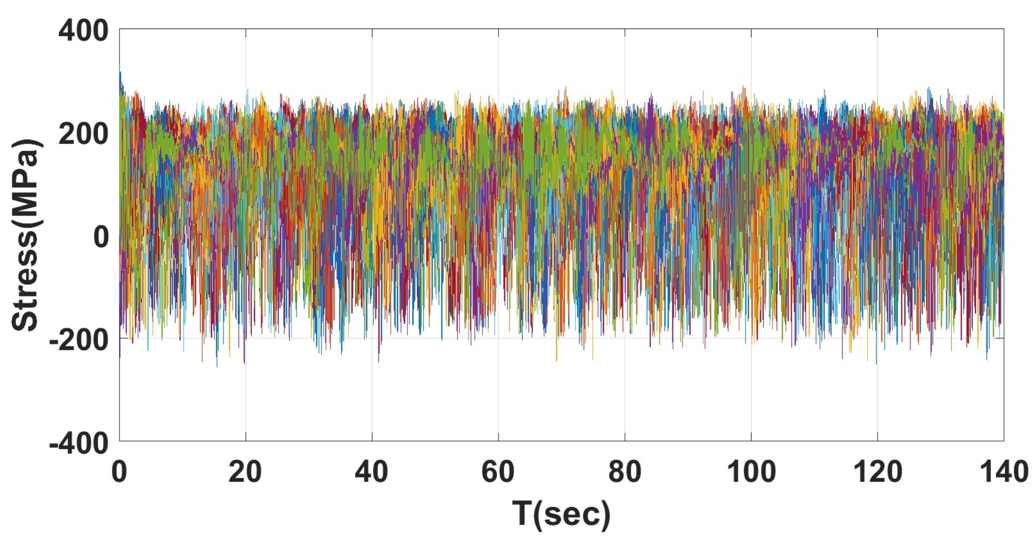

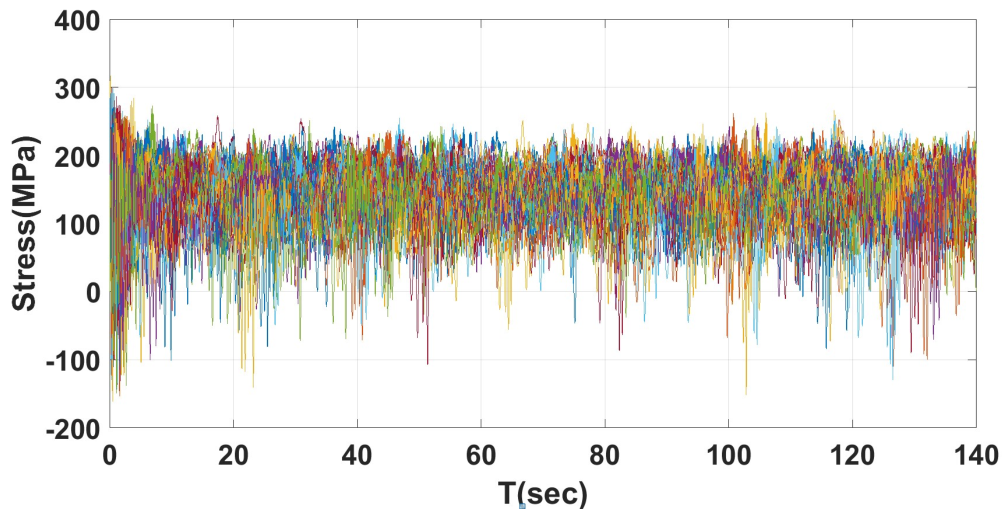


Figure 4.14 Output stresses for duffing oscillator a) Normal b) Weibull

Table 4.5 Statistical moments of output stress process

| Output Stresses | Non-Gaussian (Normal) | Non - Gaussian (Weibull) |
|---|---|---|
| Mean | 130.55 | 144.70 |
| Standard Deviation | 72.71 | 37.8 |
| Skewness | -1.73 | -0.93 |
| Kurtosis | 6.57 | 5.254 |

It should be noted that despite using a Gaussian input process, the nonlinear nature of the system produces a significantly non-Gaussian output stress process as shown in Figure 4.14. In our estimation, we exclude the response during the initial 20 seconds because it is influenced by arbitrary initial conditions. Figure 4.16 also shows the estimated output stress autocorrelation coefficient (blue line). The red line shows a smooth version which is used in order to reduce a potentially large variability of fatigue life prediction.

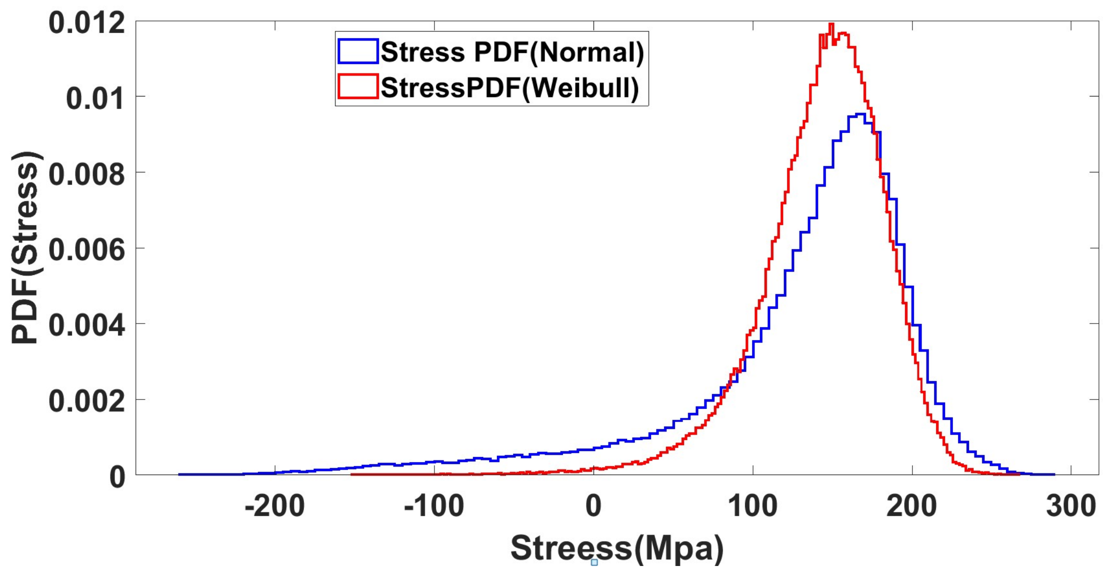


Figure 4.15 Estimated marginal PDF of output stress process.

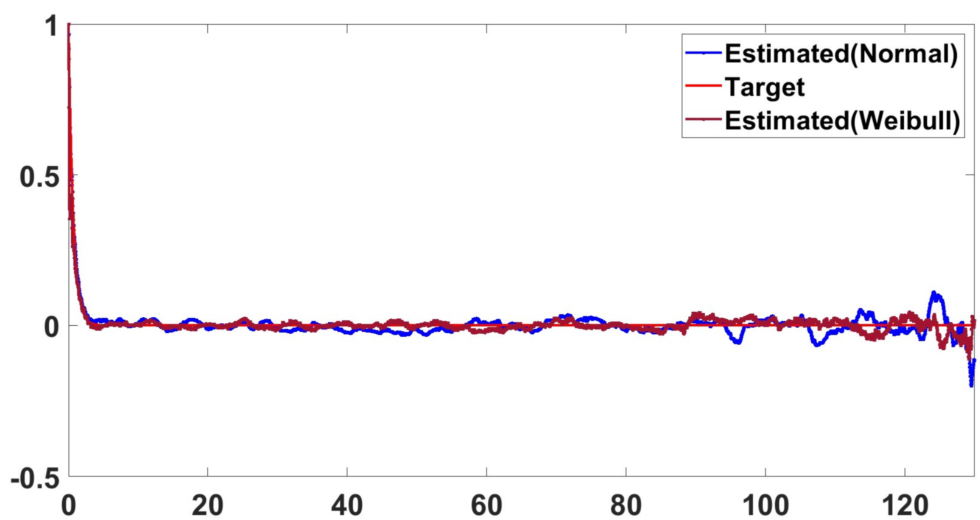


Figure 4.16 Estimated autocorrelation coefficient for output stress process for normal and Weibull marginal PDF

After successfully estimating the marginal PDF and autocorrelation function of the output stress, we employ the NG-KLE approach to generate multiple output trajectories of long duration. This reduces the computational cost of solving the equations of motion for longer durations. Figure 4.17 illustrates the generation of output stress signals using the normal marginal PDF for a duration of 240 seconds, as opposed to the original 140-second signal. The extended signal duration offers the advantage of improved accuracy in capturing cyclic loadings and high-stress cycles, which are critical for fatigue life calculations.

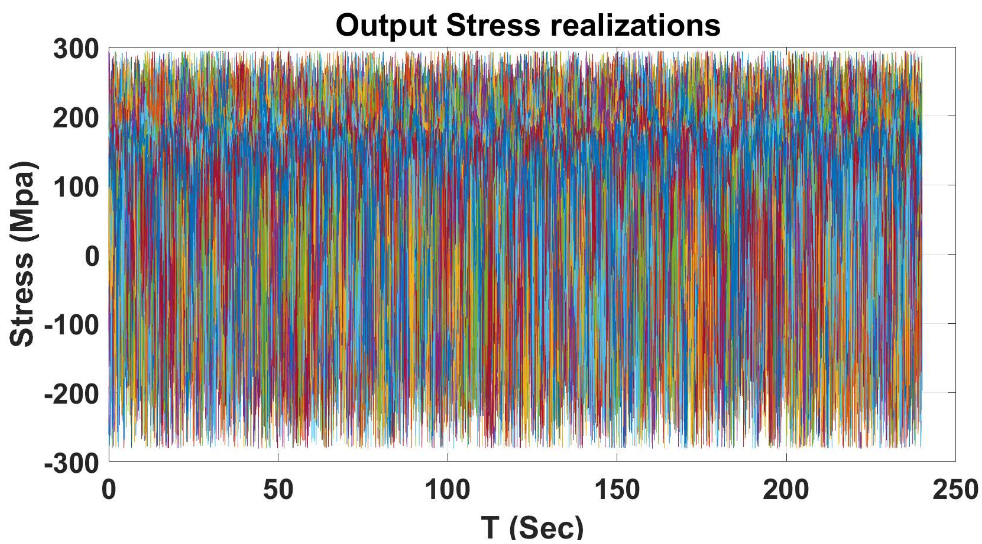


Figure 4.17 Output stress trajectories generated using NG-KLE for Normal

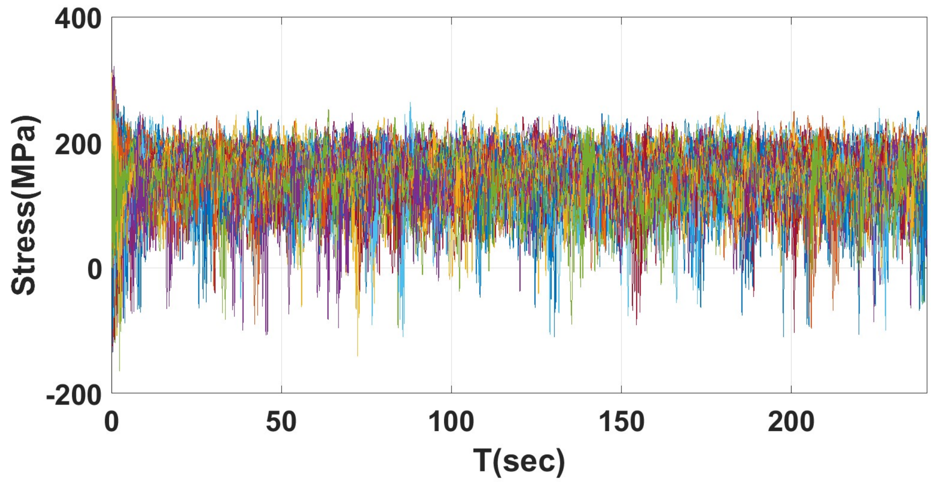


Figure 4.18 Output stress trajectories generated using NG-KLE for Weibull

We mentioned that the generation of longer output signals aids in reducing the computational cost of required system evaluations. However, the computational cost of generating these longer signals may increase, as more eigenvalues are needed in the Karhunen-Loève Expansion (KLE).

To ensure the accuracy of the generated output stress trajectories, we conducted a validation process by recalculating the marginal PDF of the stress output process. The purpose of this step was to verify that the PDFs we estimated from the generated stress data closely resembled the original ones. Figure 4.19 shows that our estimated stress PDF closely matches the original one for both the case i.e. Weibull and Normal for the duration of 240 secs. Figure 4.20 highlights the autocorrelation function for both the sample stresses generated for Normal and Weibull distribution.

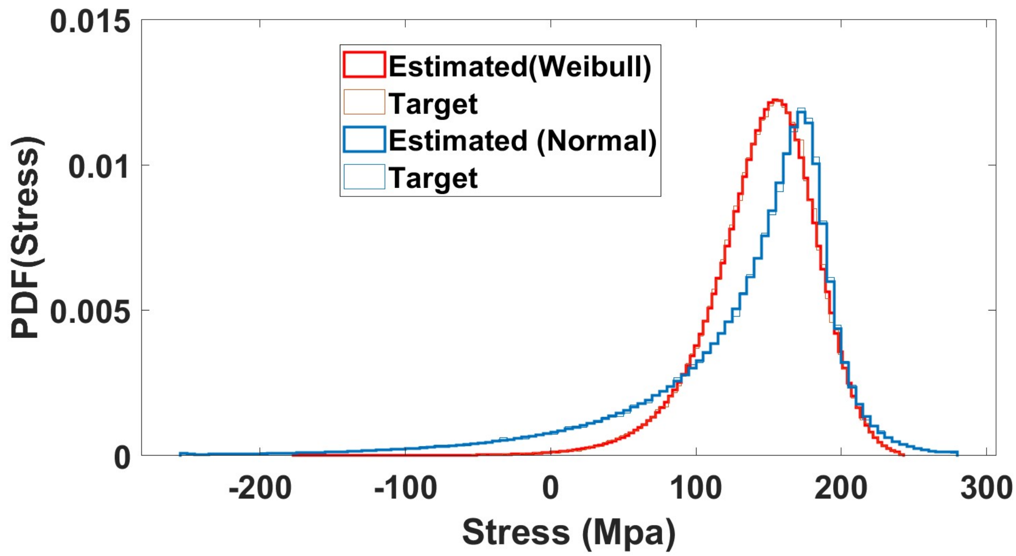


Figure 4.19 Accuracy of estimated output marginal PDF

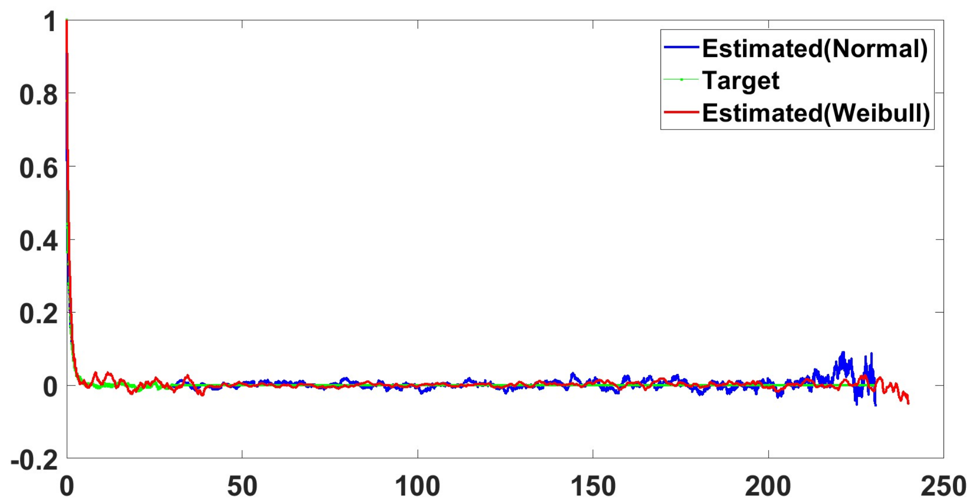


Figure 4.20 Accuracy of estimated autocorrelation function

4.4.3 Fatigue Life Estimation

Each of the generated shear stress trajectories is rain-flow counted to estimate the corresponding fatigue damage and therefore fatigue life. A large number of output stress trajectories was generated using a normal or Weibull marginal PDF. Figure 4.21(a) and (b) shows the histogram of the resulting damage from each output trajectory for the normal and Weibull marginal PDF. As expected the two histograms are very different indicating the importance of Gaussian or non-Gaussian case.

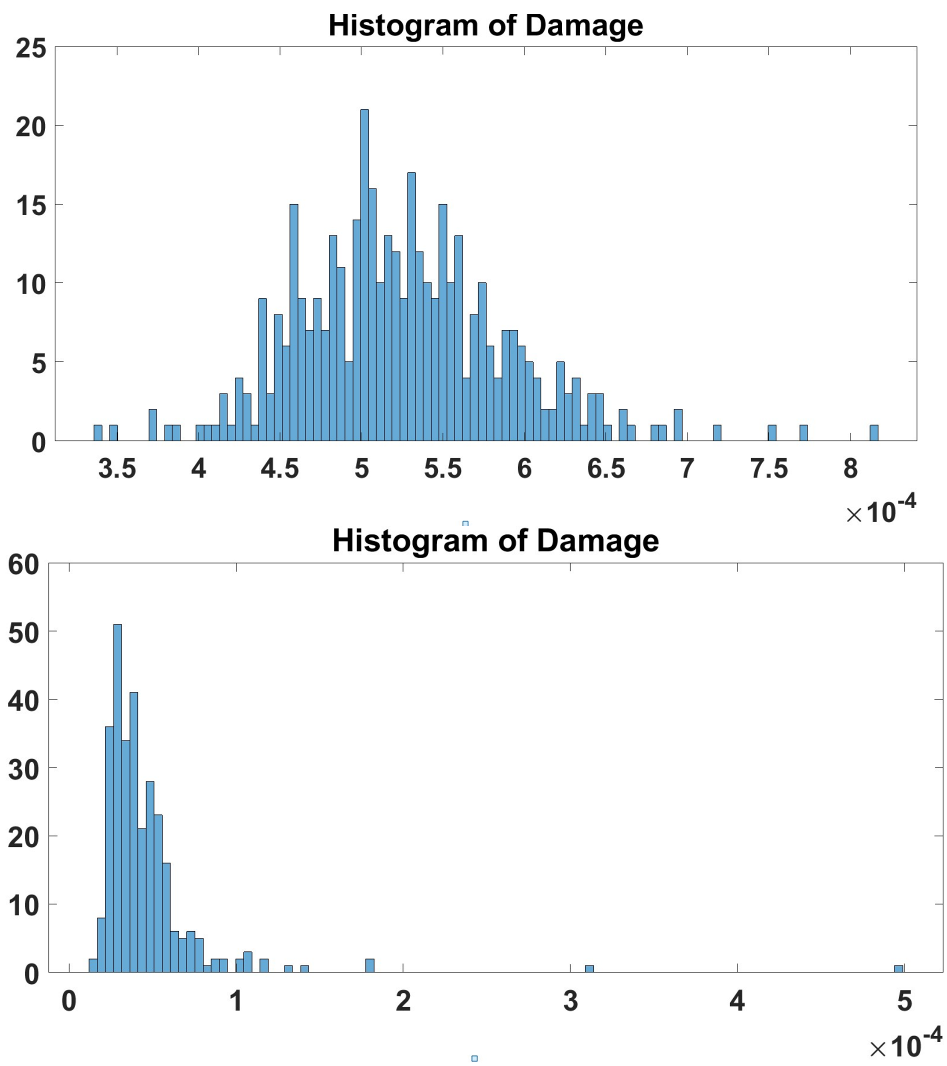

Figure 4.21 Histogram of damage for (a) Gaussian and (b) non-Gaussian marginal PDF

Figure 4.22(a) and (b) shows the histogram of the corresponding life for the Gaussian and the non-Gaussian case indicating large differences.

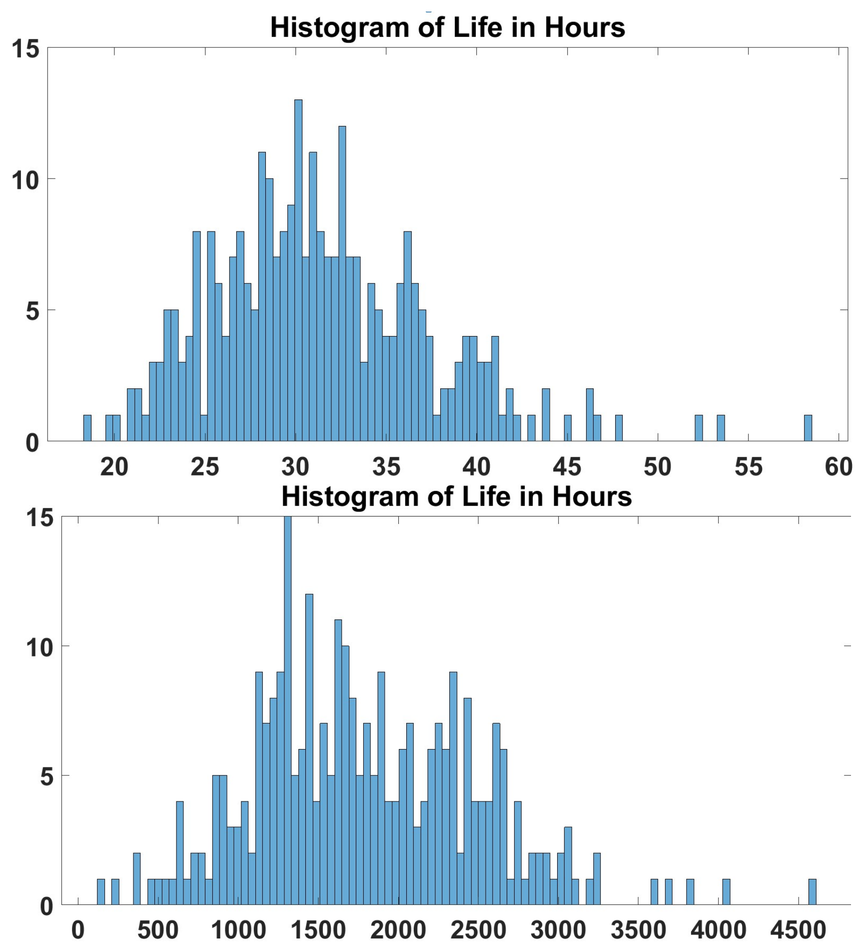


Figure 4.22 Histogram of life in hours for (a) Gaussian and (b) non-Gaussian marginal PDF

## 4.5 Summary

In this chapter, we introduced a simulation-based method for estimating the fatigue life of nonlinear vibratory systems subjected to both Gaussian and non-Gaussian excitations. Our approach, based on the NG-KLE methodology and PCE, efficiently characterizes stationary non-Gaussian processes defined by their marginal PDF and autocorrelation function. We improved the required computational efficiency by generating trajectories of long duration without solving the equations of motion for the entire long duration. To estimate fatigue life, we employed two methodologies: the total probability theorem approach and the PDF of peak stresses approach using fully reversed amplitudes. Both approaches use the Miner's linear damage model with a Morrow mean stress correction. The proposed methodology accommodates both Gaussian and non-Gaussian processes, whether narrow or wideband, ensuring accurate fatigue life predictions. We illustrated its effectiveness using a Duffing oscillator example, demonstrating the importance of accounting for non-Gaussian loading in estimating fatigue life.

CHAPTER FIVE

# A SUBDOMAIN APPROACH FOR LONG TIME HORIZON GAUSSIAN AND NON-GAUSSIAN RANDOM PROCESSES

## 5.1 Introduction

For many dynamic system applications, such as random linear and nonlinear vibrations, durability or fatigue, the system is excited by random loads represented by random processes. Their response (e.g. time-dependent stress) is required to assess durability, reliability or simply strength through time. For nonlinear problems, time trajectories of the input process are needed to calculate the corresponding output time trajectories. This operation, known as uncertainty propagation, is carried out for many trajectories to obtain accurate statistics of the output random process. Therefore, the input and output random processes must be characterized (i.e., generate time trajectories) in the time domain. For uncertainty propagation, a long-time horizon is commonly required for meaningful results.

Spectral decomposition methods are commonly employed to characterize a Gaussian random process. Many spectral decomposition methods have been developed including Borgman's method [16, 68], Shinozuka's method [17-18], Karhunen-Loeve expansion (KLE) [19,20,81] expansion and Expansion Optimal Linear Estimation. Among them, the KLE is often used mainly for Gaussian processes. However, it can also be used for non-Gaussian processes. It represents a random process as a weighted sum of uncorrelated eigenfunctions of the process covariance matrix. For a stationary process, the latter is formed if the process Power Spectral Density (PSD) is known.

The Borgman and Shinozuka spectral representation methods [16-20, 68] are based on the Fourier transform. The phase angles of all harmonics are treated as independent random variables[81]. The methods assume ergodicity in mean and autocorrelation so that the temporal and ensemble statistics for all sample trajectories are equal. The KLE method represents a random process as a weighted sum of uncorrelated eigenfunctions using a spectral decomposition of a covariance function. The EOLE method [22] is a variant of the KLE method.

Autoregressive time series models have been also used to represent a random process [82, 83] by assuming that a state depends linearly on previous states. The linear dependency coefficients are usually computed by maximizing a likelihood function. For a stationary process, the application of the KLE in a very large domain (time horizon) compared to the correlation length still remains unaffordable. For a given mean-square error, the number of needed terms in the KLE grows drastically with the size of the domain [84]. This presents two major challenges if trajectories of very long duration are needed. First, the size of the covariance matrix becomes very large especially if a small discretization step is used. As a result, the eigenvalue analysis of the covariance matrix to obtain its eigenvalues and eigenvectors may become very expensive. Second, in uncertainty propagation of nonlinear dynamic problems (or linear dynamic problems excited by non-Gaussian processes), a Quasi Monte Carlo (QMC) approach [32, 85] may be needed to make sure the input process trajectories cover the entire design space. This is necessary in order to increase the accuracy of the output process statistical moments without having to time integrate many input trajectories of long duration to calculate the corresponding output trajectories. The output statistical moments are used to estimate the marginal PDF and autocorrelation function (or equivalently PSD) of the output process [32]. A space filling set of input trajectories can be generated if the KLE random coefficients (the $\xi_i$ 's of Eq. 4) are space filled. This becomes practically impossible if there are hundreds of them due to the long duration of each trajectory.

This Chapter addresses the above two challenges by splitting the time horizon into a number of short subdomains of equal duration. The duration of each subdomain can be as short as the process correlation length. If shorter, the process correlation structure is not maintained. The aim is to generate trajectories of a random process using the KLE, if the time horizon is much longer than the process correlation length and a direct KLE is not computationally affordable [84, 85]. The spectral decomposition of the covariance matrix $\boldsymbol{\Sigma}$ is computed for only one subdomain so that a reduced number of terms is needed for the KLE and thus the computational effort of eigenvalue analysis of $\boldsymbol{\Sigma}$ is small. Then, independent random trajectories are generated for each of two adjacent subdomains and, finally, a coupling matrix is formed to condition the KLE $\xi_i$ variables of the second subdomain to ensure the process correlation is preserved across the junction of the two subdomains. Finally, a cubic-spline interpolation is used at the junction to ensure continuity of the generated trajectories up to second derivative. We note that a set of correlated random processes was proposed in [87] by imposing a correlation between the KLE coefficients of each random process. However, the connection at the junction of each subdomain was performed by overlapping the subdomains which introduces an error on the process correlation reducing therefore accuracy. In this research, we consider only Gaussian random processes. However, the proposed approach can be extended to non-Gaussian processes using for example, the method in [32, 88, 89]. This chapter is organized as follows. Section 5.2 presents a brief description of KLE and Section 5.3 provides details of the proposed subdomain KLE. Section 5.4 compares the proposed approach with the conventional one domain KLE using two examples to demonstrate its accuracy. Finally, Section 5.5 summarizes.

## 5.2 Brief Description of Karhunen-Loeve Expansion

As mentioned above in section 5.1, the KLE represents a random process $F(t)$ as a weighted sum of uncorrelated eigenfunctions using a spectral decomposition of the process covariance function. A stationary Gaussian process $F(t)$ can be characterized using only its autocorrelation function $R_F(\tau)$ where $\tau = t_2 - t_1$ is the relative time, under the assumption of the standard translation process model [38, 56]. If the time duration $[0, T]$ of the process is discretized uniformly using $N$ points, the $N$ x $N$ covariance matrix is

$$\Sigma = [C_F\ (t_i, t_j)] = [C_F\ (\tau)], 0 \leq t_i, t_j \leq T \tag{5.1}$$

Note that for a zero-mean process

$$R_F(\tau) = R_F(\tau) = \sigma^2 \rho_F(\tau) \tag{5.2}$$

where $\rho_F(\tau)$ is the process autocorrelation coefficient and $\sigma^2 = R_F(\tau = 0)$ is the process variance. Hence, a zero-mean, stationary, Gaussian process is fully characterized by its autocorrelation function $R_F(\tau)$ which is the same with the covariance function $R_F(\tau)$. The process can also be characterized in the frequency domain by specifying the Power Spectral Density (PSD) $S_{FF}(\omega)$ which is the inverse Fourier transform of $R_F(\tau)$, i.e.

$$S_F(\omega) = \int_{-\infty}^{\infty} R_F(\tau) e^{-j\omega\tau}\, d\tau \tag{5.3}$$

Eq. (5.3) is known as the Wiener-Khintchine Theorem [16].

Because of the affine transformation property of the multi-normal distribution, the following spectral representation (KL expansion) holds

$$F(t,\theta) = \mu_F + \sum_{i=1}^{r} \sqrt{\lambda_i} \cdot \Phi_i(t) \cdot \xi_i(\theta) \tag{5.4}$$

where $t = t_1, t_2, \ldots, t_N$ and $r \leq N$ is the number of dominant eigenvalues of the covariance matrix. In Eq. (5.4), $\lambda_i$ and $\Phi_i(t),\ i = 1, \ldots, r$ are the eigenvalues and the corresponding eigenvectors of the covariance matrix $\mathbf{\Sigma}$, and $\xi_i(\theta)$ are $i$ independent realizations of the standard normal distribution. Eq. (4) is used to generate sample trajectories of $F(t)$.

For a non-Gaussian process, a non-linear transformation of the underlying Gaussian process is used based on the rigorous mathematical framework of Grigoriu's translation process theory [38, 55]. A translation process is a flat transformation of a Gaussian process. An iterative process is commonly used to identify the non-linear transformation. The iterative procedure is based on the Power Spectral Density (PSD) of the process [87] or its autocorrelation function. A combination of Polynomial Chaos Expansion (PCE) and KLE has been presented in [31] to generate trajectories for a non-Gaussian process. In this research, we consider only Gaussian processes.

## 5.3 Proposed Subdomain KLE for Long-Duration Random Processes

To generate trajectories for a stationary random process with a long domain (time horizon) [0, T], the domain is partitioned into a number of subdomains resulting in a much smaller duration for each subdomain. Since the numerical cost of KLE increases drastically with increasing domain size, the basic idea is to perform the KLE only for the first subdomain, and then ensure 1) that the correlation across the junction is preserved and 2) each trajectory is continuous up to the second derivative at the junction. The correlation is preserved using the coupling matrix K of Equation (5.7)and Equation (5.8) the continuity at the junction is enforced using 1) a computationally efficient iterative process to ensure $F(t = t_1^-, \theta_1, \theta_2)$ is close to $F(t = t_1^+, \theta_1, \theta_2)$ (see Eq. 11 for the definition of $F(t, \theta_1, \theta_2)$) and 2) a cubic-spline interpolation using one or two time steps before and after the junction time $t_1$ (see Figure 5.1) to ensure continuity up to second derivative at the junction.

To describe the proposed method, we use two subdomains. An extension to multiple subdomains is easily obtained considering two adjacent subdomains at a time. We first generate two independent sets of trajectories, one for each subdomain, and then impose a relationship between the KLE coefficients of the two sets. Subsequently, a computationally efficient approach is used to generate trajectories of the process in the whole domain with up to second derivative continuity at the subdomain junction.

Let $F_1(t, \theta_1)$ and $F_2(t, \theta_2)$ with $\theta_1, \theta_2 \in \Theta$, be two independent sample trajectory sets of the random process $F(t, \theta)$ as

$$F_1(t, \theta_1) = \sum_{i=1}^{r} \sqrt{\lambda_i} \cdot \Phi_i(t) \cdot \xi_i(\theta_1) \text{ with } t \in [0, t_1] \tag{5.5}$$

$$F_2(t,\theta_2) = \sum_{i=1}^{r} \sqrt{\lambda_i} \cdot \Phi_i(t - t_1) \cdot \xi_i(\theta_2) \text{with } t \in [\,t_1, T] \tag{5.6}$$

Each set includes a number of trajectories, each denoted by $f_1(t)$ and $f_2(t)$, respectively. Figure 5.1 shows a trajectory $f(t)$ of process $F(t,\theta)$ for the time horizon $0 \le t \le T$, split in two subdomains at time $t_1$ of equal duration.

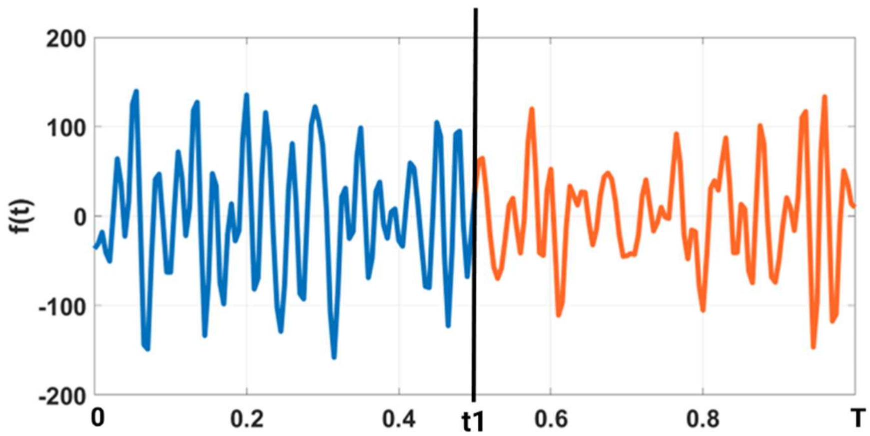


Figure 5.1 Process trajectory *f(t)* using two adjacent subdomains

The covariance function $C(|s-t|)$ of the process $F(t,\theta)$ is known for $0 \le s, t \le T$. We define the $r \times r$ matrix $\boldsymbol{K}$, called coupling matrix, where r is the number of significant eigenvalues for one subdomain (see equation 5.4). The elements of $\boldsymbol{K}$ are obtained by projecting $C(\lfloor t - \bar{t} \rfloor)$ where $t \in [0, t_1]$ and $\bar{t} \in [t_1, T]$ onto the basis $\Phi_i(t)$ as

$$F_2(t,\theta_2) = K_{ij} = \frac{1}{\sqrt{\lambda_i \lambda_j}} \int_{t=0}^{t_1} \int_{\bar{t}=t_1}^{T} C(\lfloor t - \bar{t} \rfloor) \Phi_i(t) \Phi_j(\bar{t} - T) d\bar{t} dt =$$

$$= \frac{1}{\sqrt{\lambda_i \lambda_j}} \int_{t=0}^{t_1} \int_{\bar{t}=0}^{t_1} C(\lfloor t - \bar{t} - t_1 \rfloor) \Phi_i(t) \Phi_j(\bar{t}) d\bar{t} dt \tag{5.7}$$

The matrix $\boldsymbol{K}$ expresses the correlation, the initially uncorrelated KLE coefficient sets (one for each subdomain), must have in order to properly represent the random process for the entire domain $T$ (union of the two subdomains). The coupling matrix $\boldsymbol{K}$ is explicitly represented as

$$\boldsymbol{K} = \begin{bmatrix} I & K_{12} & \cdots & K_{1r} \\ K_{21} & I & \cdots & K_{2r} \\ \vdots & \vdots & \ddots & \vdots \\ K_{r1} & K_{r2} & \cdots & I \end{bmatrix} \tag{5.8}$$

To generate sets of correlated random processes in two adjacent subdomains, a vector $\overline{\boldsymbol{H}}$ is formed in terms of matrices $\boldsymbol{K}$ and $\boldsymbol{L}$ as

$$\overline{\boldsymbol{H}}\ (\theta_1, \theta_2) = \boldsymbol{K}^T \boldsymbol{H}(\theta_1) + \boldsymbol{LH}(\theta_2) \tag{5.9}$$

where $\boldsymbol{L}$ is the lower triangular matrix of the Cholesky decomposition of $\boldsymbol{I} - \boldsymbol{K^T K}$ so that [91]

$$\boldsymbol{I} - \boldsymbol{K^T K} = \boldsymbol{LL^T} \tag{5.10}$$

where matrix $\boldsymbol{I} - \boldsymbol{K^T K}$ is positive definite.

The Cholesky decomposition of the discretized covariance function can be used to correlate a set of random variables representing a discretized random field [92]. In Eq. (5.10), $\boldsymbol{I}$ is the $r \times r$ identity matrix and $\boldsymbol{H}$ is a vector containing all random coefficients $\xi_i(\theta)$ of the KLE. Note that the numerical effort to perform the Cholesky decomposition of Eq. 5.10 depends only on the number $r$ of significant eigenvalues of only one subdomain, which in turn can be small due to the shorter duration $[0,\ t_i]$ of the subdomain.

The vector $\overline{\boldsymbol{H}}$ of equation (5.9) contains the random coefficients $\bar{\xi}_i(\theta_1, \theta_2)$ to be used in the KLE of the second subdomain. Utilizing $\bar{\xi}_i(\theta_1, \theta_2)$ ensures that the correlation between the two adjacent subdomains is preserved across their boundary. Finally, we generate sample trajectories for the two subdomains as

$$F(t, \theta_1, \theta_2) = \begin{cases} \sum_{i=1}^{r} \sqrt{\lambda_i} \Phi_i(t) \xi_i(\theta_1), & t \in [0, t_1] \\ \sum_{i=1}^{r} \sqrt{\lambda_i} \Phi_i(t - t_1) \bar{\xi}_i(\theta_1, \theta_2), & t \in [\, t_1, T] \end{cases} \tag{5.11}$$

As an example, Figure 5.2 shows two adjacent subdomains of a Gaussian process with the Pierson Moskowitz spectrum (or PSD). The correlation length is 0.5 secs (example 1 of Section 5.4). The time trajectories are generated using a time step of 0.0005 seconds. Figure 5.3 zooms in at the junction. The KLE has been used to initially generate a trajectory for each subdomain (black and red lines) using two independent sample sets $\xi_i(\theta)$ of the standard normal distribution.

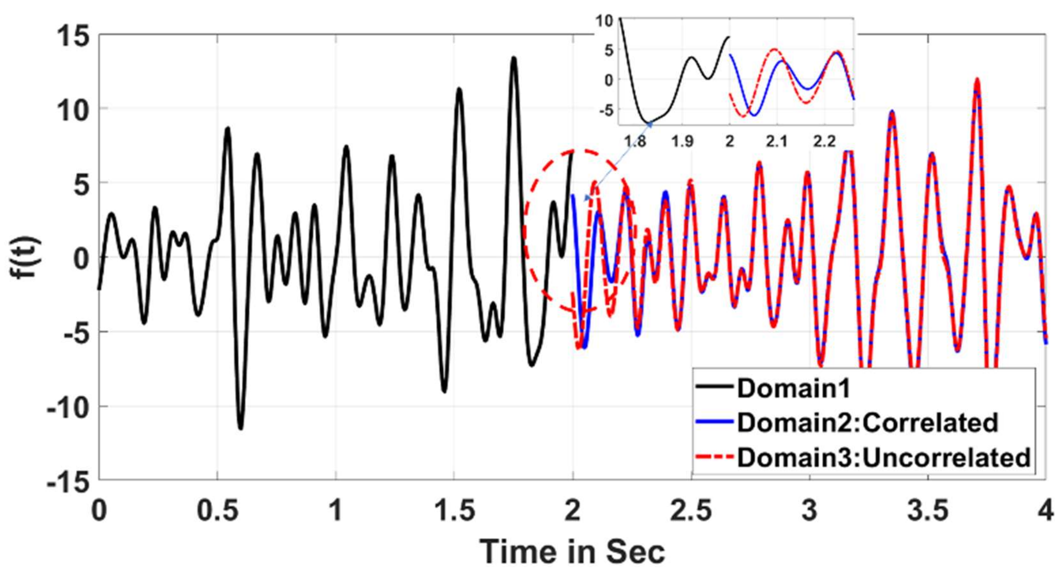


Figure 5.2 Process trajectories for two adjacent subdomains before and after correlation

The trajectory continuity is not preserved at the junction between the two subdomains. At this point, the coupling matrix $\boldsymbol{K}$ (Eqs 5.7 and 5.8) is formed and the $\xi_i(\theta_2)$ realizations for the second subdomain are modified as in Eq. (5.9). The new realizations are used to modify the uncorrelated trajectory (red line) resulting in a correlated trajectory (blue line). However, there is still a discontinuity between the black and blue lines. As Figure 5.2 shows, the modification effect using matrix $\boldsymbol{K}$ is mostly localized near the junction point at $t_i$, while it is weak far from this point. The coupling matrix *K* guarantees the preservation of the specified process correlation function across the junction but it does not guarantee the trajectory continuity at the junction. The matrix $\boldsymbol{L}$ guarantees that the new KLE coefficients $\overline{\boldsymbol{H}}\ (\theta_1, \theta_2)$ are uncorrelated as they should.

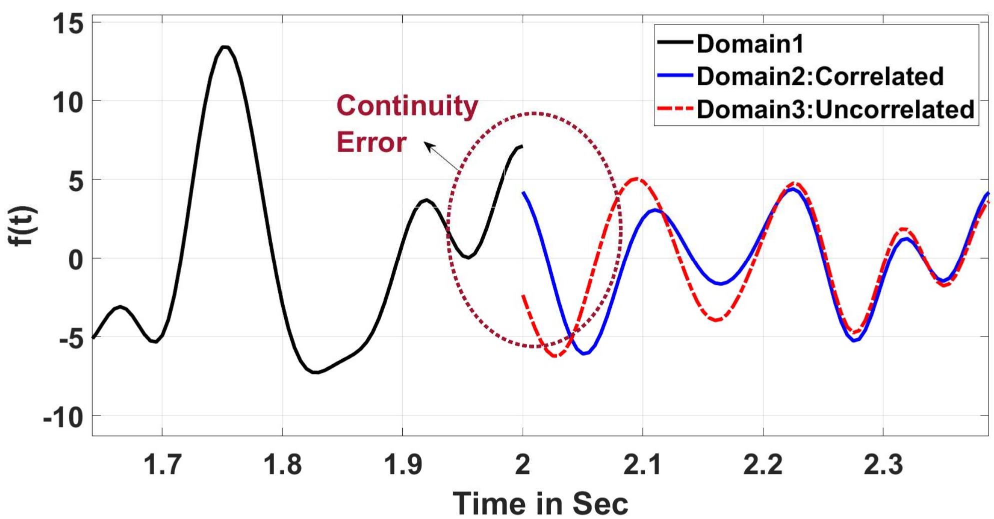


Figure 5.3 Zoomed in portion of Fig. 5.2 showing the continuity error at the junction.

The Pierson Moskowitz spectrum (or PSD). The correlation length is 0.5 secs (section 5.5.2). The time trajectories are generated using a time step of 0.0005 seconds. Figure 5.3 zooms in at the junction. The KLE has been used to initially generate a trajectory for each subdomain (black and red lines) using two independent sample sets $\xi_i(\theta)$ of the standard normal distribution.

## 5.4 Continuity at the Subdomain Junction

To ensure continuity of two trajectories at the junction location $t = t_1$, we must first have.

$$F(t = t_1^-, \theta_1, \theta_2) = F(t = t_1^+, \theta_1, \theta_2) \tag{5.12}$$

where $F(t, \theta_1, \theta_2)$ is defined in Eq. (11). The following continuity error $\in$ for $F(t, \theta_1, \theta_2)$ is defined at the junction $t = t_1$

$$\in = \frac{|F(t = t_1^-, \theta_1, \theta_2) - F(t = t_1^+, \theta_1, \theta_2)|}{|F(t = t_1^-, \theta_1, \theta_2)|} \; x \; 100 \tag{5.13}$$

For each generated trajectory of the first subdomain, we iteratively generate trajectories for the second subdomain using 1) the random coefficients $\bar{\xi}_i(\theta_1, \theta_2)$ in the vector $\overline{\boldsymbol{H}}$ (Eq. 5.9) to preserve the correlation across the junction and 2) to ensure the relative error $\in$ is less than 1% (i.e. $\in < 0.01$). After we obtain a trajectory with $\in < 0.01$, we apply a cubic-spline interpolation using one or two time steps before and after the junction time $t_1$ to enforce continuity up to second derivative at the junction. This process (i.e. above steps 1 and 2 and the cubic-spline interpolation) is repeated until the required number of trajectories is generated for the second subdomain. Note that the cubic-spline interpolation ensures continuity of value and the first two derivatives at the junction. Iterations until $\in < 0.01$ are performed to make sure the cubic-spline interpolation does not substantially modify the two trajectories at the junction altering the process correlation across the junction. For the same reason, we use only one or two time steps before and after the junction for the cubic-spline interpolation. Figure 5.4 shows the cubic-spline modification at the junction using two time steps before and after the junction (Figure 5.4a) and one time step before and after the junction (Figure 5.4b).

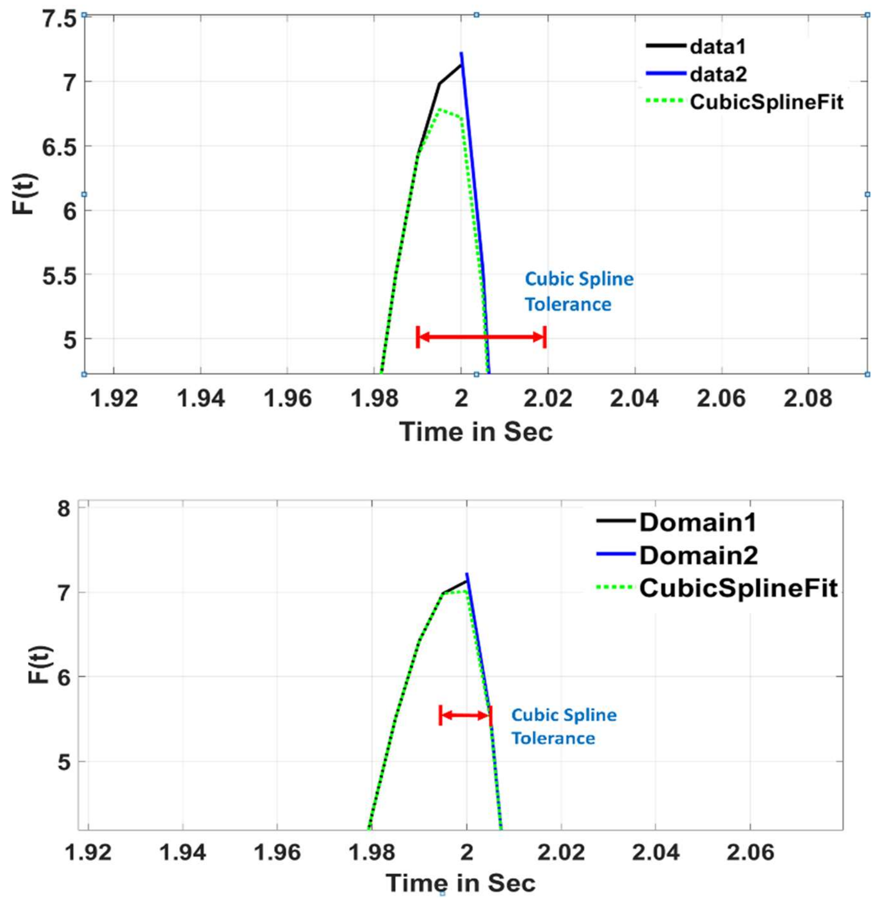


Figure 5.4 Cubic-spline interpolation using (a) two-time steps before and after the junction, and (b) one time step before and after the junction

The proposed approach is easily generalized to many subdomains considering two adjacent subdomains at a time. After a trajectory has been generated for the first and second subdomains for example, we generate a trajectory for the third subdomain using the same process between the second and third subdomains. Figure 5.5 shows a generated process trajectory using four subdomains by repeating the proposed approach three times.

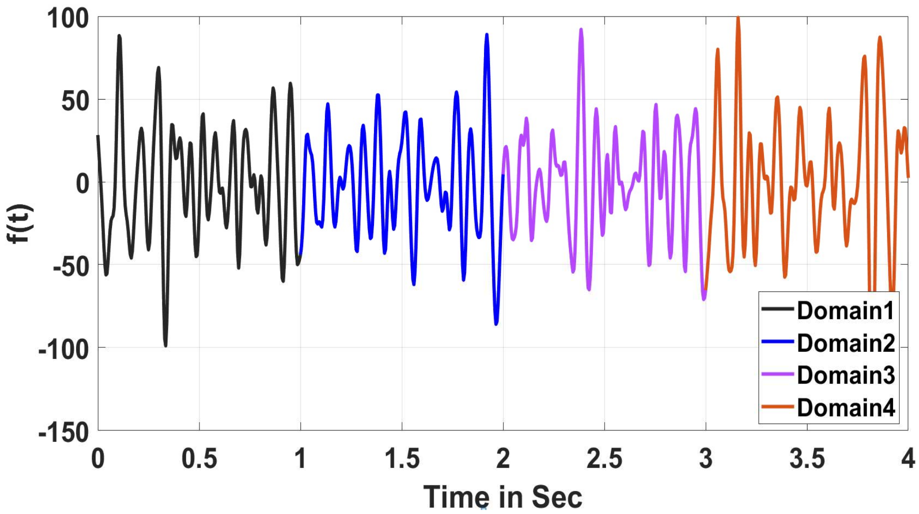


Figure 5.5 Generation of a process trajectory using 4 sub-domains

## 5.5 Numerical Applications

In this section, we will present the numerical implementation of the sub-domain-based approach by applying it to an industry-wide application involving two input spectra: Exponential and Moskowitz Power Spectral Density (PSD).

### 5.5.1 Pierson Moskowitz PSD Example

To demonstrate the accuracy of the proposed subdomain KLE approach, we compare it with the conventional KLE based on the entire time horizon (one subdomain). This section presents two examples of a stationary random process: 1) a process with a Pierson Moskowitz Power Spectral Density (PSD), and 2) [87], a process with an exponential PSD[88].

In this example, we consider a zero-mean, stationary random process *F(t)* with the following Pierson Moskowitz PSD

$$S_{FF}(\omega) = \frac{A}{\omega^5} e^{\frac{-B}{\omega^4}} \tag{5.14}$$

where, A= $1.2*10^{12}$ $N^2$ $sec^{-4}$ and B = 20,000 $sec^{-4}$ (Figure 5.6). The PSD represents a double-sided spectrum showing only the positive frequency range.

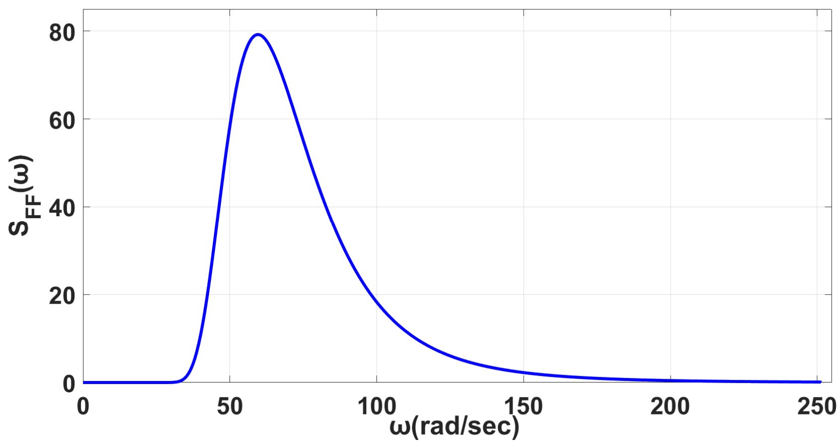


Figure 5.6 Pierson Moskowitz PSD

The inverse Fourier transform of $S_{FF}(\omega)$ normalized by the corresponding variance $\sigma^2 = R(\tau = 0)$, provides the correlation coefficient function $\rho_{FF}(t, t+\tau) = \rho_{FF}(\tau)$ (Figure 5.7).

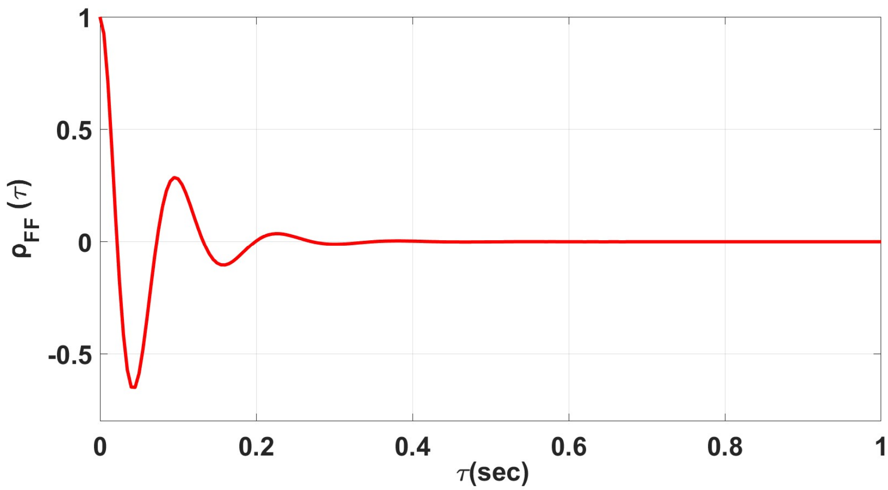


Figure 5.7 Autocorrelation coefficient for Pierson Moskowitz PSD

The domain is discretized uniformly using a time step *dt* = 0.005 sec. Figure 5.7 shows that the correlation length $t_c$ is approximately equal to 0.4 seconds, i.e. $\rho_{FF}(t, t+\tau) \approx 0$ if $\tau > 0.4$ sec. The covariance matrix of $F(t)$ was first formed, and an eigenvalue analysis was performed to calculate its eigenvalues $\lambda$ and corresponding eigenvectors $\Phi(t)$ using a simulation time (duration) of 4, 3, 2 and 1 seconds. Figure 8 shows the eigenvalues for the four simulation times indicating that the number of dominant eigenpairs used in the KLE of Eq. (5.4) increases drastically with increasing duration. If the magnitude of the last dominant eigenvalue is less than 1% of the highest, the number of dominant eigenvalues for the 4, 2, 1 and 0.5 sec duration is 189, 95, 49, and 31 respectively. Figure 5.9 shows a few trajectories from KLE for the 4 sec duration case.

Note that for acceptable accuracy, the subdomain length for the proposed approach must be larger than the process correlation length in order for the KLE to properly capture the correlation structure of the process.

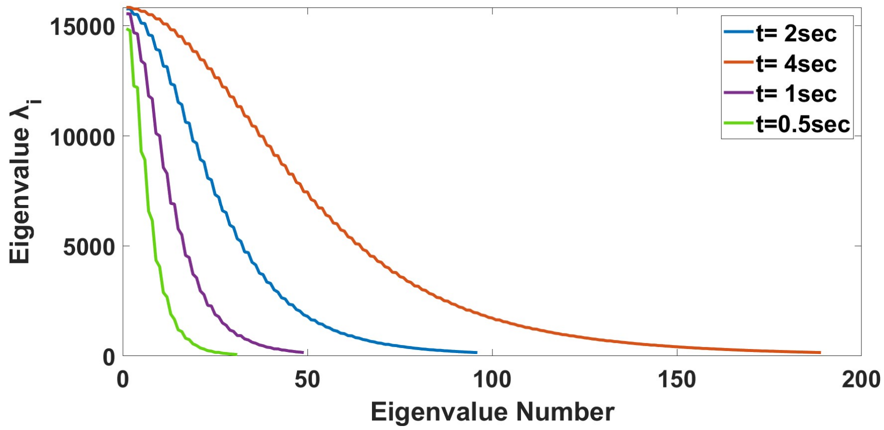


Figure 5.8 Eigenvalues of covariance matrix for Pierson Moskowitz PSD

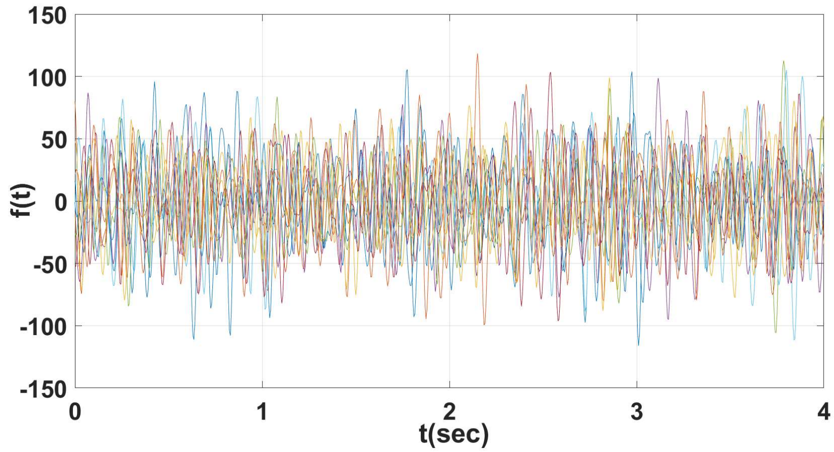


Figure 5.9 Process trajectories for Pierson Moskowitz PSD example

For this reason, we used 4 different subdomain length; i.e. $t_i = 0.5, 1, 2\ and\ 4$ sec respectively. The duration (time horizon) of interest is $0 \leq t \leq T = 4$ sec. Thus, the $t_i = 4$ sec case represents the conventional one-subdomain case. Figure (5.10) illustrates the accuracy of proposed approach using subdomains of duration 0.5, 1, 2, and 4 seconds for a simulation time of 4 seconds. To cover the 4 sec simulation time, the number of subdomains is therefore 8 (0.5 sec duration each), 4 (1 sec duration each), 2 (2 sec duration each), and 1 (4 sec duration), respectively. The one-subdomain case represents the conventional KLE. For each case, 5000 trajectories were generated for the entire 4 sec domain and were used to estimate the process PSD. Figure 5.10 shows that in all cases the accuracy is very good indicating that the proposed subdomain approach provides very good accuracy even if each subdomain is short (e.g. 8 subdomains of 0.5 sec duration each) where a small number of dominant eigenvalues is used compared to the entire simulation time case.

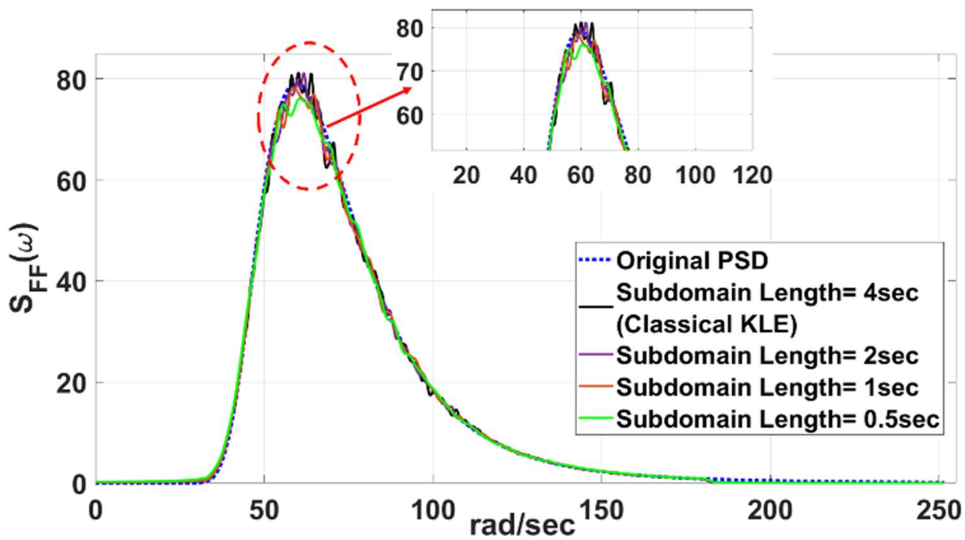


Figure 5.10 Average Pierson Moskowitz PSD estimation using subdomain approach for N=5000 trajectories and $\lambda_i = 31, 49, 95$ and 189

Note that for this example, the largest number of subdomains is eight (not shown here) with 0.5 sec duration each which is a little larger than the correlation length of 0.4 seconds. Figure 5.11 shows one realization of a long-time horizon of 16 sec generated using $t_i = 1$ sec and 16 subdomains. All subdomains are connected at the junction using the proposed methodology indicating that very long trajectories can be generated with a relatively small number of independent realizations $\xi_i(\theta)$ of the standard normal distribution in the KLE.

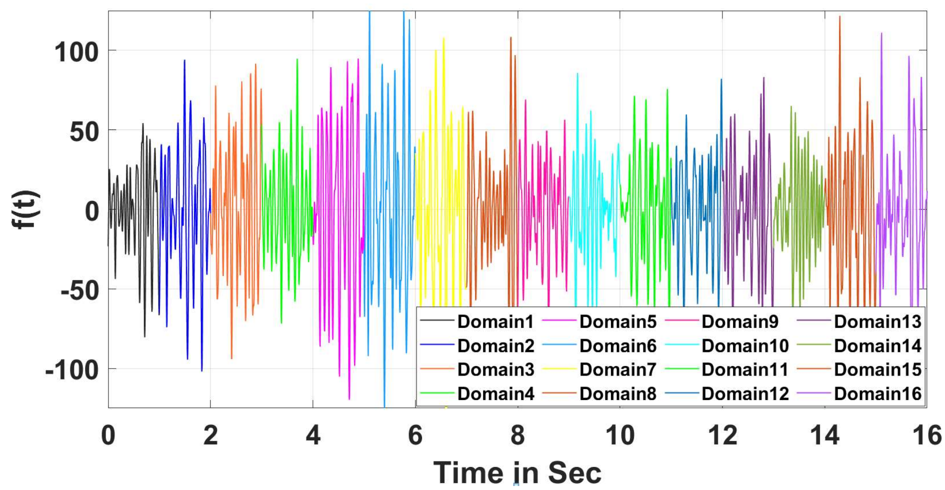


Figure 5.11 Example of a long trajectory generated with 16 subdomains of 1 sec duration each for Pierson Moskowitz PSD

### 5.5.2 Exponential PSD Example

In this example, we use the common exponential PSD[89]. (Figure 5.12)

$$S_{FF}(\omega) = 4e^{-4\omega} \tag{5.15}$$

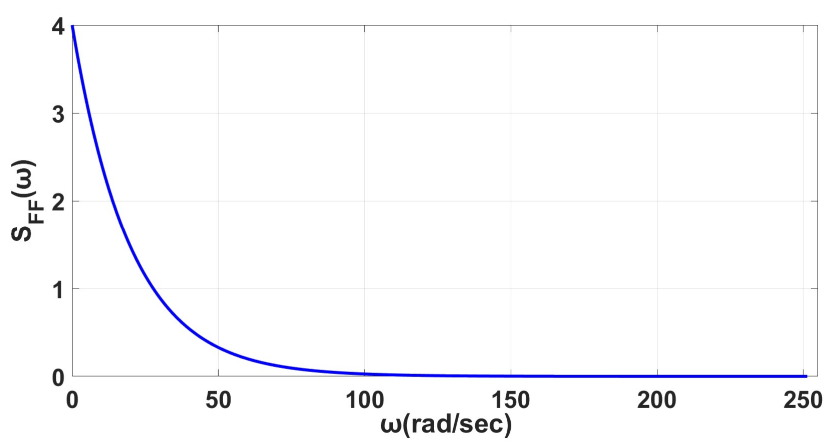


Figure 5.12 Exponential PSD

Similarly, to the previous example, the autocorrelation coefficient function $\rho_{FF}(t, t+\tau) = \rho_{FF}(\tau)$ is obtained using the inverse Fourier transform of $S_{FF}(\omega)$

normalized by the corresponding variance $\sigma^2 = R(\tau = 0)$, as shown in Figure 5.13. and it indicates that the correlation length is approximately 1 sec. We therefore use subdomains of length equal to 1 sec.

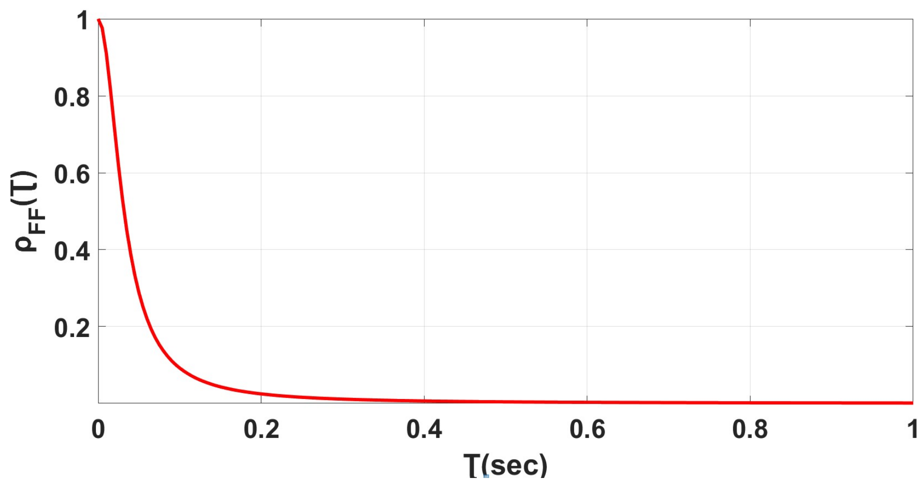


Figure 5.13  Autocorrelation coefficient for Exponential PSD

Figure 5.14 shows the eigenvalues and their maximum number of the covariance matrix if the ratio of smallest to largest eigenvalue is 1% for subdomain lengths of 1, 2, 4, and 8 seconds indicating that 31, 63, 120 and 237 terms respectively, are used in the KLE.

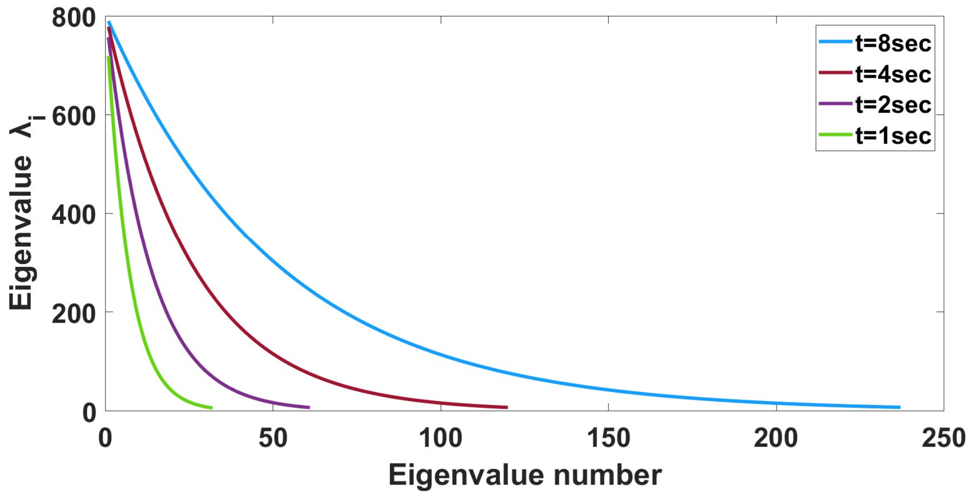


Figure 5.14 Eigenvalues of covariance matrix for exponential PSD

Figure 5.15 shows that even the smallest subdomain length of 1 sec is enough to estimate the exponential PSD accurately using $N = 5000$ trajectories. Figure 5.16 shows some of the trajectories for the time horizon of $0 \leq t \leq T = 8\ sec$.

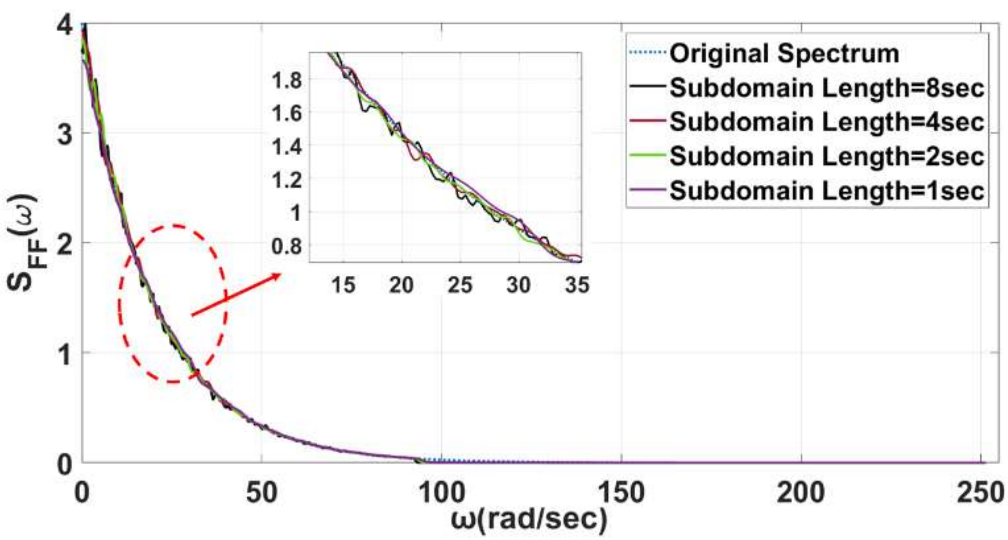


Figure 5.15 Average exponential PSD estimation using subdomain approach for N=5000 trajectories and $\lambda_i = 31, 63, 120$ and $237$

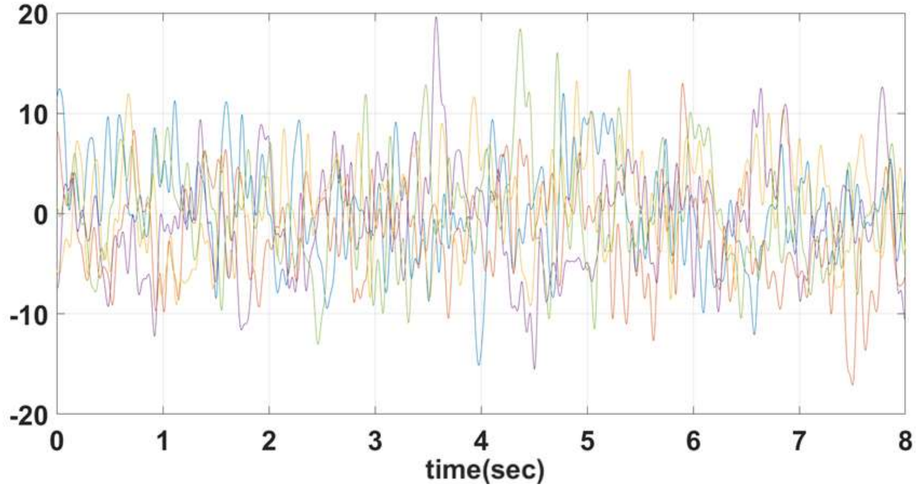


Figure 5.16   Process trajectories for exponential PSD example

## 5.4 Summary

This chapter presents a unique subdomain-based approach the KL Expansion of a stationary, Gaussian process for a domain which is much longer than the process correlation length is computationally expensive, especially if a small discretization step is used to capture high frequency content for example. To address this issue, a subdomain approach has been presented where the spectral decomposition of the process covariance matrix is computed for a short subdomain where the computational effort is much smaller since a reduced number of terms is needed for the KLE. For two subdomains for example, trajectories are generated for each subdomain independently and a coupling method is applied to the second domain trajectories to condition them so that the random process correlation is preserved across the subdomain junction. Additionally, continuity at the junction is enforced using a cubic-spline interpolation. The proposed approach is easily extended to multiple subdomains of equal duration which can be as small as the process correlation length. Two examples demonstrated the accuracy of the proposed approach.

The presented subdomain approach for Gaussian processes has also been extended to non-Gaussian processes. The non-Gaussian case is not presented however, due to its many similarities with the Gaussian case.

# CHAPTER SIX

# SIMULATION-BASED FATIGUE LIFE ESTIMATION USING SUBDOMAIN NG-KLE

## 6.1 Introduction

This Chapter combines the developments of Chapters 4 and 5 to develop a general simulation-based fatigue life estimation using a subdomain-based NG-KLE method. The subdomain part of the developed method improves computational efficiency by applying the NG-KLE method to generate short duration trajectories, and then creating very long synthetic trajectories by stitching many sort trajectories. As demonstrated in Chapter 5, both the marginal PDF and the autocorrelation function of the process are preserved. The synthetic long stress trajectories are then used to estimate fatigue life using one of the three approaches of Chapter 4. The proposed approach has three main advantages: 1) it handles both Gaussian and non-Gaussian processes, 2) it is computationally efficient, and 3) it is accurate due to the synthetically generated long output trajectories.

We demonstrate in this Chapter, all developments using two examples: A Duffing oscillator excited by a non-Gaussian load, and a truck frame excited also by a non-Gaussian load. In the latter example, a very large finite element model is used for the truck.

## 6.2 Example 1: Duffing Oscillator Under Non-Gaussian Loading

In this section, we apply the subdomain-based non-Gaussian Karhunen-Loève Expansion (NG-KLE) methodology to assess the fatigue life of the Duffing oscillator nonlinear system subjected to non-Gaussian loading. This case study demonstrates the advantages of utilizing the subdomain-based NG KLE in estimating fatigue life in combination with the developed generalized simulation-based fatigue methodology.

We used a normal or Weibull marginal PDF. In the former case, the PDF has a mean of 500 and a standard deviation of 300. The Weibull PDF has the same mean and standard deviation while the skewness coefficient is equal to 0.7 and the kurtosis coefficient is equal to 3. Figure 6.1 shows the Weibull marginal PDF.

The case study illustrates how the subdomain-based NG-KLE methodology, with its flexibility and accuracy, can effectively handle diverse input conditions, ultimately providing valuable insights into the fatigue behavior of complex systems under non-Gaussian loading.

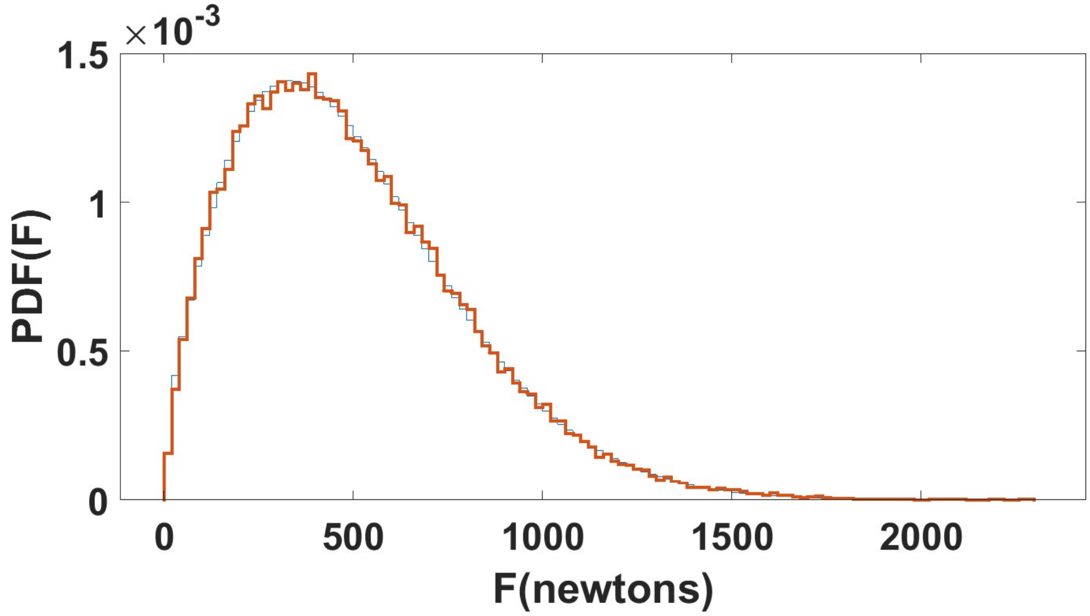


Figure 6.1 Weibull marginal PDF

6.2.1 Generation of Input Force Trajectories using the Subdomain Approach

We first generate input force trajectories using KLE of only 14 second duration. This reduces the number of significant terms in the KLE substantially improving therefore, the computational efficiency. The subdomain approach was then used to “stich” together 10 signals of 14 second duration each for a total duration of 140 seconds, as shown in Figure 6.2. The dots indicate the location where two subsequent signals were connected together. It should be noted that the provided correlation of the process is preserved through the boundaries between two adjacent subdomains. This is a key advantage of the subdomain enabling the generation of significantly longer input signals using a small number of terms in the KLE.

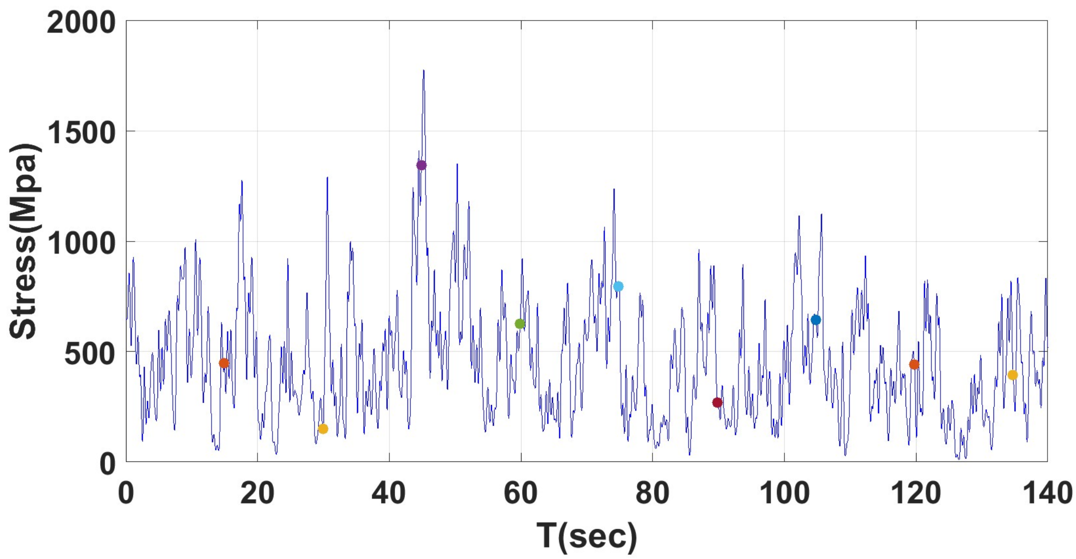


Figure 6.2  Representative input force trajectory from subdomain NG-KLE for the Weibull marginal PDF

6.2.2 Validation of Input Marginal PDF and Autocorrelation Function

In order to make sure the generated trajectories on the input process follow the provided marginal PDF and autocorrelation function, we generated 50 realizations using the NG-KLE approach (Figure 6.3).

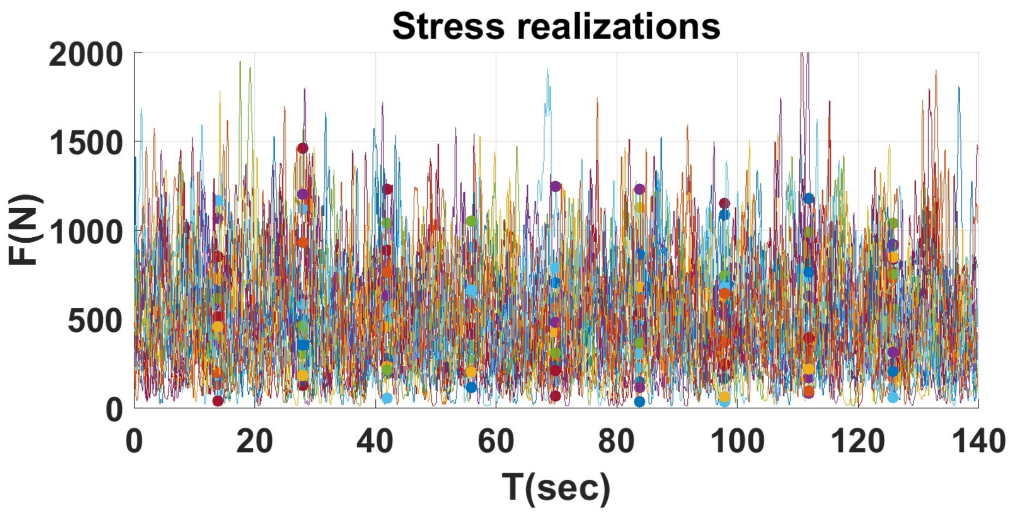


Figure 6.3 Input force trajectories from subdomain NG-KLE for the Weibull marginal PDF

With this ensemble of realizations, we estimated both the marginal PDF and the autocorrelation coefficient. Figures 6.4 and 6.5 show an excellent agreement between the estimated and provided marginal PDF and autocorrelation coefficient. This validation step ensures the accuracy of the generated trajectories, affirming their fidelity in representing the target system behavior.

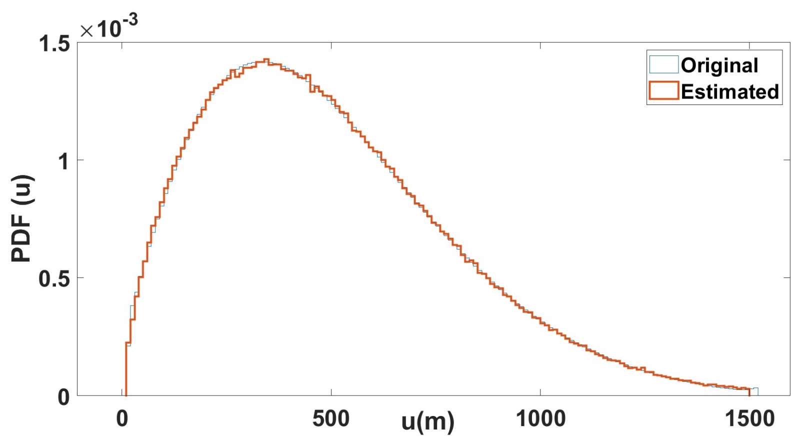


Figure 6.4 Comparison of estimated and target marginal PDF

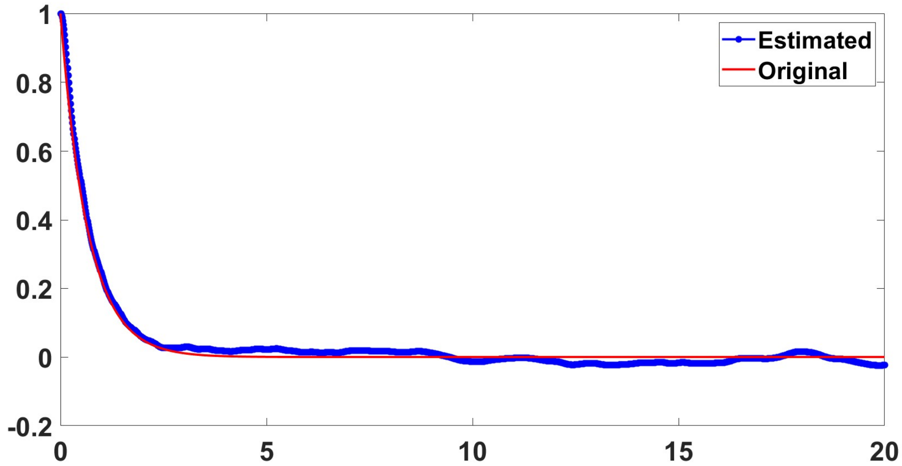


Figure 6.5 Comparison of estimated and target autocorrelation coefficient

6.2.3 Estimation of Output Marginal PDF and Autocorrelation Function

The 50 input force trajectories of Figure 6.3 were used as excitation of the Duffing oscillator and the corresponding output displacement trajectories were obtained using Runge-Kutta time integration. Subsequently, the output displacements were converted to shear stress of the linear spring coil as shown if Figure 6.6. Note that the small number of 50 output trajectories ensures computational efficiency.

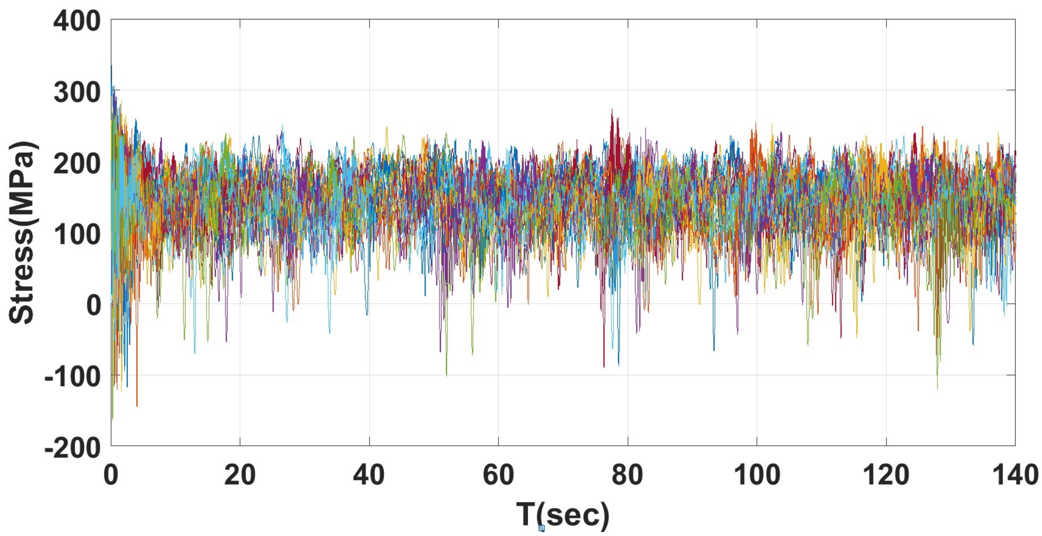


Figure 6.6 Output stress trajectories from Duffing oscillator

The 50 stress output signals were then used to estimate the marginal output stress PDF and the autocorrelation function. For that, we omitted the initial 10 seconds of each trajectory which are dominated by arbitrary initial conditions used in the Runge-Kutta time integration. Figure 6.7 compares the estimated marginal PDF from the subdomain approach with the classical NG-KLE based on 140 second trajectories without the subdomain "stitching." The accuracy of the subdomain approach is very good.

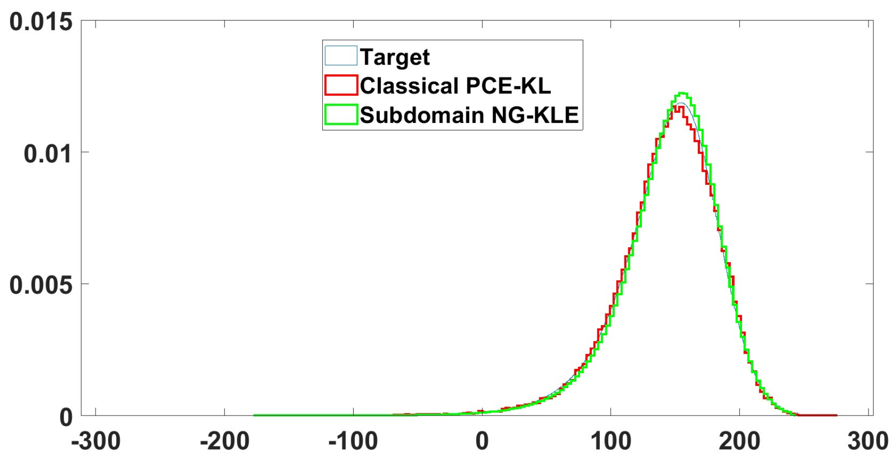


Figure 6.7 Estimated output marginal PDF of output stress

6.2.4 Generation of Long Output Stress Trajectories Using Subdomain NG-KLE

After we obtained the estimated marginal PDF and autocorrelation function of the output stress process, as explained in Section 6.3.2, we used the NG-KLE approach to generate many trajectories of 30 seconds each. This short duration ensures computational efficiency of the NG-KLE. The subdomain approach was then used to “stich” together 150 trajectories of 30 second each generating therefore trajectories of 4500 second each (Figure 6.8). This approach allows us to generate many output stress signals that capture the system’s statistics over a very long period without increasing the computational cost.

To validate the statistical accuracy of the 4500 second trajectories, we estimated their first four statistical moments and compared them with 240 second trajectories generated by the NG-KLE without using the subdomain approach. Table 6.1 compares the two cases, indicating the statistical accuracy of the trajectories generated by the subdomain approach.

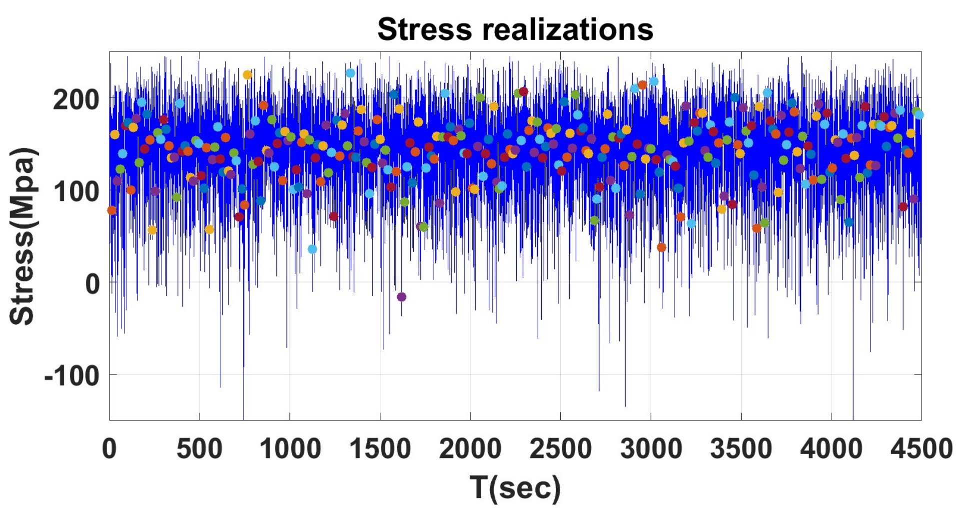


Figure 6.8 Long stress realizations generated using the subdomain NG-KLE (150 subdomains of 30 sec each)

Table 6.1 Statistics for the output trajectories

| Quantity | Weibull (t=240 sec) NG-KLE | Weibull (t=4500sec) Subdomain NG-KLE |
|---|---|---|
| Mean | 144.70 | 144.35 |
| Standard Deviation | 37.8 | 37.92 |
| Skewness Coef. | -0.93 | -0.8686 |
| Kurtosis Coef. | 5.254 | 5.0965 |

The long-duration trajectories of Figure 6.8 highlight the ability to capture high-stress areas (stress peaks) that might have been overlooked with shorter signals. This extended signal duration is critical in the estimation of fatigue life which is dominated by rare events of high stresses which are difficult to obtain with short-duration signals.

6.2.5 Fatigue Life Estimation

The long-duration trajectories of Figure 6.8 were used to estimate the fatigue life using the total probability theorem approach (Section 4.3.2) and the PDF of peak stresses approach (Section 4.3.3). The table shows that the two approaches show similar fatigue life estimation. In addition, the estimated life using long-duration signals of 4500 seconds based on the subdomain NG-KLE, is substantially lower (e.g. 774.99 versus 1437 for the total probability theorem approach) compared to the short signals of 240 second duration. This is expected because the long signals have a high probability of capturing large stress peaks which dominate and reduce the fatigue life. Although not shown in the table, the fatigue life using 4500 second signals, was similar if longer signals were used (e.g. 9000 seconds) indicating convergence of fatigue life estimation.

Table 6.2 Fatigue life estimation summary

| Input Spectrum | Weibull t=240 Sec | Weibull t=4500sec (Subdomain-NG-KLE) |
|---|---|---|
| Total Probability Theorem (hrs) | 1437 | 774.99 |
| PDF of Peak Stresses (hrs) | 1441 | 731.44 |
| Number of Eigenvalues | 650 | 72 |

## 6.3 Appropriate Duration of Output Stress Trajectories

The length of stress signals needed for fatigue analysis can vary depending on several factors, including the complexity of the system, the nature of the loading conditions, and the specific fatigue analysis method being employed. However, in general, longer stress signals are often beneficial for more accurate fatigue analysis. Here are some considerations:

- Loading Conditions: For systems subject to simple, repetitive loads, shorter stress signals may be sufficient. However, if the loading conditions are complex or involve non-Gaussian behavior, longer signals become more important.
- Complex Systems: Complex engineering systems with multiple components and interactions typically require longer stress signals. This is because such systems

can exhibit intricate stress variations that must be captured for accurate fatigue analysis.

- Fatigue Life Estimation Methods: The method used for fatigue life estimation plays a significant role. Some methods, like the rain-flow counting algorithm, work well with shorter signals. In contrast, advanced methods that consider non-Gaussian behavior often require longer signals to capture statistical characteristics accurately.
- Non-Gaussian Behavior: If the stress signals exhibit non-Gaussian behavior, which is common in real-world applications, longer signals are essential. Non-Gaussian behavior includes features like heavy tails, skewness, kurtosis, and complex temporal patterns, which necessitate more extensive data for accurate analysis.
- Statistical Confidence: Longer signals provide more data points, leading to greater statistical confidence in the results. This is crucial for estimating fatigue life, especially when dealing with uncertainties.

For the above reasons, we propose the approach shown in Figure 6.9 to determine the most appropriate stress signal length for accurately calculating fatigue life. It leverages both traditional counting methods such as rain-flow counting and advanced techniques such as the subdomain NG-KLE that account for non-Gaussian behavior. The key is incrementally increasing the signal length and re-estimating fatigue life until convergence within a predefined tolerance.

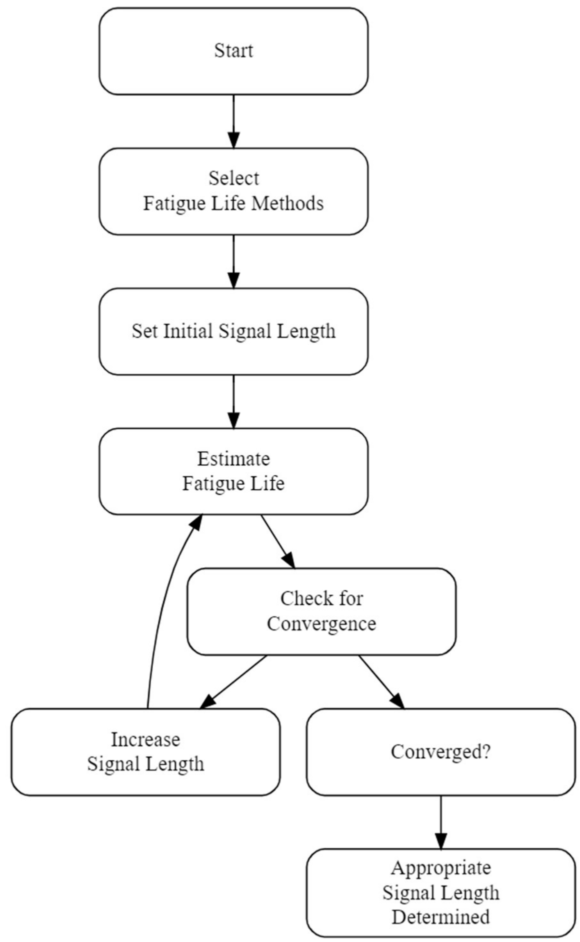


Figure 6.9 Flowchart of incremental increase of signal length

The process begins by selecting a combination of fatigue life estimation methods suitable for the expected loading conditions as per Section 4.3. An initial short length input random process is chosen based on expected real-world duration and computational resources. The selected methods then estimate fatigue life using the short length input process. If the fatigue estimates between two successive iterations do not converge within a defined limit, the process length is systematically increased, and the estimation is repeated until satisfactory convergence is achieved. The length can be easily increased using the developed subdomain approach. A key enabler is that the subdomain NG-KLE allows generating arbitrary length signals once the marginal PDF and autocorrelation are determined, without needing expensive re-evaluations. This iterative data-driven methodology identifies the minimum signal length required for the selected methods to yield acceptably consistent fatigue life predictions. The final converged result provides greater confidence in obtaining an accurate fatigue life even under non-Gaussian loading.

## 6.4 Example 2: Automotive Pickup Truck with Non-Linear Mounts Subjected to Non-Gaussian Loading

The chassis is a critical component in trucks that integrates major systems such as axles, suspension, powertrain, and the cab [100]. It must be rigid to withstand the operational stresses yet have adequate bending stiffness for good handling. Key design criteria are minimizing stress, deflection, and maximizing energy absorption. Fatigue loading is a major consideration as the chassis experiences complex dynamic loads in service. Factors affecting fatigue life include stress state, geometry, surface quality, material type, defects, and loading direction [101-104]. Many researchers have focused on chassis design and manufacturing. The objective in this example is to apply the proposed fatigue analysis techniques for truck frames to access their fatigue life while reducing the number of FEA simulations. Fatigue life estimation is critical to prevent in-service failures.

To demonstrate the industrial application of the developed general simulation-based fatigue methodology we use an open-source Chevrolet Silverado pickup truck model as shown in Figure 6.10. The system is a large automotive finite element model with non-linear components.

Figure 6.10 Finite element model of Silverado pickup truck

6.4.1 Description of Model and Input Random Force

The FEA model consists of 4.5 million degrees of freedom. The cab and the truck bed are mounted on the frame at the mounting locations as shown in Figure 6.11. The frame is supported at all other suspension mounting locations using flexible constraints. The non-linear stiffness of the bushings in the direction of the strut is also shown in Figure 6.11. The tactile response is measured at the seat mounting location. A viscous damping of 5 Ns/mm applied at each cab, bed and suspension mounting locations. The excitation (input) random process is stationary and non-Gaussian with a Weibull marginal PDF and is applied at the front left shock tower through a non-linear bushing in the direction of the strut (Figure 6.11).

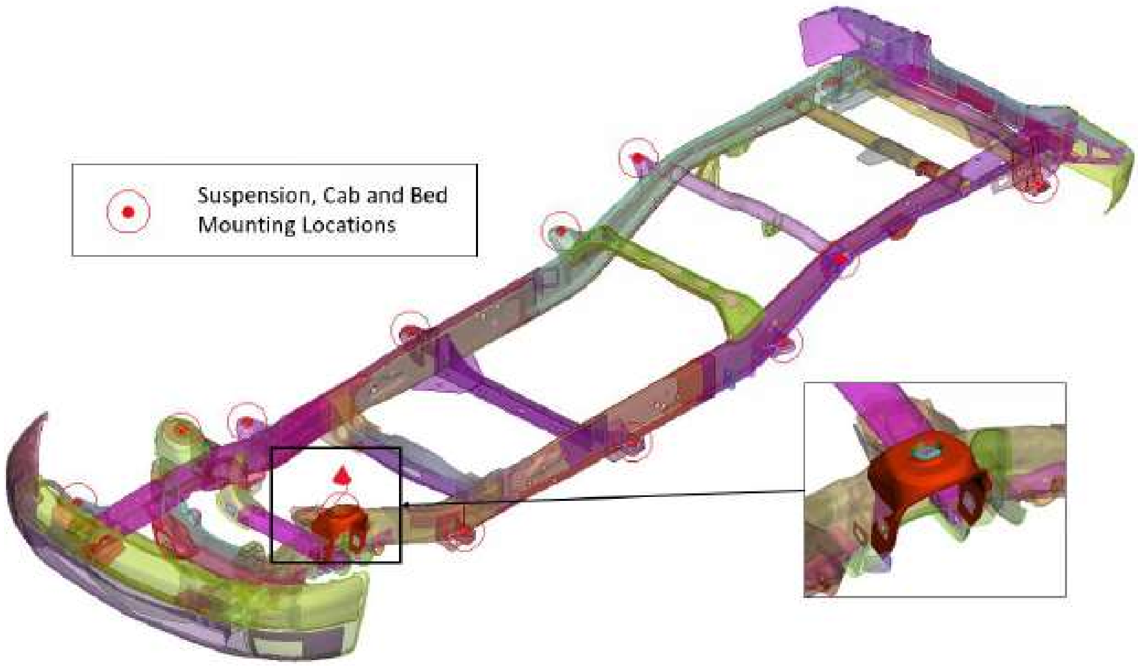


Figure 6.11 Location of cab mount, nonlinear bushing, and non-Gaussian load location

Because of the presence of the non-linear bushings at the suspension mount, a direct non-linear transient analysis is needed, which is very expensive and impractical even for one simulation for this large system. Component Mode Synthesis (CMS) is effectively used to address this. In CMS, the dynamics of the structure are described by the normal modes of its individual components, and a set of modes called constraint modes. The Craig-Bampton method is the most accurate and widely used CMS method. It uses component normal modes which are calculated with the interface between connected component structures held fixed. The attachment to the interface is achieved by a set of constraint modes. A constraint mode shape is the static deflection of the structure if we apply a unit displacement to one interface DOF while all other interface DOF are held fixed. Thus, the motion at the interface is completely described by the constraint modes.

The truck model is partitioned into three large linear vibratory sub-structures as shown in Figure 6.12 and one small non-linear substructure separated at the mounting locations (coupling DOFs) [97-100]. The original DOFs of each substructure are represented by the constraint modes and the normal modes. This CMS approach reduces large vibratory substructures to modal models with few DOFs each. The frequency range of interest is from 0-30 Hz but the modal content up to 60 Hz is captured for each substructure in order to improve the accuracy of the simulation.

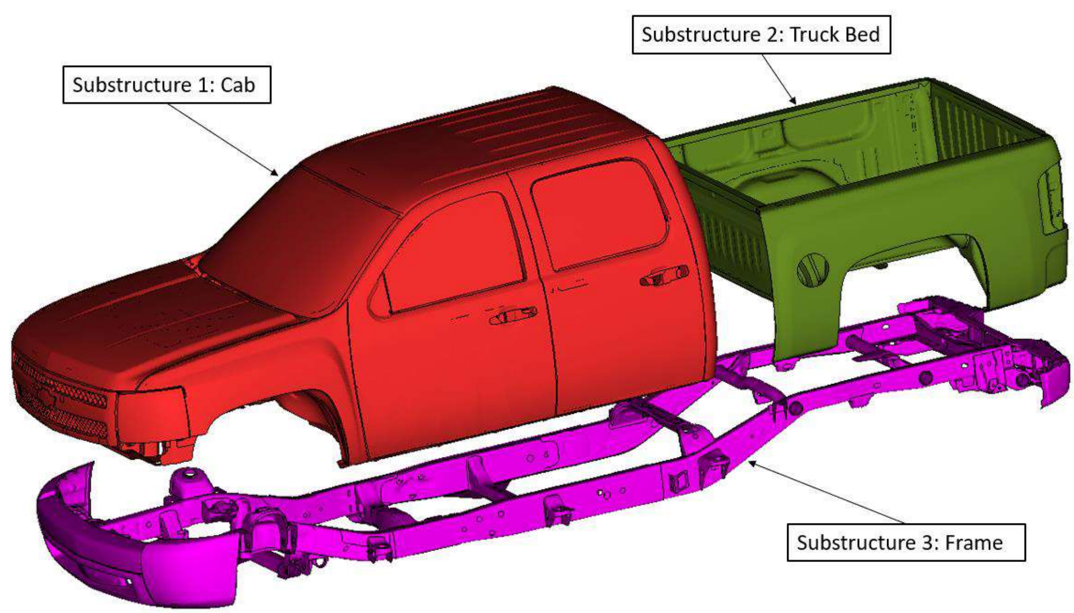


Figure 6.12 Substructures of pickup truck finite element model

Finally, the dynamic substructures and the residual non-linear substructure along with the applied loads and appropriate boundary conditions are assembled together to form a finite element model of 336 DOFs [97]. Table 6.3 shows the details of the super elements (substructures) and the residual structure for this the truck example. This non-linear model is then solved using the non-linear direct transient analysis in MSC/Nastran. The method uses the Newmark-Beta method for integration in time and the Quasi-Newton techniques known as BFGS (Broyden-Fletcher-Goldfarb-Shanno) to update the Hessian for iterations at each time.

The non-linear stiffness of the mounts is approximated using a linear fit as shown in Figure 6.13. An equivalent linear stiffness of 1600 *N/m3* is used instead of the actual non-linear stiffness to “linearize” the system.

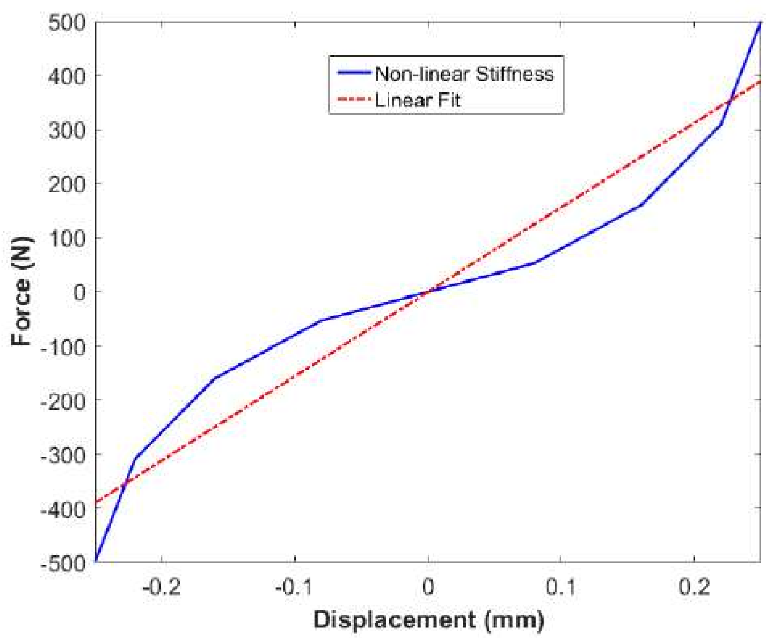


Figure 6.13 Nonlinear stiffness of suspension mount bushing

Table 6.3 Details of substructures and residual structure for the truck example

| No. | Joint From-To | Modal DOFs | Physical DOFs | Total DOFs |
|---|---|---|---|---|
| 1 | Cab | 163 | - | - |
| 2 | Bed | 64 | - | - |
| 3 | Frame | 103 | - | - |
| 4 | Residual | - | 6 | 336 |

6.4.2 Generation of non-Gaussian Force excitation trajectories

First, we generated the input random force realizations which are used as input excitations for the system. These excitations represent forces that act on the truck from the road, similarly to those experienced by a truck during operation. A Weibull marginal PDF is used for the input force random process with a heavy right tail, to capture the probability of extreme loading resulting in early failures. To generate realistic output stresses, the marginal PDF has a mean of 28 KN and a standard deviation of 15. The Weibull parameters lambda and kappa are then computed to match the desired mean and standard deviation, ensuring that the Weibull marginal PDF accurately represents the statistical properties of the input forces. Figure 6.14 shows the Weibull marginal PDF of the input force process and compares it with the normal distribution.

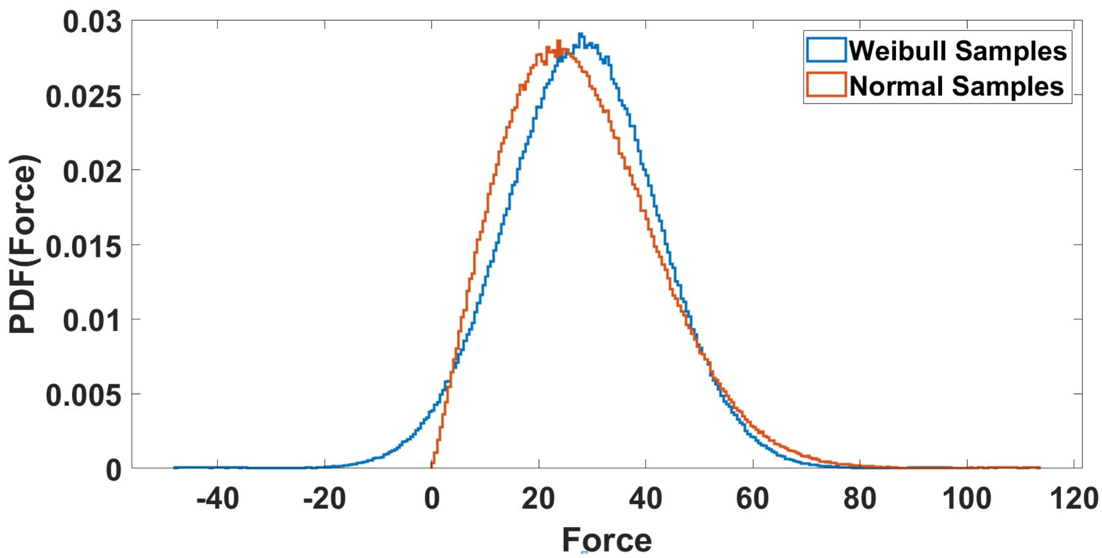


Figure 6.14 Marginal PDF for input force random process

An exponentially decaying autocorrelation coefficient (Figure 6.15) is used to capture the correlation structure of the input force process.

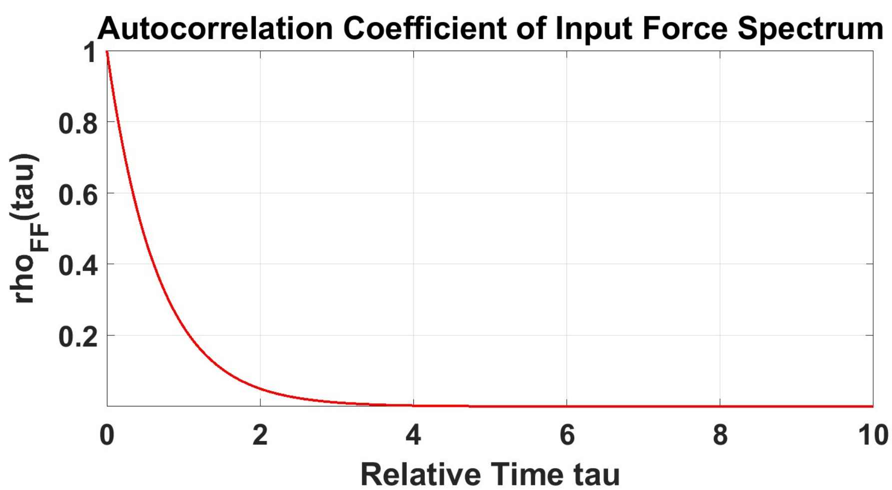


Figure 6.15 Autocorrelation coefficient of input force random process

Using the marginal PDF and the autocorrelation coefficient, we generated a 30 second force trajectories using the subdomain NG-KLE by stitching 3 subdomains of 10 second each (Figure 6.16). The color dots indicate the location where different segments of these force trajectories are stitched together.

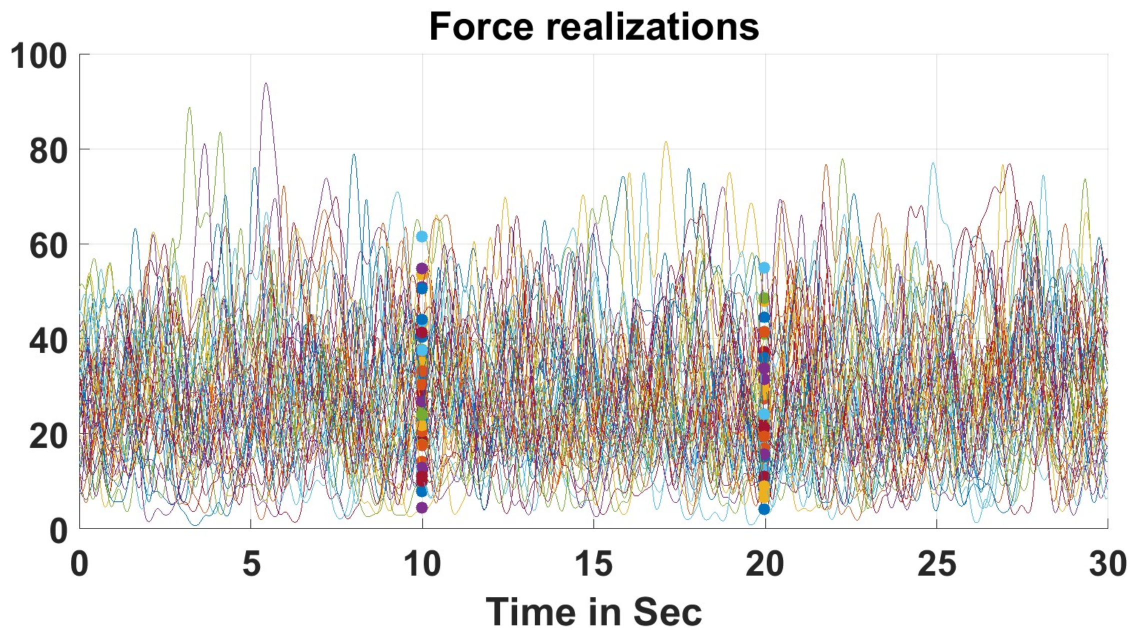


Figure 6.16 Input excitation force realizations from subdomain NG-KLE

To demonstrate the accuracy of the developed general fatigue estimation methodology, we repeat the fatigue estimation approach three independent times. Each time, we generate 50 input force realizations and calculate the corresponding 50 system responses. We use the low number of 50 evaluations to also demonstrate the computational efficiency of the method. Table 6.4 shows the statistics for the 50 input realizations. We observe that the estimated four statistical moments of the input process are similar.

Table 6.4 Input statistics of the fifty realizations per iteration

| Quantity | Non - Gaussian Iteration 1 | Non - Gaussian Iteration 2 | Non - Gaussian Iteration 3 |
|---|---|---|---|
| Mean | 27.8 | 28.1 | 27.4 |
| Standard Deviation | 14.60 | 15.10 | 14.80 |
| Skewness | 0.5666 | 0.5366 | 0.49 |
| Kurtosis | 3.12 | 2.99 | 3.08 |

For each input realization, a finite element model is run using NASTRAN's transient Sol 108. The corresponding output displacement realization is then used to calculate a stress realization at a particular location where the fatigue life will be estimated.

### 6.4.3 Output Stress Process and Generation of Long Stress Trajectories

Figure 6.17 shows the location of the input excitation and the response. The latter is obtained at a circular beam of the chassis which is typically the second-highest stress area. We avoid areas near welds which could experience the highest stress region because the properties of the welding material can vary and are proprietary to the manufacturer. Figure 6.18 shows the 50 realizations of the calculated stress process for iteration 1. Their non-negative values are due to the Weibull marginal PDF of the input force process. Table 6.5 shows the statistics of the stress output process based on the 50 realizations.

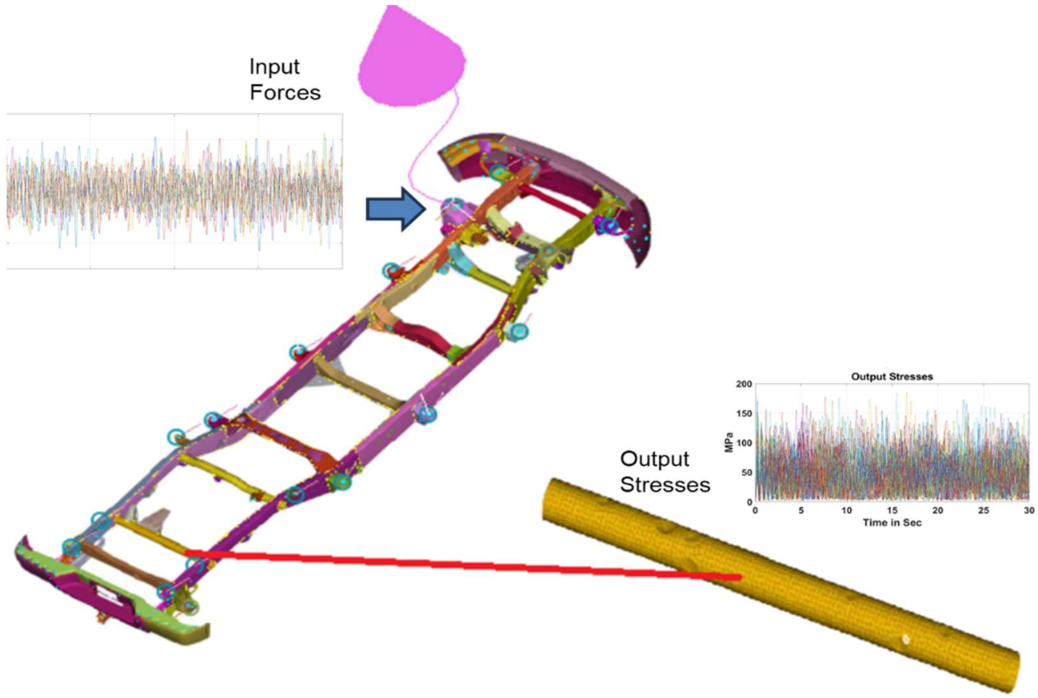


Figure 6.17 Input and output locations for the truck example

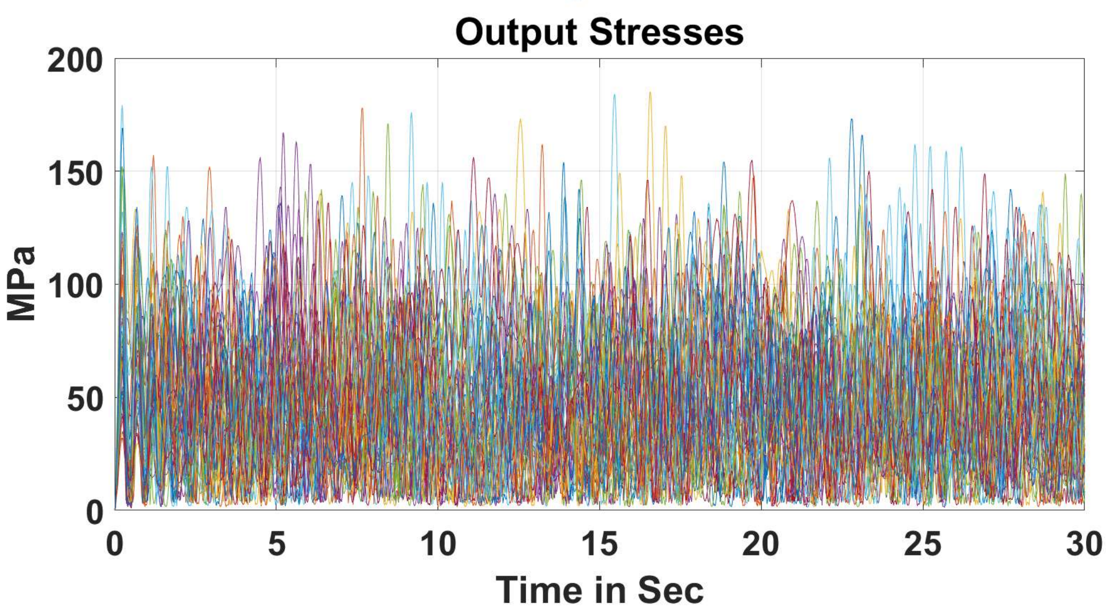


Figure 6.18 Output stresses for the 50 realizations of iteration 1

Table 6.5 Statistics of the output stress process

| Quantity | Non - Gaussian Iteration 1 | Non - Gaussian Iteration 2 | Non - Gaussian Iteration 3 |
|---|---|---|---|
| Mean | 47.98 | 53.1 | 42.10 |
| Standard Deviation | 28.05 | 30.5 | 36.4 |
| Skewness | 0.72 | 0.77 | 0.65 |
| Kurtosis | 3.41 | 3.6 | 3.5 |

Using the 50 output stresses trajectories, we estimated the marginal PDF (Figure 6.19) and the autocorrelation coefficient (Figure 6.20). The latter is smoothed using a Savitzky-Golay filter to reduce noise.

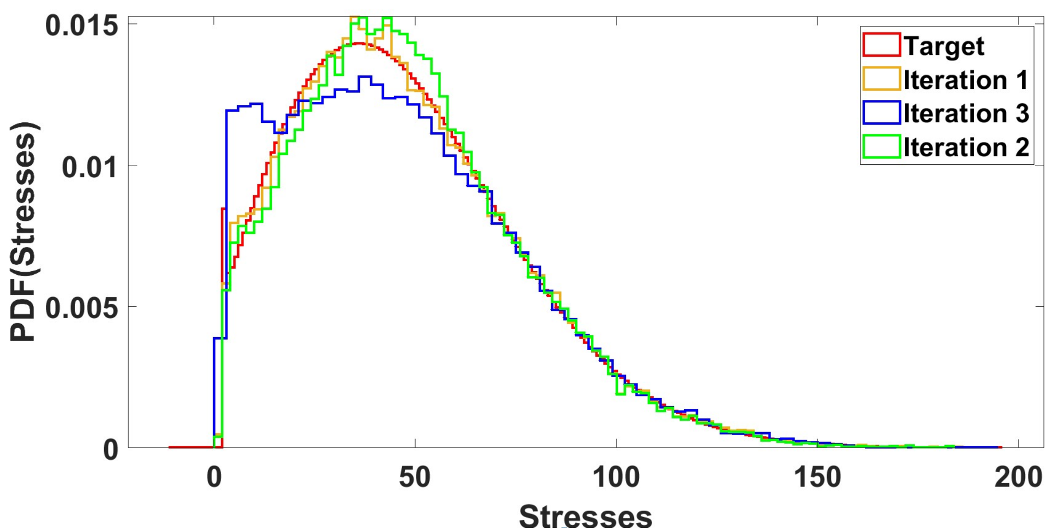


Figure 6.19 Estimated marginal PDF of output stress.

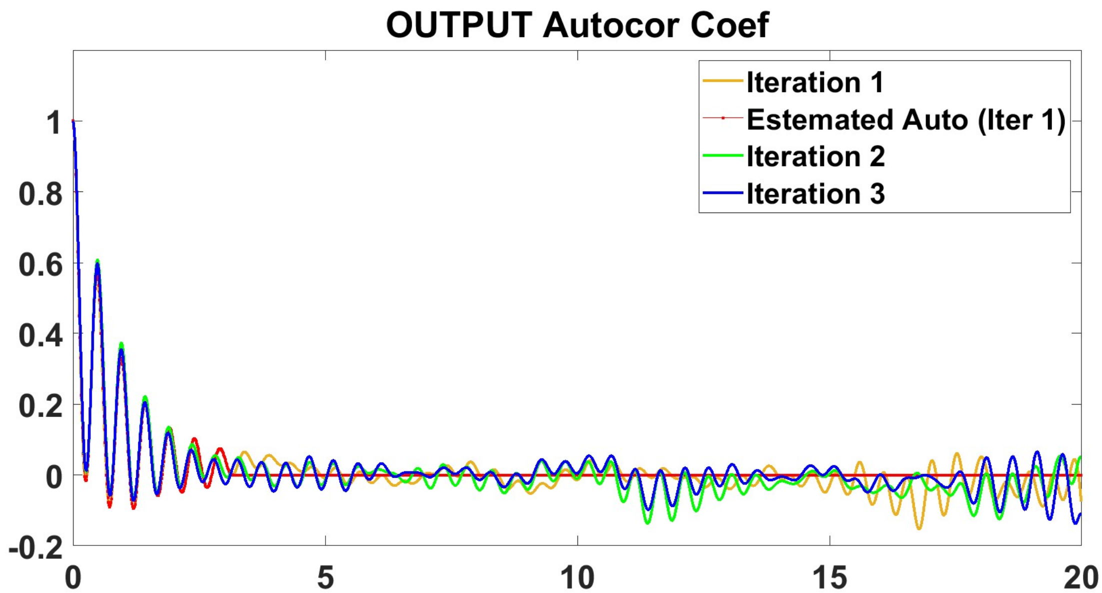


Figure 6.20 Estimated autocorrelation coefficient for output stress

After the marginal PDF and the autocorrelation coefficient are estimated, the subdomain NG-KLE approach is employed to generate very long stress trajectories spanning 5000 seconds as shown in Figure 6.21 demonstrating how the stress realizations evolve over extended periods. For each trajectory, 250 subdomains of 20 seconds each were used.

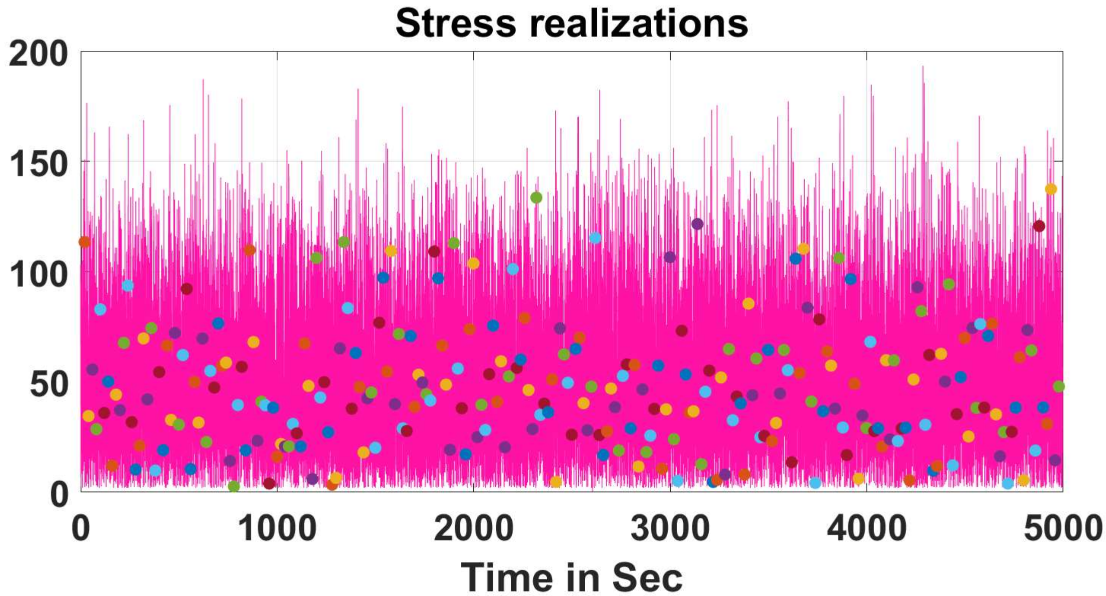


Figure 6.21 Long stress realizations using subdomain NG-KLE with 250 subdomains of 20 seconds each.

6.4.4 Fatigue Life Estimation

The fatigue life of a chassis frame is typically measured in terms of the number of loading cycles it can withstand before failure rather than in hours or years because it depends on how the vehicle is used and on the loading conditions it experiences. For example, a manufacturer might test a chassis frame to determine that it can withstand 1 million loading cycles, using also a safety factor of 2.5 – 3 times the actual number of cycles to failure. The actual duration in hours or years this represents depends on the frequency and magnitude of the loads the chassis frame experiences during its operational life. In a real-world scenario, the fatigue life of a chassis frame varies from vehicle to vehicle and can range from several years to decades, depending on factors such as the vehicle's usage, maintenance, and design. Commercial vehicles designed for heavy-duty

applications may have longer fatigue lives than passenger cars. It's also worth noting that manufacturers use safety factors and design considerations differently to ensure that the chassis frame will last well beyond the expected lifespan of the vehicle.
The spe'ific number of hours or years it would take for a chassis frame to reach its fatigue life can only be determined if the vehicle's operating conditions are known through its lifespan.

Using a large number of 5000-second long synthetic stress realizations as in Figure 6.21, we estimated the PDF of the fatigue cycles using the three methodologies of Section 4.3. Table 6.6 summarizes the results. The fatigue life is expressed both in hours and in terms to cycles to failure.

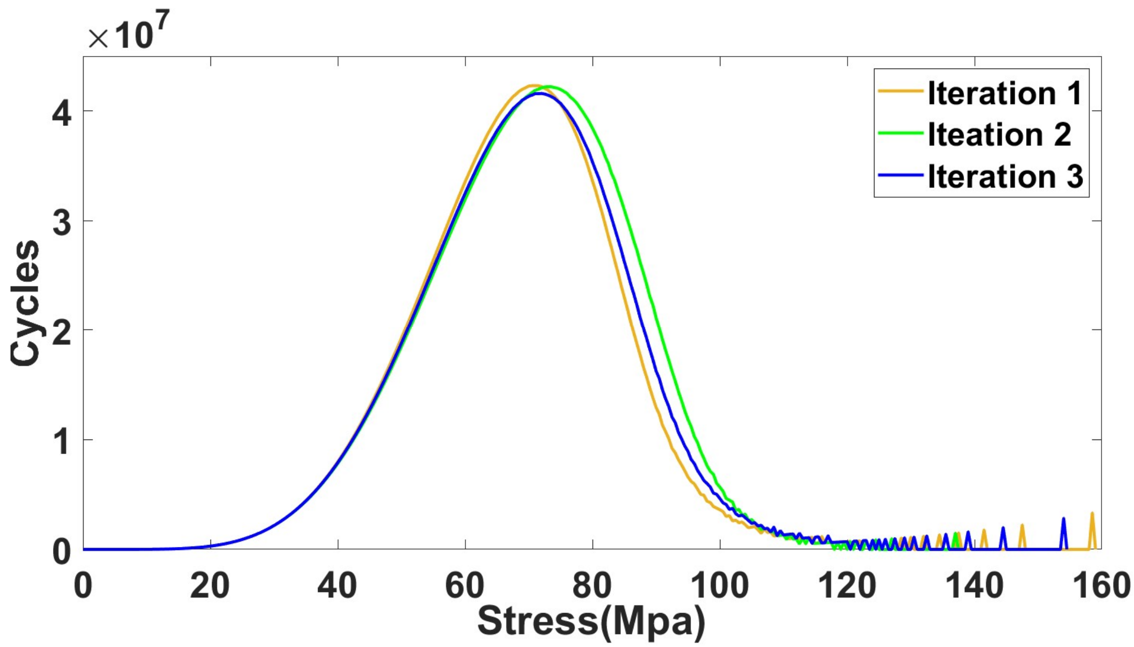


Figure 6.22 PDF of fatigue strength cycles

Table 6.6 Fatigue life estimation for the truck example

| Method | Iteration 1 | Iteration 2 | Iteration 3 |
|---|---|---|---|
| Mean Life (Hrs) | 7579 | 8009 | 7800 |
| Total Probability theorem | 7516 | 8190 | 7789 |
| PDF of peak stresses | 7359 | 8290 | 7692 |
| Number of cycles | 453589 | 434590 | 443002 |

## 6.5 Summary

This Chapter presented a subdomain-based NG-KLE method for fatigue life estimation. The method is computationally efficient and accurate and handles both Gaussian and non-Gaussian loads.

All developments were demonstrated using two examples: A Duffing oscillator excited by a non-Gaussian load, and a truck frame excited also by a non-Gaussian load. In the latter example, a very large finite element model is used for the truck.

# CHAPTER SEVEN

# CONTRIBUTIONS AND FUTURE WORK

## 7.1 Dissertation Contributions

This dissertation presents a range of contributions aimed at advancing the accurate and computationally efficient estimation of fatigue life for nonlinear systems excited by Gaussian or non-Gaussian loads. The main contributions are summarized below.

- Novel techniques were developed to estimate fatigue life for both Gaussian and non-Gaussian excitation.
- A subdomain-based approach was developed using KLE for Gaussian processes. The approach was also extended to non-Gaussian processes resulting in a NG-KLE. The methodology allows us to generate very long trajectories of a process enhancing therefore, the accuracy of fatigue life estimation without increasing the computational cost substantially as is the case for the conventional KLE. The method particularly benefits problems with non-normal stochastic excitations, facilitating efficient uncertainty propagation and fatigue life estimation.
- The computational and accuracy advantages of the developed subdomain NG-KLE were demonstrated using a Duffing oscillator nonlinear system as well as a nonlinear truck model example. A non-Gaussian excitation was used for both examples.

In an era dominated by the relentless advance of Artificial Intelligence and Machine Learning (AI/ML), this dissertation offers new mathematical techniques for efficient and accurate uncertainty propagation and fatigue life estimation for complex nonlinear systems excited by non-Gaussian loads.

## 7.2 Recommendations for Future Work

Below are potential future work avenues based on the contributions of this dissertation:

- Extend the subdomain KLE approach to non-stationary random processes.
- Develop more automated and adaptive ways to optimize the subdomain partitioning and continuity enforcement for greater efficiency.
- Explore multi-scale and multi-physics extensions of the fatigue modeling techniques for complex systems.
- Create user-friendly software implementations, to make the dissertation techniques more accessible to the wider research community.
- Create hybrid methods combining the dissertation techniques with physics-based and data-driven models to further improve efficiency and accuracy.

REFERENCES


[1] Tasdemir, B., and D. Coker. "Comparison of damage mechanisms in curved composite laminates under static and fatigue loading." *Composite Structures* 213 (2019): 190-203.

[2] Fatemi, A., and Yang, L., 1998, "Cumulative fatigue damage and life prediction theories: a survey of the state of the art for homogeneous materials", *International Journal of Fatigue*, 20(1), 9-34. K.

[3] Fan, Wenliang, et al. "The higher-order analysis method of statistics analysis for response of linear structure under stationary non-Gaussian excitation." *Mechanical Systems and Signal Processing* 166 (2022): 108430.

[4] Cai, G. Q., and YK0765 Lin. "Response distribution of non-linear systems excited by non-Gaussian impulsive noise." *International journal of non-linear mechanics* 27.6 (1992): 955-967.

[5] Steinwolf, A., and R. A. Ibrahim. "Numerical and experimental studies of linear systems subjected to non-Gaussian random excitations." *Probabilistic engineering mechanics* 14.4 (1999): 289-299..

[6] YU, Ying-yang, and Tong-min JIANG. "Generation of non-Gaussian random vibration excitation signal for reliability enhancement test." *Chinese Journal of Aeronautics* 20.3 (2007): 236-239..

[7] Geroulas, Vasileios, et al. "Reliability analysis of nonlinear vibratory systems under non-Gaussian loads." *Journal of Mechanical Design* 140.2 (2018): 021404..

[8] Dasgupta, Abhijit, and Michael Pecht. "Material failure mechanisms and damage models." *IEEE Transactions on Reliability* 40.5 (1991): 531-536..

[9] Tsianika, Vasiliki. Improved Fatigue Reliability and Accelerated Testing Methods for Vibratory Systems under Gaussian and Non-Gaussian Excitation. Diss. *Oakland University*, 2018..

[10] Tsianika, Vasiliki, et al. "A methodology for fatigue life estimation of linear vibratory systems under non-Gaussian loads." *SAE International Journal of Commercial Vehicles* 10.2017-01-0197 (2017): 460-472.

[11] Sakamoto, Shigehiro, and Roger Ghanem. "Polynomial chaos decomposition for the simulation of non-Gaussian nonstationary stochastic processes." *Journal of engineering mechanics* 128.2 (2002): 190-201.

[12] Zhao, Tengyuan, and Yu Wang. "Non-parametric simulation of non-stationary non-gaussian 3D random field samples directly from sparse measurements using signal decomposition and Markov Chain Monte Carlo (MCMC) simulation." *Reliability Engineering & System Safety* 203 (2020): 107087.

[13] Colin, Bruno. "Characterization of random Gaussian and non-Gaussian stress processes in terms of vibration fatigue." *Mechanics & Industry* 18.8 (2017): 809..

[14] Palmieri, Massimiliano, et al. "Non-Gaussianity and non-stationarity in vibration fatigue." *International Journal of Fatigue* 97 (2017): 9-19..

[15] Jiang, Y., Tao, J., Chen, X. (2022). Fatigue Life Analysis Under Non-Gaussian Random Vibration Excitation. In: Non-Gaussian Random Vibration Fatigue Analysis and Accelerated Test. *Springer, Singapore. https://doi.org/10.1007/978-981-16-3694-3_5*.

[16] Borgman, L., 1969, “Ocean Wave Simulation for Engineering Design”, *Journal of the Waterways and Harbors Division*, 95, 557-583..

[17] Shinozuka, M., and Deodatis, G., 1991, “Simulation of Stochastic Processes by Spectral Representation”, *Applied Mechanics Reviews*, 44, 191-203.

[18] Shinozuka, M., and Jan, C., 1972, “Digital Simulation of Random Processes and its Applications”, *Journal of Sound and Vibration,* 25, 111-128..

[19] Sudret, B., and Der Kiureghian, A., 2000, "Stochastic Finite Element Methods and Reliability: A State-of-the-art Report", Report UCB/SEMM-2000/08, *University of California, Berkeley*, CA.

[20] Phoon, K. K., Huang, S. P., and Quek, S. T., 2002, "Simulation of Second-Order Processes Using Karhunen-Loeve Expansion", *Computers and Structures*, 80, 1049-1060.

[21] Wu, S. Q., and S. S. Law. "A reduced polynomial chaos expansion model for stochastic analysis of a moving load on beam system with non-Gaussian parameters." *Journal of vibroengineering* 17.3 (2015): 1560-1577.

[22] Stefanou, George. "The stochastic finite element method: past, present and future." *Computer methods in applied mechanics and engineering* 198.9-12 (2009): 1031-1051.

[23] Xu, Huan, Feng Ding, and Erfu Yang. "Modeling a nonlinear process using the exponential autoregressive time series model." *Nonlinear Dynamics 95* (2019): 2079-2092..

[24] Adhikari, Ratnadip, and Ramesh K. Agrawal. "An introductory study on time series modeling and forecasting." *arXiv preprint arXiv:*1302.6613 (2013)..

[25] Liu, Zhangjun, Zixin Liu, and Yongbo Peng. "Dimension reduction of Karhunen-Loeve expansion for simulation of stochastic processes." *Journal of Sound and Vibration 408 (2017)*: 168-189..

[26] Vio, Roberto, et al. “Numerical Simulation of Non-Gaussian Random Fields with Prescribed Marginal Distributions and Cross-Correlation Structure. II. Multivariate Random Fields.” *Publications of the Astronomical Society of the Pacific, vol*. 114, no. 801, 2002, pp. 1281–89.

[27] Carrara, Pietro, et al. "A framework to model the fatigue behavior of brittle materials based on a variational phase-field approach." *Computer Methods in Applied Mechanics and Engineering* 361 (2020): 112731..

[28] Sakamoto, S., and Ghanem, R., 2002, "Simulation of Multidimensional Non-Gaussian Non-stationary Random Fields", *Probabilistic Engineering Mechanics*, 17, 167-176.

[29] "A Methodology for Fatigue Life Estimation of Linear Vibratory Systems under Non-Gaussian Loads", *Proceedings of SAE World Congress*, Research# 2017-01-0197,Detroit, MI, 2017.

[30] Buldygin, Valeriĭ Vladimirovich, and IU V. Kozachenko. Metric characterization of random variables and random processes. Vol. 188. *American Mathematical Soc.* 2000.

[31] Geroulas, V., Mourelatos, Z.P., Tsianika, V., and Baseski, I., "Reliability of Nonlinear Vibratory Systems Under Non-Gaussian Loads", *ASME Journal of Mechanical Design*, MD-17-1368, August 2017 (in press)..

[32] Kim, Hwanpyo, and Michael D. Shields. "Modeling strongly non-Gaussian non-stationary stochastic processes using the iterative translation approximation method and Karhunen–Loève expansion." *Computers & Structures* 161 (2015): 31-42..

[33] Montoya-Noguera, Silvana, et al. "Simulation of non-stationary non-Gaussian random fields from sparse measurements using Bayesian compressive sampling and Karhunen-Loève expansion." *Structural Safety 79 (2019): 66-79*.

[34] Braccesi, C., et al. "The importance of dynamic behaviour of vibrating systems on the response in case of non-Gaussian random excitations." *Procedia Structural Integrity* 12 (2018): 224-238..

[35] Debusschere, Bert J., et al. "Numerical challenges in the use of polynomial chaos representations for stochastic processes." *SIAM journal on scientific computing* 26.2 (2004): 698-719..

[36] Soong, T. T., and Grigoriu, M., 1993, Random Vibration of Mechanical and Structural Systems, *Prentice Hall, Englewood Cliffs*, *NJ*.

[37] Lee, Yung-Li, and Tana Tjhung. "Rain-flow cycle counting techniques." Metal Fatigue Analysis Handbook: *Practical Problem-solving Techniques for Computer-aided Engineering* 89 (2011).

[38] Meneghetti, Giovanni, et al. "The peak stress method applied to the fatigue assessment of tube-tube steel joints with weld ends under multiaxial loadings." *MATEC Web of Conferences*. *Vol. 300. EDP Sciences*, 2019..

[39] Li, H.; Wen, D.; Lu, Z.; Wang, Y.; Deng, F. Identifying the Probability Distribution of Fatigue Life Using the Maximum Entropy Principle. *Entropy 2016*, 18, 111.

[40] E. Santecchia, A. M. S. Hamouda, F. Musharavati, E. Zalnezhad, M. Cabibbo, M. El Mehtedi, S. Spigarelli, "A Review on Fatigue Life Prediction Methods for Metals", *Advances in Materials Science and Engineering, vol. 2016*, Article ID 9573524, 26 pages, 2016.

[41] Sun, Qin, Hong-Na Dui, and Xue-Ling Fan. "A statistically consistent fatigue damage model based on Miner's rule." *International Journal of Fatigue 69* (2014): 16-21..

[42] Lee, Y.-L., Pan, J., Hathaway, R., and Barkey, M., 2005, *Fatigue Testing and Analysis, Elsevie*r, 2005.

[43] Wirsching, P. H., Paez, T. L., and Ortiz, H., 1995, Random Vibrations: Theory and Practice, *John Wiley & Sons, New York, NY*.

[44] Chen, Jie, et al. "Piecewise stochastic rain-flow counting for probabilistic linear and nonlinear damage accumulation considering loading and material uncertainties." *International Journal of Fatigue* 140 (2020): 105842..

[45] Ballard, P., et al. "High cycle fatigue and a finite element analysis." *Fatigue & Fracture of Engineering Materials & Structures* 18.3 (1995): 397-411.

[46] Dowling, N. E., 1979, "Fatigue at notches and the local strain and fracture mechanics approaches", *American Society of Testing and Materials, Fracture Mechanics*, ASTM STP 677

[47] Matsuishi, M. and Endo, T., Fatigue of metals subjected to varying stress. *Presented to the Japanese Society of Mechanical Engineers, Fukuoka, Japan*, 1968.

[48] Zalaznik, Aleš, and Marko Nagode. "Experimental, theoretical and numerical fatigue damage estimation using a temperature modified dirlik method." *Engineering Structures* 96 (2015): 56-65.

[49] Singh, Jaskirat, and Sachin Sapatnekar. "Statistical timing analysis with correlated non-Gaussian parameters using independent component analysis." Proceedings of the 43rd annual Design Automation Conference. 2006. G. Glinka, J.C.P. Kam,Rain-flow counting algorithm for very long stress histories,*International Journal of Fatigue,Volume 9, Issue 4,1987,Pages 223*

[50] Hafner, Christian M., and Hans Manner. "Dynamic stochastic copula models: Estimation, inference and applications." *Journal of applied econometrics* 27.2 (2012): 269-295.

[51] Dai, Hongzhe, Zhibao Zheng, and Huihuan Ma. "An explicit method for simulating non-Gaussian and non-stationary stochastic processes by Karhunen-Loève and polynomial chaos expansion." *Mechanical Systems and Signal Processing* 115 (2019): 1-13.

[52] Obermayr, Martin, Christian Riess, and Jürgen Wilde. "A novel online 4-point rain-flow counting algorithm for power electronics." *Microelectronics Reliability 120 (2021)*: 114112.

[53] Shao, Weiming, Zhiqiang Ge, and Zhihuan Song. "Semisupervised Bayesian Gaussian mixture models for non-Gaussian soft sensor." *IEEE Transactions on Cybernetics* 51.7 (2019): 3455-3468.

[54] Raveri, Marco, and Cyrille Doux. "Non-Gaussian estimates of tensions in cosmological parameters." *Physical Review D* 104.4 (2021): 043504.

[55] Ince, A. "A mean stress correction model for tensile and compressive mean stress fatigue loadings." *Fatigue & Fracture of Engineering Materials & Structures* 40.6 (2017): 939-948.

[56] Bader, Qasim, and Emad Kadum. "Mean stress correction effects on the fatigue life behavior of steel alloys by using stress life approach theories." *Int. J. Eng. Technol* 14.04 (2014): 50-58.

[57] Grigoriu, M., "Simulation of Stationary Non-Gaussian Translation Processes," *Journal of Engineering Mechanics* 124, no. 2 (1998): 121-126.

[58] Papageorgiou, A., 2003, "Sufficient Conditions for Fast Quasi Monte Carlo Convergence," *Journal of Complexity*, 19, 332-351

[59] Xiu, D., and Karniadakis, G., 2002, "The Wiener-Askey Polynomial Chaos for Stochastic Differential Equations", SIAM Journal on Scientific Computing, 24(2), 619-644.

[60] Kim, Kwang-Ki K., et al. "Wiener's polynomial chaos for the analysis and control of nonlinear dynamical systems with probabilistic uncertainties [historical perspectives]." *IEEE Control Systems Magazine* 33.5 (2013): 58-67.

[61] Dutta, Parikshit, and Raktim Bhattacharya. "Nonlinear estimation of hypersonic state trajectories in Bayesian framework with polynomial chaos." *Journal of guidance, control, and dynamics 33*.6 (2010): 1765-1778..

[62] Debusschere, Bert J., et al. "Numerical challenges in the use of polynomial chaos representations for stochastic processes." *SIAM journal on scientific computing* 26.2 (2004): 698-719.

[63] Zhang, Yi, et al. "Reliability analysis with consideration of asymmetrically dependent variables: discussion and application to geotechnical examples." Reliability Engineering & System Safety 185 (2019): 261-277.Klink, Dieter, and Petrie Meyer. "A comparison of techniques for finding coefficients of polynomial chaos models for antenna problems." *International Journal of RF and Microwave Computer-Aided Engineering 31.8 (2021): e22729*.

[64] Cheng, Haiyan, and Adrian Sandu. "Efficient uncertainty quantification with the polynomial chaos method for stiff systems." Mathematics and Computers in Simulation 79.11 (2009): 3278-3295. Borgman, L., 1969, "Ocean Wave Simulation for Engineering Design", *Journal of the Waterways and Harbors Division*, 95, 557-583.

[65] Yang, S., Xiong, F., & Wang, F. (2017). Polynomial Chaos Expansion for Probabilistic Uncertainty Propagation.

[66] Huang, S. P., S. T. Quek, and KK0994 Phoon. "Convergence study of the truncated Karhunen–Loeve expansion for simulation of stochastic processes." *International journal for numerical methods in engineering* 52.9 (2001): 1029-1043..

[67] Wu, S. Q., and S. S. Law. "A reduced polynomial chaos expansion model for stochastic analysis of a moving load on beam system with non-Gaussian parameters." *Journal of vibroengineering* 17.3 (2015): 1560-1577.

[68] Majcher, M., Mourelatos, Z.P., Geroulas, V., Baseski, I., and Singh, A., "An Efficient Method to Calculate the Failure Rate of Dynamic Systems with Random Parameters using the Total Probability Theorem", *SAE International Journal of Materials & Manufacturing,* 8(3), 623-631, 2015.

[69] Xu, Huan, Feng Ding, and Erfu Yang. "Modeling a nonlinear process using the exponential autoregressive time series model." *Nonlinear Dynamics 95* (2019): 2079-2092..

[70] Adhikari, Ratnadip, and Ramesh K. Agrawal. "An introductory study on time series modeling and forecasting." *arXiv preprint arXiv:*1302.6613 (2013)..

[71] Liu, Zhangjun, Zixin Liu, and Yongbo Peng. "Dimension reduction of Karhunen-Loeve expansion for simulation of stochastic processes." *Journal of Sound and Vibration 408 (2017)*: 168-189..

[72] Quigley, J. P., Lee, Y.-L., and Wang, L., 2016, “Review and Assessment of Frequency-Based Fatigue Damage Models”, *SAE International Journal of Materials and Manufacturing*, 9(3), 565-577.

[73] Norouzi, M., and Nikolaidis, E., 2012, "Efficient Method for Reliability Assessment Under High-cycle Fatigue", *International Journal of Reliability, Quality and Safety Engineering*, 19(5), 1250022

[74] Shigley, J. E., Mischke, C. R., and Budynas, R. G., 2003, *Mechanical Engineering Design, McGraw Hill*.

[75] "A Methodology for Fatigue Life Estimation of Linear Vibratory Systems under Non-Gaussian Loads", *Proceedings of SAE World Congress*, Research# 2017-01-0197,Detroit, MI, 2017.

[76] ISO 8608, 1995, Mechanical Vibration - Road Surface Profiles - Reporting of Measured Data, *International Organization for Standardization, Geneva.*

[77] Geroulas, V., Mourelatos, Z.P., Tsianika, V., and Baseski, I., "Reliability of Nonlinear Vibratory Systems Under Non-Gaussian Loads", *ASME Journal of Mechanical Design*, MD-17-1368, August 2017 (in press).

[78] Schueller, G.I., “A State-of-the-art Report on Computational Stochastic Mechanics,” *Probabilistic Engineering Mechanics* 12, no. 4 (1997): 197-321.

[79] Samaras, E., Shinozuka, M., and Tsurui, A., “ARMA Representation of Random Processes,” *Journal of Engineering Mechanics* 111 (1985): 449-461.

[80] Kudryashov, Nikolay A. "The generalized Duffing oscillator." *Communications in Nonlinear Science and Numerical Simulation* 93 (2021): 105526.

[81] Gersch, W. and Yonemoto, J., “Synthesis of Multivariate Random Vibration Systems: A Two-stage Least Squares ARMA Model Approach,” *Journal of Sound and Vibration* 52, no. 4 (1977): 553-565.

[82] Dick, J., Kuo, F.Y., and Sloan, I.H., “High Dimensional Integration – the Quasi Monte Carlo Way,” *Acta Numerica* (2014): 1-157.

[83] Betz, W., Papaioannou, I., and Straub, D., “Numerical Methods for the Discretization of Random Fields by Means of the Karhunen – Loève Expansion,” *Computer Methods in Applied Mechanics and Engineering* 271 (2014): 109-129.

[84] Panunzio, A.M., Cottereau, R., and Puel, G., “Large Scale Random Fields Generation Using Localized Karhunen Loève Expansion,” Advanced Modeling and Simulation in Engineering Sciences (2018): 5-20.

[85] Panunzio, Alfonso M., et al. "Sensitivity of the wheel–rail contact interactions and Dang Van Fatigue Index in the rail with respect to irregularities of the track geometry." *Vehicle system dynamics* 56.11 (2018): 1768-1795.

[86] Mande, O.K., Mourelatos, Z.P., and Papadimitriou D., "A Subdomain Approach for Uncertainty Quantification of Long Time Horizon Random Processes, " in press, *SAE International Journal of Advances and Current Practices in Mobility*, 2024 (issue 1). Also, SAE Technical Paper 2023-01-0083, WCX SAE World Congress Experience, 2023.

[87] Cottone, Giulio, and Mario Di Paola. "A new representation of power spectral density and correlation function by means of fractional spectral moments." *Probabilistic Engineering Mechanics* 25.3 (2010): 348-353.

[88] Ohtomo, Norio, et al. "Exponential characteristics of power spectral densities caused by chaotic phenomena." *Journal of the Physical Society of Japan* 64.4 (1995): 1104-1113.

[89] Rutigliani, Vito, et al. "Setting up a proper power spectral density (PSD) and autocorrelation analysis for material and process characterization." *Metrology, Inspection, and Process Control for Microlithography XXXII*. Vol. 10585. SPIE, 2018.

[90] E. Santecchia, A. M. S. Hamouda, F. Musharavati, E. Zalnezhad, M. Cabibbo, M. El Mehtedi, S. Spigarelli, "A Review on Fatigue Life Prediction Methods for Metals", *Advances in Materials Science and Engineering, vol. 2016*, Article ID 9573524, 26 pages, 2016.

[91] Newland, D.E., An Introduction to Random Vibrations, Spectral and Wavelet Analysis, 3rd ed. (Mineola, NY: Dover Pubications, Inc., 1993) Lee, Y.-L., Pan, J., Hathaway, R., and Barkey, M., 2005, *Fatigue Testing and Analysis, Elsevie*r, 2005.

[92] Wirsching, P. H., Paez, T. L., and Ortiz, H., 1995, Random Vibrations: Theory and Practice, *John Wiley & Sons, New York, NY*.

[93] Tong, Ming-Na, Yan-Gang Zhao, and Zhao Zhao. "Simulating strongly non-Gaussian and non-stationary processes using Karhunen–Loève expansion and L-moments-based Hermite polynomial model." *Mechanical Systems and Signal Processing* 160 (2021): 107953.

[94] Cho, H., Venturi, D., and Karniadakis, G.E., "Karhunen-Loeve Expansion for Multi-correlated Stochastic Processes,".

[95] Rue, H., "Fast Sampling of Gaussian Markov Random Fields," Journal of Royal Statistical Society B 63, no. 2 (2001):

[96] Wang, Limin. Karhunen-Loeve expansions and their applications. *London School of Economics and Political Science (United Kingdom)*, 2008..

[97] Patil, Santosh Anandrao. Time-Dependent Reliability-Based Design Optimization of Large Vibratory Systems. Diss. *Oakland University, 2019*.

[98] Patil, S., Papadimitriou, D., and Mourelatos, Z.P., "Time-Dependent Reliability-Based Design Optimization of Vibratory Systems," *SAE Int. J. Commer. Veh.* 10(1):56-65, 2017.

[99] Patil, Santosh, Dimitrios Papadimitriou, and Zissimos Mourelatos. "Time-Dependent Reliability-Based Design Optimization of Vibratory Systems." *SAE International Journal of Commercial Vehicles* 10.2017-01-0194 (2017): 56-65.

[100] Barton, David C., and John D. Fieldhouse. *Automotive Chassis Engineering*. Berlin: Springer, 2018.

[101] Moaaz, Ahmad O., and Nouby M. Ghazaly. "A review of the fatigue analysis of heavy duty truck frames." *American Journal of Engineering Research (AJER)* 3.10 (2014): 1-6

[102] Vijayakumar, M. D., Kannan, C. R., Manivannan, S., Vairamuthu, J., Tilahun, S., & Ram, P. B. (2020, December). Finite element analysis of automotive truck chassis. In *IOP Conference Series: Materials Science and Engineering* (Vol. 988, No. 1, p. 012114). IOP Publishing.

[103] Abd Rahman, Roslan, Mohd Nasir Tamin, and Ojo Kurdi. "Stress analysis of heavy duty truck chassis as a preliminary data for its fatigue life prediction using FEM." *Jurnal Mekanikal* (2008).

[104] Gao, Yunkai, Ze Yuan, and Yuexing Duan. "The Study on Fatigue Bench Test and Durability Evaluation of a Light Truck Cab." *SAE International Journal of Advances and Current Practices in Mobility* 2.2020-01-0760 (2020): 1569-1577.

[105] Wirsching, P. H., Paez, T. L., and Ortiz, H., 1995, *Random Vibrations: Theory and Practice*, John Wiley & Sons, New York, NY.

[106] Damati, Ahlam, Omar Daoud, and Qadri Hamarsheh. "Enhancing the odd peaks detection in OFDM systems using wavelet transforms." *Advances in Systems, Signals and Devices* (2016): 161.

RELATED PUBLICATIONS

**Journal Papers**

- Mande, O.K., Mourelatos, Z.P., and Papadimitriou D., "A Subdomain Approach for Uncertainty Quantification of Long Time Horizon Random Processes, " in press, *SAE International Journal of Advances and Current Practices in Mobility*, 2024 (issue 1). Also, SAE Technical Paper 2023-01-0083, WCX SAE World Congress Experience, 2023.

- Mande, O.K, and Mourelatos, Z.P. “A Simulation-based Fatigue Life Estimation Method for Nonlinear Systems Under Non-Gaussian Loads,” in preparation, *International Journal of Fatigue*, Oct. 2023.